

AFWAL-TR-81-3012

2

AD A104542

LEVEL II

FLIGHT TRAJECTORY CONTROL INVESTIGATION

INSTRUMENT DIVISION
LEAR SIEGLER, INC.
GRAND RAPIDS, MICHIGAN

DECEMBER 1980



Final Report for Period 15 May 1978 - 30 Oct. 1980

APPROVED FOR PUBLIC RELEASE;
DISTRIBUTION UNLIMITED



AIR FORCE FLIGHT DYNAMICS LABORATORY
AIR FORCE WRIGHT AERONAUTICAL LABORATORIES
AIR FORCE SYSTEMS COMMAND
WRIGHT-PATTERSON AIR FORCE BASE, OHIO 45433

DTIC FILE COPY

NOTICE

When Government drawings, specifications, or other data are used for any purpose other than in connection with a definitely related Government procurement operation, the United States Government thereby incurs no responsibility nor any obligation whatsoever; and the fact that the government may have formulated, furnished, or in any way supplied the said drawings, specifications, or other data, is not to be regarded by implication or otherwise as in any manner licensing the holder or any other person or corporation, or conveying any rights or permission to manufacture use, or sell any patented invention that may in any way be related thereto.

This report has been reviewed by the Office of Public Affairs (ASD/PA) and is releasable to the National Technical Information Service (NTIS). At NTIS, it will be available to the general public, including foreign nations.

This technical report has been reviewed and is approved for publication.

William L. Young
WILLIAM L. YOUNG JR.
Project Engineer
Control Systems Development Branch
Flight Control Division

FOR THE COMMANDER

James W. Morris
JAMES W. MORRIS, Acting Chief
Control Systems Development Branch
Flight Control Division

H. Max Davis
H. MAX DAVIS
Assistant Chief
Flight Control Division

"If your address has changed, if you wish to be removed from our mailing list, or if the addressee is no longer employed by your organization please notify AFWAL/FIGL, W-PAFB, OH 45433 to help us maintain a current mailing list".

Copies of this report should not be returned unless return is required by security considerations, contractual obligations, or notice on a specific document.

SECURITY CLASSIFICATION OF THIS PAGE (When Data Entered)

REPORT DOCUMENTATION PAGE		READ INSTRUCTIONS BEFORE COMPLETING FORM
1. REPORT NUMBER AFWAL-TR81-3012	2. GOVT ACCESSION NO. AD-A104	3. RECIPIENT'S CATALOG NUMBER
4. TITLE (and Subtitle) FLIGHT TRAJECTORY CONTROL INVESTIGATION	5. TIME PERIOD COVERED Final Report 15 May 1980 - 30 Oct 1980	6. PERFORMING ORGANIZATION NUMBER ID-05R
7. AUTHOR(s) Dr. M. J. Bird Dr. J. Karmarker, Systems Control, Inc. (Vt)	8. CONTRACT NUMBER F33615-78-C-3607	9. PROGRAM ELEMENT, PROJECT, TASK AREA & WORK UNIT NUMBERS 62201F 2403/02/34
11. CONTROLLING OFFICE NAME AND ADDRESS Flight Dynamics Laboratory (AFWAL/FIGL) Air Force Wright Aeronautical Laboratories AF Systems Command, Wright Patterson AFB, OH 45433	12. REPORT DATE March 1981	13. NUMBER OF PAGES 164
14. MONITORING AGENCY NAME & ADDRESS (if different from Controlling Office)	15. SECURITY CLASS. (of this report) UNCLASSIFIED	15a. DECLASSIFICATION/DOWNGRADING SCHEDULE
16. DISTRIBUTION STATEMENT (of this Report) Approved for public release; distribution unlimited.		
17. DISTRIBUTION STATEMENT (of the abstract entered in Block 20, if different from Report)		
18. SUPPLEMENTARY NOTES		
19. KEY WORDS (Continue on reverse side if necessary and identify by block number) Four Dimensional Guidance Optimal Control Laws Optimal Profile Synthesis Avionics Systems Flight Test Plan Avionics Systems Simulation		
20. ABSTRACT (Continue on reverse side if necessary and identify by block number) Optimal control algorithms for four-dimensional guidance of a transport aircraft were investigated for feasibility. Cost function constraints on the optimal reference path generator appeared impossible to achieve and the optimal guidance algorithms do not achieve significant performance improvement without excessive increases in sophistication and cost of the onboard avionics computer. A modularized existing Mission Management system allows a three-phase flight test plan to demonstrate the operational capability of the existing classical integrated flight trajectory control algorithms.		

BLANK

FOREWORD

This is the final engineering report of the Flight Trajectory Control investigation program under Contract F33615-78-C-3607 of Air Force Wright Aeronautical Laboratories, Flight Dynamics Laboratory, to determine the feasibility of applying optimal control theory to four-dimensional guidance of a transport aircraft. The investigations, in conformance with techniques previously developed for four-dimensional guidance of transport aircraft using classical control system theory, included application of optimal algorithms to both generation of a three-dimensional reference path trajectory through a sequence of waypoints specified in space coordinates, and to the guidance commands that controlled the aircraft along the reference trajectory at a velocity necessary to achieve a specified time of arrival at the waypoints.

The general result of this investigation is that the anticipated degree of improvement in aircraft control, using optimal rather than classical algorithms, could not justify the large increase in computational requirements of the on-board avionics computer and the associated increased costs inherent in state-of-the-art computer hardware technology.

A plan, specifically generated as part of this investigation to demonstrate the optimal algorithms by both man-in-the-loop simulation using a transport fixed-base cockpit and by flight test in a transport aircraft, can be implemented for demonstration of the existing classical guidance algorithms.

The work of this report is based on previous engineering development of four-dimensional guidance of transport aircraft using classical algorithms as reported in Technical Report AFFDL-TR-77-120.

The principal contributors to this report are the project engineer, Dr. M. Bird, Dr. R. Fredricks, and Dr. J. Karmarker, Systems Control, Inc. (Vt). Detailed analyses were provided by Mr. J. Ring.

The investigations of this report were accomplished during the period May 1978 through October 1980.

Accession For	
NTIS GRA&I <input checked="" type="checkbox"/>	
DTIC TAB <input type="checkbox"/>	
Unannounced <input type="checkbox"/>	
Justification	
By _____	
Distribution/	
Availability Codes	
Dist	Avail and/or Special
R	



D

BLANK

TABLE OF CONTENTS

Paragraph	Page	
1	INTRODUCTION	1
2	PROGRAM SUMMARY	3
2.1	PROGRAM PLAN	3
2.2	PROGRAM HISTORY	3
3	ALGORITHM DEVELOPMENT	9
3.1	TRAJECTORY GENERATOR DEVELOPMENT	9
3.1.1	Development Method	9
3.1.2	Dynamics of Problem	12
3.1.3	Cost Function	17
3.1.4	The Discrete Stage Optimal Control Algorithm	19
3.1.5	Representative Iterative Solution For $\vec{x}, \vec{\lambda}, \vec{u}$	
	(N given) Via Steepest Descent First	
	Iteration (k=1)	21
3.1.6	Solution Constraints	25
3.1.7	Trajectory Generator Review	25
3.2	OPTIMAL CONTROLLER ALGORITHM DEVELOPMENT	27
3.2.1	Simplified Aerodynamic Coefficients	27
3.2.2	Aircraft State Model	34
3.2.3	Dynamic Linearization of State Model Equations	44
3.2.4	Design of Linear Quadratic Regulator	51
3.2.4.1	LQ Design - Step 1	55
3.2.4.2	LQ Design - Step 2	57
3.2.4.3	LQ Design - Step 3	62
3.2.4.4	LQ Design - Step 4	65
3.2.4.5	Mechanization Requirements	65
3.3	THREAT AVOIDANCE ALGORITHM	70
3.3.1	Task Definition	70
3.3.2	Resource Management Concepts	71
3.3.3	Threat Avoidance Review	74
3.3.4	Threat Modeling Survey	74
3.3.5	Conclusions	76
3.4	SIMULATOR DEVELOPMENT	76
3.4.1	Aerodynamics and Stability Augmentation System	77
3.4.1.1	SAS Design	77
3.4.1.2	SAS Mechanization	85
3.4.1.3	SAS Performance	85
3.4.1.4	KC-135 Aerodynamics	91
3.4.2	Rehosting of IFTC Algorithms	102
3.4.3	Controller/Display Modification	105
4	RECOMMENDED FLIGHT TEST PLAN	107
4.1	FLIGHT TEST PLAN OVERVIEW	107
4.2	FLIGHT TEST FUNCTIONAL REQUIREMENTS ANALYSIS .	109

TABLE OF CONTENTS (Continued)

Paragraph		Page
4.2.1	General Navigation	109
4.2.2	Guidance	110
4.2.3	Flight Plan Management	110
4.2.4	Performance	111
4.2.5	Controller/Display	112
4.2.6	Communications	112
4.3	FLIGHT TEST SYSTEM MECHANIZATION	112
4.3.1	Functional Description	112
4.3.2	Physical Description	116
4.3.2.1	Phase One Configuration: Baseline System	116
4.3.2.2	Phase Two Configuration: Interim System	119
4.3.2.3	Phase Three Configuration: All-up MMS	119
4.3.3	Flight Test System Installation Plan	121
4.3.3.1	Avionics Equipment Bay Installation	121
4.3.3.2	Cockpit-Mounted Controller/Display Units	121
4.4	FLIGHT TEST OPERATIONS	124
4.4.1	Test Sequence 1	128
4.4.2	Test Sequence 2	129
4.4.3	Test Sequence 3	130
4.5	AIRCRAFT INSTALLATION AND CHECKOUT	130
4.5.1	Class II Modification Document Details	130
4.5.2	Aircraft Installation Design	131
4.6	FLIGHT TEST SUPPORT	132
4.6.1	Aircraft Modifications	133
4.6.2	Ground Checkout	133
4.6.3	Data Analysis	134
5	CONCLUSIONS AND RECOMMENDATIONS	135
10	APPENDIX A	
	AIRCRAFT TRANSFER FUNCTIONS	136
20	APPENDIX B	
	STOCHASTIC THREAT MODEL	146
30	APPENDIX C-1	
	ANALOG CIRCUIT DIAGRAMS	152
40	APPENDIX C-2	
	DIGITAL FLOW CHART	162

LIST OF FIGURES

Figure		Page
1	PROGRAM PLAN, FLIGHT TRAJECTORY CONTROL . . .	4
2	MOVING TARGET COORDINATE SYSTEM	42
3	LINEAR QUADRATIC CONTROLLER BLOCK DIAGRAM . . .	53
4	ROOT LOCUS FOR VARYING δV_{max}	58
5	ROOT LOCUS FOR VARYING $\delta \psi_{max}$	58
6	ROOT LOCUS FOR VARYING $\delta \gamma_{max}$	59
7	ROOT LOCUS FOR VARYING $\delta x_{AT_{max}}$	59
8	ROOT LOCUS FOR VARYING $\delta y_{CT_{max}}$	60
9	ROOT LOCUS FOR VARYING δh_{max}	60
10	ROOT LOCUS FOR VARYING $\delta \alpha_{max}$	61
11	ROOT LOCUS FOR VARYING $\delta \phi_{max}$	61
12	ROOT LOCUS FOR VARYING δt_{max}	62
13	ROOT LOCUS FOR NOMINAL FLIGHT PATH ANGLE VARIATION	63
14	ROOT LOCUS FOR NOMINAL BANK ANGLE VARIATION .	63
15	ROOT LOCUS FOR NOMINAL ALTITUDE VARIATION . .	64
16	ROOT LOCUS FOR NOMINAL VELOCITY VARIATION . .	64
17	δV_{max} = SCHEDULING	66
18	$\delta \psi_{max}$ = SCHEDULING	67
19	$\delta \gamma_{max}$ = SCHEDULING	68
20	REAL-TIME RESOURCE CONTROLLER	73
21	OPTIMUM FLIGHT PATH ASSUMING FIRST OBJECTIVE IS COMPLETED AND A POP-UP THREAD IS DETECTED BY ON-BOARD SENSORS	75
22	SAS PITCH AXIS BLOCK DIAGRAM	77
23	PITCH AXIS ROOT LOCUS - DOMINANT POLES	80
24	SAS YAW DAMPER BLOCK DIAGRAM	81
25	YAW DAMPER ROOT LOCI - DOMINANT POLES	82
26	ROLL AXIS BLOCK DIAGRAM	83
27	ROLL SAS ROOT LOCI	84
28	STABILITY AUGMENTATION SYSTEM CIRCUIT DIAGRAMS	88
29	LONGITUDINAL SAS RESPONSE TO PULSE ELEVATOR DEFLECTION	89
30	LATERAL SAS RESPONSE TO PULSE AILERON DEFLECTION	90

LIST OF FIGURES (Continued)

Figure		Page
31	BODY, STABILITY, AND WIND AXIS SYSTEM GEOMETRIES	93
32	SIMULATION BLOCK DIAGRAM	97
33	LONGITUDINAL AIRCRAFT RESPONSE TO PULSE ELEVATOR DEFLECTION	103
34	LATERAL AIRCRAFT RESPONSE TO PULSE AILERON DEFLECTION	104
35	NEW DUAL SEAT COCKPIT CONTROLLER/DISPLAY CONFIGURATION	106
36	TASK FLOW DIAGRAM, FLIGHT TEST PLAN	108
37	PERFORMANCE NAVIGATION COMPUTER SYSTEM	113
38	FUNCTIONAL BLOCK DIAGRAM, FLIGHT TEST SYSTEM	114
39	INTERFACE DIAGRAM, BASELINE SYSTEM	118
40	INTERFACE DIAGRAM, INTERIM SYSTEM	120
41	INTERFACE DIAGRAM, MISSION MANAGEMENT SYSTEM	122
42	BASELINE SYSTEM INSTALLATION	123
43	INTERIM SYSTEM INSTALLATION	125
44	FINAL CONFIGURATION INSTALLATION	126
45	FLIGHT TEST SEQUENCE	127
46	SYSTEM DEMO TASK FLOWCHART - PHASE III	132

LIST OF TABLES

Table		Page
I	INITIAL Q AND R SELECTION	56
II	SOLUTION OF STEADY STATE LQ PROBLEM	56
III	FINAL Q AND R SELECTION	69
IV	SUMMARY OF A/C FLIGHT CONDITIONS	78
V	PITCH SAS RESPONSE CHARACTERISTICS	79
VI	LATERAL SAS RESPONSE CHARACTERISTICS	83
VII	TERM DEFINITION, EQUATIONS 99 through 105 . . .	86
VIII	PROBLEM VARIABLE SCALING	87
IX	SAS DESIGN VERIFICATION	91
X	MAXIMUM VALUES	101
XI	AIRCRAFT DYNAMICS VERIFICATION	102

FINAL REPORT
FLIGHT TRAJECTORY CONTROL INVESTIGATION

1 INTRODUCTION

This report details the results of the Flight Trajectory Control Investigation (FTCI) conducted by Lear Siegler, Instrument Division, Grand Rapids, Michigan under Air Force contract F33615-78-C-3607.

The intent of the FTCI program was to develop improved algorithms incorporating optimal control techniques for guidance and control of a transport aircraft, to verify these algorithms by simulation, and to design a demonstration flight test.

The basic algorithms, developed under previous Air Force contracts¹, implemented classical control techniques for real-time generation of a flight path through a sequential series of waypoints defined in four dimensions (x, y, z, t) and for control of a transport aircraft to the generated flight path.

These basic algorithms had been demonstrated, using fixed-base cockpit, man-in-the-loop simulations, to provide excellent functional and operational guidance and control capability for a transport aircraft. However, these algorithms were not 'optimal' in the sense of minimizing a specified cost function that could be defined in terms of space position and time control performance trade-offs.

A principal issue in this FTCI program was the cost effectiveness of any optimal control algorithms, as compared to the classical control algorithms. The increased cost of applying optimal control, as measured by increased processing speed and memory requirements of the airborne avionics computer to handle the more sophisticated algorithms, must be paid by increased performance as measured by deviations of the actual aircraft flight path from the specified waypoints that define the desired flight path.

Early in the program it became apparent that the cost for initially developing the optimal algorithms for generation of the trajectory in four dimensions would greatly exceed the contractual resources. The program was redirected to develop the optimal algorithms to control the aircraft to a four-dimensional trajectory defined by the existing classical algorithms. The initial control algorithms developed in the form of a

¹Feasibility Study for Integrated Flight Trajectory Control (Airlift). LSI Report # GRR-008-0177A, AFFDL-TR-77-120, contract F33615-74-C-3083.

linear quadratic estimator, did not show any improvement in control performance when compared to the classical algorithms. As a result, the flight test plan, while useful for demonstrating either optimal or classical algorithms, is based on an avionics system mechanization that incorporates only the classical algorithms.

Although the major findings of this program indicate that optimal control applied to the basic Integrated Flight Trajectory Control functions is not yet within the state-of-the-art, continuing advances in methods of implementing optimal algorithms for aircraft guidance and control and in airborne processor mechanizations may yet make the FTCI concepts not only feasible but desirable.

PROGRAM SUMMARY

2.1 PROGRAM PLAN

Two key elements of the general plan to achieve the tasks of the FTCI program were (1) to utilize the assets accruing from the preceding IFTC program program and (2) to obtain specialized technical support, through a subcontract, from System Control Incorporated (SCI) of Florida.

The major program tasks included development of optimal trajectory generator and aircraft control algorithms, verification of these algorithms by man-in-the-loop simulation using a fixed-base cockpit, and design of a flight test program to demonstrate the performance of the algorithms in a typical operational system.

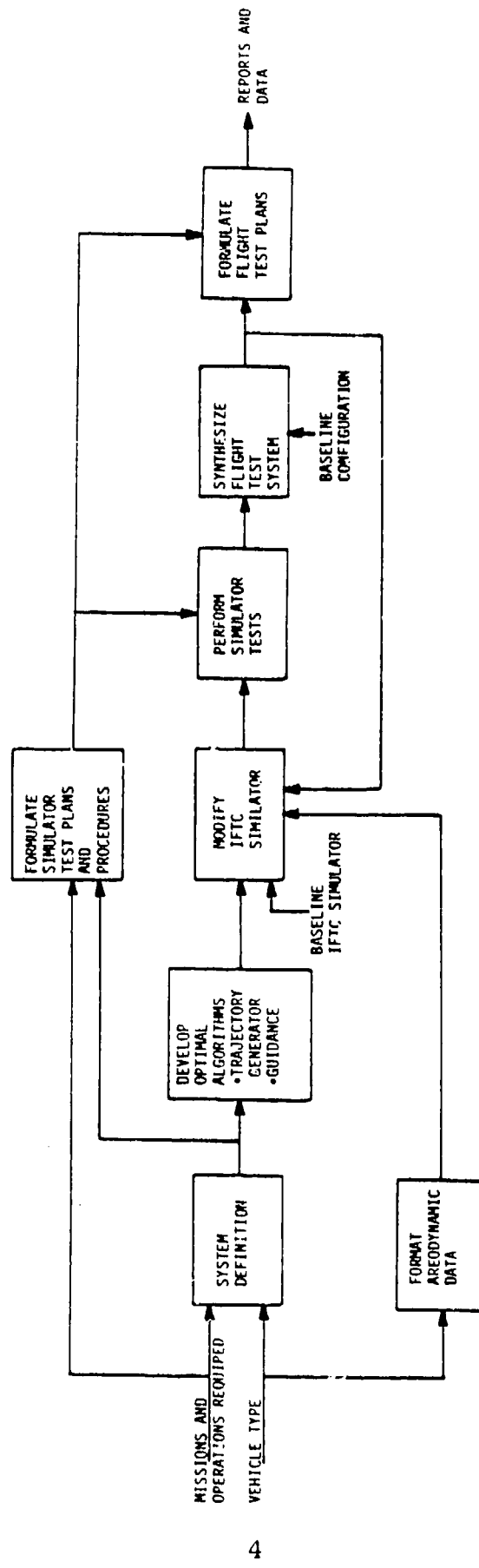
The assets or background for this program that were derived from IFTC included classical algorithms that were the functional, but not necessarily the performance, equivalent of the desired optimal algorithms. In addition, the assets included a fixed-base transport cockpit simulator equipped with man-machine interface specifically developed for the operational requirements of IFTC mission management systems.

The subcontract with SCI (Vt) was designed to provide Lear Siegler, Inc. (LSI) with experienced technical advice and support in the application of nonlinear optimal control theory to the general task of algorithm development and to provide novel concepts, developed by SCI, for threat modeling and avoidance capabilities for the trajectory generator. The expertise of SCI (Vt) in these areas is based on successful related programs. A typical example is the Advanced Weapons Management Systems (AWMS) for the Navy. In this program SCI (Vt) developed a dynamic programming solution for determining an optimum flight path and allocation of other resources for threat avoidance by a manned aircraft on any enemy defense penetration mission.

2.2 PROGRAM HISTORY

The initial task in developing the algorithms, as shown in Figure 1, was to develop a first-cut approach to applying optimal control theory to the trajectory generator.

The approach, described in 3.1, was straightforward and amounted basically to adapting the classical two-point boundary value formulation to a six-degree-of-freedom point mass aircraft with all the structural, maneuver, and mission constraints accounted for by using penalty functions (both terminal and enroute) in J , the overall cost function. An



PROGRAM PLAN, FLIGHT TRAJECTORY CONTROL
FIGURE 1

eight-dimensional discrete state vector (\vec{x}) was formulated consisting of east, north, and vertical aircraft displacements, true airspeed, flight path angle, heading angle, vehicle mass, and elapsed time. The last state variable was introduced because ground track distance was used as the independent variable rather than time. The control vector (\vec{u}) chosen consisted of three elements, namely, angle of attack (alternatively pitch), craft roll angle, and effective engine power setting or EPR.

- A zero-th order solution for the complete trajectory including a terminal value (R_o) for the ground-track variable (r) was assumed to be obtainable from the existing conventional IFTC trajectory generator which has already been developed. The solution for the state (\vec{x}), costate ($\vec{\lambda}$) (also eight-dimensional), and control vectors over the complete trajectory was obtained using a steepest descent technique to minimize the gradient of the Hamiltonian (H) at each discrete state of each iteration. The control vector trajectory was continually perturbed via the steepest descent algorithm until $\nabla_u H$, the gradient of H with respect to \vec{u} , became sufficiently small at each of the assumed N discrete track stages in the profile that a stopping criteria was satisfied. This process yielded a candidate optimal solution $[\vec{x}\{r\}, \vec{\lambda}\{r\}, \vec{u}\{r\}]$ for the trajectory, valid from $r=0$ to $r=R_o$. New candidate optimal solutions were obtained using an outer iteration loop where R_o was perturbed from the conventional IFTC generator value. By calculating the actual cost associated with each candidate optimal solution, the true optimum could be determined.

It was felt that this algorithm was amenable to a real-time airborne implementation due to the speed and small size of current military microprocessors. However, an algorithm review, by subcontractor SCI, indicated that the task of implementing this algorithm in our simulator would exceed substantially the manpower and dollar resources allotted to the FTCI program. In addition to excessive algorithm development costs, SCI indicated that the penalty function approach to constraint satisfaction was too "soft", even though it did make the full two-point boundary value quite suitable for the steepest descent solution. Although the constraints could be forced to be satisfied more exactly if more complex optimization methods, such as gradient projection, were used to augment the steepest descent approach, proper investigations of these techniques would only exacerbate the time, manpower, and financial overload of the program.

As an alternative, SCI suggested implementing a piecemeal procedure that would generate suboptimal flight profiles. This approach would first determine a horizontal plane profile which avoided all threats and satisfied all the waypoint and endpoint constraints. This profile could then be displayed to the pilot for his approval. Next would be to use an energy-state optimal control algorithm, similar to that being pursued by Erzberger, et al.², to calculate the vertical profile, speed, and time schedules associated with the accepted horizontal trajectory. This approach would take maximum advantage of the threat avoidance (minimum exposure) horizontal profile generator previously developed during the AWMS program and of the considerable previous work based upon Erzberger's energy-state algorithm, as reported in the literature.

The piecemeal approach, however, had the disadvantage of limited inherent performance improvement capability.

The problem was resolved by rescoping the FTCI program to concentrate the remaining resources in developing the linear quadratic optimal control algorithms for control of the aircraft to a trajectory developed using the IFTC classical techniques but modified with increased survivability capability by incorporating algorithms developed by SCI. These algorithms are defined in Section 3.3.

The development of the linear quadratic optimal controller, as detailed in Section 3.2, began with definition of dimensionless force and moment equations for the KC-135 aerodynamics. These equations were derived by simplification of the standard aerodynamic equations defined by Boeing Military Aircraft Division for the KC-135 aircraft.

With these aerodynamic forces and moments the equations of motion in six degrees of freedom were generated for simulation of the KC-135 aircraft. The state model of the aircraft, for this purpose, was defined in terms of nine state variables: airspeed, angle of attack, angle of sideslip, and body axis angular rates in inertial space and attitude. This aircraft model was simulated by hybrid computer and the simulation was verified by comparing the response of the simulated system to simulated aileron and elevator deflections to calculated responses of identical analytic inputs.

The inner control loop of the aircraft simulation was closed by design and simulation of the stability augmentation system (SAS) using attitude and rate feedback.

²H. Erzberger, et al., "Fixed Range Optimum Trajectories for Short-Haul Aircraft", NASA TN-D-8115, December 1975.

The SAS and autothrottle design were based on the current digital flight control system being installed on the Speckled Trout aircraft.

To complement these simulations an IR&D project rehosted the IFTC algorithms from our IBM 370 to a PDP-11/70 laboratory computer. This improved operating time because the IBM-370 was entered through an often unreliable time-sharing real-time monitor system while the PDP-11/70 is a dedicated machine for avionics systems simulation. In addition, the controller/display unit of the cockpit simulator was modified to provide improved operability.

To reduce the complexity of the linear quadratic (LQ) controller, the aircraft equations of motion were reduced to point mass rather than the six-degree-of-freedom equations employed for the simulation. These point mass equations were linearized and used to develop a simplified form of the aircraft state equations. To analytically determine the steady-state performance of the optimal controller to a deterministic disturbance such as a change in horizontal wind magnitude and direction, the simplified aircraft state model was developed as a function of the following state variables: airspeed, heading, flight path angle, position in along-/across-track coordinates, and altitude. The driving functions were modeled as assumed rates of change of wind magnitude and direction. For this input, an analytic solution of the state perturbation matrix and control correction matrix were obtained to demonstrate feasibility of the LQ optimal controller, with a constant value for the state (Q) and control (R) gain feedback weighting matrices.

- a. A diagonal form of the weighting matrices was selected to allow independent selection of values for individual states and controls.
- b. Initial values, Q_0 and R_0 , were established for a particular flight condition by assigning maximum values to the plant state and computing maximum allowable controls corresponding to these states.
- c. The components of the matrices were varied to determine the effect on the closed-loop system optimal controller stability by eigenvalue analysis.
- d. A sensitivity analysis determined that three elements of the Q matrix (δV_{\max} , $\delta \psi_{\max}$ and $\delta \lambda_{\max}$) which penalized errors in velocity, heading, and flight path angle must be modified as a function of flight profile to achieve the desired response.

- e. The weighting matrices were scheduled as a function of flight condition by selecting a performance index for a sample of representative flight conditions that resulted in a critically damped closed-loop system.

The simplification of the controller by incorporating a point mass aircraft model and a stability augmentation control, rather than an attitude flight control system, minimized computation time in the airborne processor but also degraded probable performance. The cross-coupling terms derived by the controller would make aircraft transient responses to pilot overrides and to scheduled gain changes as a function of flight condition unacceptable to the pilot. No further funds were expended directly for optimal control.

A flight test program to mechanize the Speckled Trout test aircraft for demonstration of IFTC characteristics of time control and in-flight mission redirect was generated. This flight test plan was designed as a three-phase program because of the limited modification time availability of the Speckled Trout test aircraft and because of the difficulty in complete single step replacement of large sections of the avionics on an operational aircraft. This flight demonstration plan, as described in Section 4, includes the avionics equipment description, the flight test scenarios, and the installation plan.

3. ALGORITHM DEVELOPMENT

Algorithm development was initiated by a preliminary definition of a preferred approach to the solution based on the concepts of the original proposal. This initial approach was expanded in further detailed developmental analyses for both the optimal trajectory generator and optimal controller.

The optimal control problem was based on the classical algorithms developed on the previous Flight Trajectory Control System Investigation. These algorithms defined a flight path of an aircraft which started from an "initial point" and terminated at a desired "end point". A "point" is defined as a four-dimensional (space, time) coordinate set that specifies a trajectory as well as the state vector of the aircraft (heading, velocity, and flight path angle) with respect to the specified trajectory.

The objective of this present Flight Trajectory Control Investigation was to develop algorithms, based on optimal control techniques, that would most nearly control the aircraft to the optimized trajectory. Because the constraints on optimization were the aircraft dynamics, the optimized trajectory had to most nearly conform to the capabilities of the aircraft while achieving the desired mission requirements; and the optimized controller had to minimize the actual excursions of the aircraft from the trajectory during flight.

Classical deterministic optimal control algorithms were developed by applying the principles of variational calculus to the initial, non-optimal, trajectory generator and control algorithms developed on the IFTC program. The high computational workload required to implement these classical optimal control techniques has, to date, made them unsuitable in applicability to airborne processors. The rate of advance in speed of digital processors, however, makes these optimal algorithms feasible for advanced avionics system mechanizations.

3.1 TRAJECTORY GENERATOR DEVELOPMENT

3.1.1 Development Method

A six-degree-of-freedom point mass model is generated for the aircraft equations of motion. Thus x , y , z , v , γ and ψ are automatically state variables with x east, y north, z up, v the true airspeed, γ the flight path angle and ψ the heading. To these add aircraft mass, m , and since ground-track distance, r , is the independent variables, time, t , is also a state variable.

The control vector, \vec{u} , consists of three elements: angle of attack, α , roll angle, ϕ , and effective power setting, π . The latter control variable is a number between zero and 100 per cent and represents the rotor RPM (effective rotor RPM for multi-engine craft) normalized to the maximum allowable RPM. Given a power setting command, π , the autopilot can readily set the throttle levers to achieve the desired RPM.

The cost function (J) includes terminal costs (K) and integral (path) losses (I). The integral losses incorporate constraints such as maximum and minimum velocities or altitudes, and avoidance regions such as cylindrical volumes about some given ground coordinate. Penalty functions incorporate all such path constraints into J .

The state (\vec{x}) and costate ($\vec{\lambda}$) vector difference equations are solved iteratively for each path increment Δr , where the magnitude of Δr will be determined by simulation. A probable "safe" value of Δr suitable for transport dynamics is ~ 0.1 nautical mile. The number of the iterative multipass stages in the solution of the algorithm is designated by N_k^{ℓ} .

This number is fixed for a given ℓ independent of k . The nominal initial trajectory has a total ground track, R_0 . Thus the number of all iterations of the first pass of the algorithm is

$$N^1 = \frac{R_0}{\Delta r}$$

where Δr is small enough to give accurate results and selected to make N^1 integer.

The index (i) on discrete increments of ground track then runs from $i=0$ to $i=N^{\ell}$ for the k th iteration of the ℓ th pass. The state, costate, and Hamiltonian, are solved for at each r_i . The control vector, however, is considered to vary more slowly and the steps in the discrete control vector occur only ever $j=10i$ units in discrete ground track with the dummy variable i running from 0 through $\frac{N-10}{10}$.

The relatively simple steepest descent algorithm for updating the control vector ($\vec{u}_{j,k}$) at the $(k+1)$ st iteration of a particular pass was implemented. Conjugate gradient and gradient projection techniques, although improving convergence time, are too complex for incorporation in an airborne computer.

In addition to updating the control vector $(\vec{u}_{j,k})$ by a steepest descent iterative approach, an ad-hoc, multi-pass technique will be used to slightly modify N^ℓ , the number of Δr stages. The approach of replacing time as the independent variable with ground track (r) results in a problem with length of ground track. Thus for the ℓ th pass, a change in N^ℓ represents an alteration of R_O . The constraint on time is represented in the terminal cost function (K) as a term of the form $k_{tt}(t_{N^\ell,k} - t_D)^2$ where t_D is the desired terminal time, $t_{N^\ell,k}$ is the value of the state variable "t" at the terminal state N^ℓ for the k th iteration of the ℓ th pass, and k_{tt} is some non-negative penalty function.

Then the complete algorithm requires iteration on $\vec{u}_{j,k,\ell}$ at each stage j for a given pass ($\ell = \text{Constant}$) with k representing the iteration number. When a stopping criteria is satisfied, the iterations for terminated at $k=k^*$ and the candidate optimal control discrete sequence $\{\vec{u}_{j,k^*,\ell}\}$ is used to evaluate an overall cost function J . Next, ℓ is incremented, i.e., N is perturbed (both above and below N^1) and new control sequences calculated via iterative steepest descent techniques.

The final optimal trajectory is then taken as the state vector generated by the optimal choice of both N^ℓ and $\{\vec{u}_{j,k^*,\ell}\}$. Letting ℓ^* denote the optimal terminal distance (via $R^* = N^{\ell^*} \Delta r$), the control sequence for the various stages is given by $\{\vec{u}_{j,k^*,\ell^*}\}$ where $j=10i$ and $i = 0, 1, 2, \dots, \frac{N^{\ell^*}-10}{10}$

The optimal solution, N^ℓ , is the point of minimum J , the cost. Thus J is a function of both the iteration k and the number of stages N^ℓ , i.e., $J=J\{k,\ell\}$.

Only a limited search was made in ℓ , i.e., $\ell=1, 2, 3$ was used when N^1 was as given previously, $N^2=N^1(1.1)$ and $N^3=N^1(0.9)$ say. The best of these three was used to define the final optimal flight path.

3.1.2 Dynamics of Problem

The aircraft equations of motion assuming zero sideslip angle and neglecting round, rotating earth effects, can be written as

$$\dot{x} = V \cos\{\gamma\} \sin\{\psi\} + w \sin\{\sigma\} \quad (1)$$

$$\dot{y} = V \cos\{\gamma\} \cos\{\psi\} + w \cos\{\sigma\} \quad (2)$$

$$\dot{z} = V \sin\{\gamma\} \quad (3)$$

$$\dot{v} = \frac{T}{m} \cos\{\alpha + \alpha_T\} - \frac{\rho}{2} (V)^2 C_D \frac{S}{m} - g \sin\{\gamma\} \quad (4)$$

$$\dot{v} = \left[\frac{T}{mV} \sin\{\alpha + \alpha_T\} + \frac{\rho}{2V} (V)^2 C_L \frac{S}{m} \right] \cos\{\phi\} - \frac{g}{V} \cos\{\gamma\} \quad (5)$$

$$\dot{\psi} = \left[\frac{T}{m} \sin\{\alpha + \alpha_T\} + \frac{\rho}{2} (V)^2 C_L \frac{S}{m} \right] \frac{\sin\{\phi\}}{\cos\{\gamma\}} \quad (6)$$

$$\dot{m} = w\{T, V, z\} \quad (7)$$

The ground track continuous dynamics may be derived from these equations by substitution of equation 8 for the time differential, dt . Then equations 1 through 7 become equations 9 through 15.

$$\frac{dt}{dr} = \frac{1}{V \cos\{\gamma\}} ; t\{0\} \triangleq 0 \quad (8)$$

$$\frac{dx}{dr} = \sin\{\psi\} + \left(\frac{w}{V} \right) \frac{\sin\{\sigma\}}{\cos\{\gamma\}} \quad (9)$$

$$\frac{dy}{dr} = \cos\{\psi\} + \frac{w \cos\{\sigma\}}{V \cos\{\gamma\}} \quad (10)$$

$$\frac{dz}{dr} = \tan\{\gamma\} \quad (11)$$

$$\frac{dv}{dr} = \frac{T\{V, z, \pi\} \cos\{\alpha + \alpha_T\}}{mV \cos\{\gamma\}} - \frac{\rho\{z\} C_D\{z, V, \alpha\} S}{2m \cos\{\gamma\}} \quad (12)$$

$$- \frac{g \tan\{\gamma\}}{V}$$

$$\frac{dy}{dr} = \left[\frac{T\{a, V, \pi\} \sin\{\alpha + \alpha_T\}}{mV^2 \cos\{\gamma\}} + \frac{\rho\{z\} C_L\{z, V, \alpha\} S}{2m \cos\{\gamma\}} \right] \quad (13)$$

$$\cdot \cos\{\phi\} - \frac{g}{V^2}$$

$$\frac{d\psi}{dr} = \left[\frac{T\{z, V, \pi\} \sin\{\alpha + \alpha_T\}}{mV \cos^2\{\gamma\}} + \frac{\rho\{z\} V C_L\{z, V, \alpha\} S}{2m \cos^2\{\gamma\}} \right] \quad (14)$$

$$\cdot \sin\{\phi\}$$

$$\frac{dm}{dr} = \frac{-w\{z, V, \pi\}}{V \cos\{\gamma\}} \quad (15)$$

In these equations

V = airspeed

γ = angle of velocity vector with respect to the x - y plane; positive γ corresponds to a climb angle

ψ = velocity vector heading measured in the x - y plane clockwise from North to the projection of the velocity vector in the x - y plane

m = mass of aircraft

α = angle of attack; positive α corresponds to aircraft longitudinal axis pitched above the velocity vector

ϕ = roll angle, positive right wing down

T = aircraft thrust

α_T = constant angle of thrust with respect to the lift line of the aircraft

w, σ = wind magnitude and heading with respect to North
 ρ = atmospheric density
 C_D = drag coefficient
 S = vehicle reference area
 g = gravitational acceleration (positive)

The complex functional interrelationships of the KC-135 vehicle and atmospheric parameters are summarized by the following equations:

$$C_L = C_L\{\alpha, z, \#M, q\} \quad (16)$$

$$= k_0 + k_1 \alpha$$

$$C_D = C_D\{C_L, \#M\} \quad (17)$$

$$= C_{D_0}\{\#M\} + k_2\{\#M\} (C_L - 0.1)^2 \quad (18)$$

$$T \triangleq NRT \cdot TS \quad (19)$$

where

$\#M$ = Mach number
 q = dynamic pressure
 NRT = normal rated thrust from all aircraft engines
 TS = effective throttle setting
 T = thrust

In equations 12 through 15, however, thrust (T) and fuel flow (w) are expressed directly in terms of π , the effective power setting that denotes actual rotor RPM, and pressure and temperature factors, δ and θ , respectively. Then

$$T = \delta f_T \{\pi/\sqrt{\theta}, \#M\} \quad (20a)$$

$$w = \delta \sqrt{\theta} f_F \{\pi/\sqrt{\theta}, \#M\} \quad (20b)$$

with

$$\theta = (\tau\{z\}/\tau_0)(1 + 0.2 \#M^2) \quad (20c)$$

$$\delta = (P\{z\}/P_0)(1 + 0.2 \#M^2)^{3.5} \quad (20d)$$

where we have assumed the specific heat ratio of air at constant pressure to that of air at constant volume to be 1.4 and where $\tau\{z\}/\tau_0$ and $P\{z\}/P_0$ are atmospheric temperature and pressure ratios obtained from the 1962 standard atmospheric model. Measurement of the stagnation pressure and static pressure allows direct determination of Mach number. The latter is, of course, linearly relatable to V , if the free stream static air temperature is known.

The control vector (\vec{u}) is three-element vector given by

$$\vec{u} \triangleq \begin{bmatrix} u_1\{t\} \\ u_2\{t\} \\ u_3\{t\} \end{bmatrix} = \begin{bmatrix} \alpha\{t\} \\ \phi\{t\} \\ T\{t\} \end{bmatrix} \quad (21)$$

In the preceding equations we have assumed a flat earth coordinate system with x east, y north, and z vertical.

Given N and Δr , the discrete versions of equations 8 through 15 are:

$$t_{i+1} = t_i + \frac{\Delta r}{V_i \cos\{\gamma_i\}} \quad (8')$$

($i=0,1,\dots,[N-1]$ and $t_0=0$)

$$x_{i+1} = x_i + \sin\{\psi_i\} + \frac{w_i \sin\{\sigma_i\}}{V_i \cos\{\gamma_i\}} \Delta r \quad (9')$$

($i=0,1,\dots,[N-1]$)

$$y_{i+1} = y_i + \cos\{\psi\} + \frac{w_i \sin\{\alpha_i\}}{V_i \cos\{\gamma_i\}} \Delta r \quad (10')$$

(i=0,1,...,[N-1])

$$z_{i+1} = z_i + [\tan\{\gamma_i\}] \Delta r \quad (11')$$

(i=0,1,...,[N-1])

$$v_{i+1} = v_i + \left[\frac{T\{z_i, v_i, \pi_i\} \cos\{\alpha_i + \alpha_T\} - g \tan\{\gamma_i\}}{m_i v_i \cos\{\gamma_i\}} \right. \\ \left. - \frac{\rho\{z_i\} C_D\{z_i, v_i, \alpha_i\} S}{2m_i \cos\{\gamma_i\}} \right] \cdot \Delta r \quad (12')$$

(i=0,1,...,[N-1])

$$\gamma_{i+1} = \gamma_i + \left[\frac{T\{z_i, v_i, \pi_i\} \sin\{\alpha_i + \alpha_T\}}{m_i (v_i)^2 \cos\{\gamma_i\}} \right. \\ \left. + \frac{\rho\{z_i\} C_L\{z_i, v_i, \alpha_i\} S}{2m_i \cos\{\gamma_i\}} \right] \cdot \cos\{\phi_i\} \Delta r - \frac{g}{(v_i)^2} \Delta r \quad (13')$$

(i=0,1,...,[N-1])

$$\psi_{i+1} = \psi_i + \left[\frac{T\{z_i, v_i, \pi_i\} \sin\{\alpha_i + \alpha_T\}}{m_i v_i \cos^2\{\gamma_i\}} \right. \\ \left. + \frac{\rho\{z_i\} v_i C_L\{z_i, v_i, \alpha_i\} S}{2m_i \cos^2\{\gamma_i\}} \right] \cdot \sin\{\phi_i\} \Delta r \quad (14')$$

(i=0,1,...,[N-1])

$$m_{i+1} = m_i - \left[\frac{w\{z_i, v_i, \pi_i\}}{V_i \cos\{\gamma_i\}} \right] \Delta r \quad (15')$$

(i=0,1,...,[N-1])

3.1.3 Cost Function

Assuming an N stage process the total cost function (J) is the sum of the terminal (K) and integral (I) (summation) costs. We write

$$J = K + I \quad (22)$$

where K is defined by

$$K = (\vec{x}_N - \vec{x}_{EP})^T [K_N] (\vec{x}_N - \vec{x}_{EP}) \quad (23)$$

and

$$(\vec{x}_N - \vec{x}_{EP}) \triangleq \begin{bmatrix} t_N - t_{EP} \\ x_N - x_{EP} \\ y_N - z_{EP} \\ z_N - z_{EP} \\ v_N - v_{EP} \\ \gamma_N - \gamma_{EP} \\ \psi_N - \psi_{EP} \\ m_N - m_{EP} \end{bmatrix} \quad (24)$$

with the subscript "EP" denoting the end point.

$[K_N]$ itself is an 8×8 diagonal matrix representing the terminal cost weights.

$$[K] = \begin{bmatrix} K_{tt} & & & & & & & \\ & K_{xx} & & & & & & \\ & & K_{yy} & & & & & \\ & & & K_{zz} & & & 0 & \\ & & & & K_{vv} & & & \\ 0 & & & & & K_{\gamma\gamma} & & \\ & & & & & & K_{\psi\psi} & \\ & & & & & & & K_{mm} \end{bmatrix} \quad (25)$$

where some elements such as K_{mm} or $K_{\gamma\gamma}$ may be zero, reflecting "don't care" conditions.

$$I = \sum_{i=0}^{N-1} \begin{bmatrix} \alpha_i \\ \phi_i \\ \pi_i \end{bmatrix}^T [R] \begin{bmatrix} \alpha_i \\ \phi_i \\ \pi_i \end{bmatrix} + \frac{k_{fuel} w\{z_i, v_i, \pi_i\}}{v_i \cos\{\gamma_i\}} \quad (26)$$

$$+ Lz_i + LV_i + La_i$$

where

Lz_i = altitude constraints

LV_i = velocity constraints

La_i = avoidance constraints

A possible formulation of Lz_i is

$$Lz_i = k_z \exp\{-(z_i - z_{min_i})/\sigma_z\} + k_z' \exp\{+(z_i - z_{max_i})/\sigma_z\} \quad (27)$$

where $\sigma_z \approx 200$ feet and z_{min_i} , z_{max_i} are determined in an ad hoc manner from the initial trajectory solution. Without any ATC constraints, z_{min_i} might be set equal to 1000 feet above the highest obstacle anywhere within a 0.5° forward look angle of the aircraft. Similarly, without any ATC constraints z_{max_i} might be set at 40,000 feet MSL for all i . Under Air Traffic Control, z_{min_i} might be set at a flat 18,000 feet MSL and z_{max_i} equal 40,000 feet MSL. During takeoff and approach segments, z_{min_i} must, of course, be suitably reduced. The demarcation boundaries separating such segments from those of cruise, cruise/climb, or cruise/ descent can be determined in terms of r_i , the independent variable, from the nominal trajectory, $\{\vec{x}_i, \vec{u}_i\}_0$.

A possible formulation of LV_i is

$$LV_i = k_v \exp - \left[\frac{(v_i - v_{min})}{\sigma_v} \right] + k_v' \exp + \left[\frac{(v_i - v_{max})}{\sigma_v} \right] \quad (28)$$

where

$$\begin{aligned}
 V_{\min} &= 1.2 V_{\text{stall}} \\
 V_{\max} &= \text{max dash velocity} \\
 \sigma_V &= 5 \text{ kts}
 \end{aligned}$$

A possible formulation for La_i is

$$La_i = \frac{k_{xaya}}{\exp\left[\frac{(x_i - x_a)^2 + (y_i - y_a)^2}{\sigma_{xy}^2}\right] - 1} \quad (29)$$

where, typically, σ_{xy} might be 50,000 feet to 500,000 feet and the avoidance cylinder is centered at (x_a, y_a) . These might be the x,y coordinate of the SAM site or of a mountain peak. Similar cost functions may be formulated for other avoidance geometries.

The cost function for fuel (k_{fuel}) in I represents the penalty for using too much fuel per unit of distance. The symmetric positive semi-definite matrix R represents the penalty on too much control action. It might be more meaningful to penalize control deviations from the original nominal control strategy, i.e., use

$$\begin{bmatrix} \alpha_i - \alpha_{i,0} \\ \phi_i - \phi_{i,0} \\ \pi_i - \pi_{i,0} \end{bmatrix} \text{ in place of } \begin{bmatrix} \alpha_i \\ \phi_i \\ \pi_i \end{bmatrix} \text{ in J}$$

where it is assumed the nominal control $(\alpha_{i,0}; \phi_{i,0}; \pi_{i,0})$ is slowly varying vector with respect to path length. This control strategy penalizes excessive perturbation that requires continuous new inputs to the autopilot/autothrottle.

3.1.4 The Discrete Stage Optimal Control Algorithm

The general form of the discrete state dynamic equations 8' through 15' may be written,

$$\begin{array}{ccc}
 & \leftarrow 1 \rightarrow & \\
 \begin{array}{c} \uparrow \\ 8 \left[\vec{x}_{i+1} \right] \\ \downarrow \end{array} & = & \begin{array}{c} \uparrow \leftarrow 1 \rightarrow \\ 8 \left[\vec{A} \{ \vec{x}_i, \vec{u}_i \} \right] \end{array} ; \vec{x}_0 \text{ given} \\
 & (i=0, 1, \dots, [N-1]) &
 \end{array} \quad (30)$$

For a given pass, N is considered fixed. The Hamiltonian (H_i) is defined as a scalar quantity given by

$$H_i = I_i + \vec{\lambda}_{i+1}^T \vec{A} \{ \vec{x}_i, \vec{u}_i \} \quad (31)$$

where I_i is an element of the integral cost function as defined in equations 26 through 29, and

$$\vec{\lambda}_N = \left[K_N \right] \left[\vec{x}_N - \vec{x}_{EP} \right] \quad (32)$$

is the final value of the costate vector. In general the costate vector satisfies the equation:

$$\left[\vec{\lambda} \right]_i = \left[\frac{\partial H}{\partial \vec{x}} \right]_i \quad (33)$$

where \vec{x} is an eight-state vector.

The necessary condition for a maximum of H is that

$$\begin{array}{ccc}
 \uparrow & \left[\frac{\partial H}{\partial \vec{u}} \right] & = \vec{0} \\
 \downarrow & \left[\frac{\partial H}{\partial \vec{u}} \right]_{i=j} &
 \end{array} \quad (34)$$

where u is a three-element control vector, given in equation 21, which drives the state vector.

In equation 34, index j is a multiple of a base number of, say, 10, i.e.,

$$(j = 0, 10, 20, \dots, (N-10))$$

This relationship of j to i is selected so that the control will vary only 1/10 as rapidly as the state or co-state for a given Δr . This assumption reduces the number of individual necessary equations that must be solved from $3N$ to $3(\frac{N}{10})$.

Our total number of unknowns (given \vec{x}_0 and $\vec{\lambda}_N$) is $nN+nN+m \frac{N}{10}$ where $n=9$ states and $m=3$ controls. The state dynamics given by vector equation 30 yields nN scalar equations as does vector equation 33. Finally, the necessary vector condition of equation 34 yields $m \frac{N}{10}$ scalar equations when expanded. Thus, a solution is possible as shown in Section 3.1.5 below.

3.1.5 Representative Iterative Solution For $\vec{x}, \vec{\lambda}, \vec{u}$ (N given) Via Steepest Descent First Iteration (k=1)

a. Given $\vec{u}_{j,0}$, the nominal trajectory, define the first iteration control vector $\vec{u}_{j,1}$ by

$$\vec{u}_{j,1} \triangleq \vec{u}_{j,0} \quad (35)$$

where

$$(j=0, 10, 20, \dots, (N-10))$$

b. "Fill in" the control vector using $\vec{u}_{i,1} = \vec{u}_{j,1}; i=j, j+1, \dots, j+9$ to get $\vec{u}_{i,1}$ where now $i=0, 1, 2, \dots, N-1$.

Then

$$\vec{x}_{i+1,1} = A\{\vec{x}_{i,1}, \vec{u}_{i,1}\} \quad i=0, 1, \dots, N-1 \quad (36)$$

with

$$\vec{x}_{0,1} = \vec{x}_{0,k} \triangleq \vec{x}_0, \text{ which is given}$$

c. Using $\vec{x}_{N,1}$ solve equation 32 for $\vec{\lambda}_{N,1}$ where \vec{x}_{EP} is specified by the aircrew. Entries in the diagonal matrix $[K_N]$ (equation 25) may be zero for control errors at the end point that are not significant.

d. Solve equation 33 backwards for $\vec{\lambda}_{i,1}$ ($i=N-1, N-2, \dots, 1, 0$) using the definition for H_i given by equation 31.

e. Using the $\{\vec{x}_{i,1}; \vec{\lambda}_{i,1}; \vec{u}_{i,1}\}$, evaluate equation 34 numerically.

Let

$$\vec{s}_{j,1} \triangleq \frac{\partial H_{j,1}}{\partial \vec{u}_{j,1}} \quad (37)$$

where

$$j = (0, 10, 20, \dots, (N-10))$$

Second Iteration ($k = 2$)

Ideally, $\vec{s}_{j,1}$ should equal 0 for all j . Then for the next estimate for the optimal control,

$$\vec{u}_{u,2} = \vec{u}_{j,1} - \tau_1 \vec{s}_{j,1} \quad (38)$$

where

$$\tau_1 = \frac{q_1}{100} \frac{|J\{1,N\}|}{\left\| \frac{\partial H_{j,1}}{\partial \vec{u}_{j,1}} \right\|^2}$$

Typically $q_1 = 10\%$ and $J\{1,N\}$ may be evaluated via equations 22 through 26. The denominator in the above is defined by

$$\left\| \frac{\partial H_{j,1}}{\partial \vec{u}_{j,1}} \right\|^2 = \sum_{j=0}^{(N-10)} \left[\left(\frac{\partial H_{j,1}}{\partial \vec{u}_{j,1}} \right)^T \left(\frac{\partial H_{j,1}}{\partial \vec{u}_{j,1}} \right) \right] \quad (39)$$

Given $\{\vec{u}_{j,2}\}$, "fill in" the control sequence to obtain the dense sequence $\{\vec{u}_{i,2}\}$ for $i=0, 1, 2, \dots, N-1$. Then repeat the steps of the first iteration and obtain a new control sequence $\{\vec{u}_{j,3}\}$ where

$$\vec{u}_{j,3} = \vec{u}_{j,2} - \tau_2 \vec{s}_{j,2} \quad (40)$$

Subsequent Iterations (k=3...N)

In general, we have for the kth iteration

$$\vec{s}_{j,k} \triangleq \frac{\partial H_{j,k}}{\partial \vec{u}_{j,k}} \quad (41)$$

$$\tau_k = \frac{q_k}{100} \frac{|J\{k,N\}|}{\left\| \frac{\partial H_{j,k}}{\partial \vec{u}_{j,k}} \right\|^2} \quad (42)$$

where q_k decreases from $q_1=10\%$ to perhaps 1% as k increases according to some assumed schedule that can be determined by computer simulation. Finally, the next control update is given by

$$\vec{u}_{j,k+1} = \vec{u}_{j,k} - \tau_k \vec{s}_{j,k} \quad (43)$$

Termination Criteria

If k becomes greater than k_{\max} , where k_{\max} is a limit that will be determined by computer simulation, we terminate the optimal trajectory generator algorithm. No attempt to further refine N is then made. $J\{k_{\max},N\}$ is, however, displayed to the pilots as is $J\{1,N\}$ the cost of the nominal trajectory. The pilots may then decide to utilize the trajectory $\{\vec{x}_{i,k_{\max}}, \vec{u}_{i,k_{\max}}\}$ after inspection and comparison with the nominal trajectory.

Normally the stopping criteria on k is when

$$\left\| \frac{\partial H_{i,k}}{\partial \vec{u}_{i,k}} \right\|_{[w]}^2 < \epsilon_1 \quad (44)$$

where ϵ_1 is determined by the simulation and where

$$\left\| \frac{\partial H_{i,k}}{\partial \vec{u}_{i,k}} \right\|_{[w]} = \sum_{i=0}^{N-1} \left[\frac{\partial H_{i,k}}{\partial \vec{u}_{i,k}} \right]^T [w] \left[\frac{\partial H_{i,k}}{\partial \vec{u}_{i,k}} \right] \quad (45)$$

with $[w]$ also determined via simulation.

Multi-Pass Refinement on N

Given a convergent steepest descent solution for the control with

$$N = N_1 \triangleq \frac{R_0}{\Delta r}$$

repeat the iterative solution until the termination criteria is achieved using $N=N_2 > N_1$ (say 10% greater). If this second pass is successful, then again repeat the iterative solution procedure using $N=N_3 < N_1$ (say 10% less).

Then compare the computed values of the cost functions $J\{k_1, N_1\}$, $J\{k_2, N_2\}$ and $J\{k_3, N_3\}$ to see which is least and choose the associated N_ℓ and $\{\vec{u}_{i,k}, N_\ell\}$ sequence.

While an initial guess at the control with $N=N_3$ is simply the control $\{\vec{u}_{i,0}\}$ suitably truncated, an ad hoc approach must be used when $N=N_2$ to come up with an initial guess for the control $\{\vec{u}_{i,0}\}$ in the discrete interval

$$i = N_1, N_1+1, N_1+2, \dots, N_2-1$$

A possible value is to set $\{\vec{u}_{i,0}\} = \vec{u}_{N_1-1,0}$ to initiate our steepest descent iterative procedures.

After successful completion of the complete optimal trajectory determination the $\{\vec{x}_i, \vec{u}_i\}$ sequence is displayed graphically to the pilots for their approval before being inserted into the autopilot. The pilots may elect to accept or reject the trajectory or even change some of the penalty functions or constraints and compute a new optimal trajectory.

3.1.6 Solution Constraints

The use of the penalty function approach rather than absolute bounds to constrain the aircraft state or to constrain the control vector commands means that it is possible that the original absolute bounds may not always be satisfied within the optimal trajectory. For crew safety then, if the generated commands exceed the absolute bounds specified by the crew or generated internally by the computer, this condition must be flagged for the crew's attention before the "optimal" trajectory is engaged into the flight controller's memory.

The complete set of partial derivatives required by the algorithm will be obtained during the actual algorithm development. Some of the required derivatives, however, are analytically available. For example,

$$\frac{\partial x_{i+1}}{\partial \psi_i} = \Delta \cos\{\psi_i\} \quad (46)$$

On the other hand, the partial derivatives

$$\frac{\partial T\{z_i, v_i, \pi_i\}}{\partial \pi_i} \triangleq T_{\pi_i} \quad (47)$$

must be evaluated numerically via the definition of a partial derivative, i.e.,

$$T_{\pi_i} \triangleq \frac{T\{z_i, v_i, \pi_i + \delta \pi_i\} - T\{z_i, v_i, \pi_i\}}{\delta \pi_i}$$

using stored tables

3.1.7 Trajectory Generator Review

In compliance with the overall program plan, System Control, Inc. (SCI) reviewed the preceding trajectory generator algorithm as derived from non-linear optimal control. They recommended abandoning the general approach as described in favor of adopting a piecemeal procedure for generating the trajectory. This procedure was

- a. To generate and display the horizontal projection of the trajectory, and
- b. After pilot acceptance, compute the associated vertical position/speed profile of the trajectory using assigned altitudes and minimum fuel algorithm.

The rationale of SCI (Vt) for this recommendation is stated below:

- a. The general non-linear optimal control theory approach to computing trajectories is too risky for this type of investigation. The implementation and successful development of this type of algorithm will be time consuming with a high possibility of failure. Furthermore, the trajectories computed with this type of algorithm will not be any more acceptable from an operational, flight control point of view than those generated using more straightforward techniques. In other words, the performance improvements of an "optimal control" trajectory generator for the 4-D end point attainment problem does not warrant the development time, risk, or on-board computer resources.
- b. To successfully compute realizable trajectories, the optimal control approach may need to be modified. The penalty function method for modeling speed, attitude, and thrust constraints makes these constraints "soft". There may be places on the trajectory where the constraints will be violated. In fact, because of the characteristics of the endpoint attainment problem, the constraints imposed by the penalty function method will probably always be violated at the end of the trajectory. The penalty function method of imposing constraints is the simplest to implement in a computer. To place stiffer constraints on the optimal control trajectories significantly increases the complexity of the numerical technique needed to compute the optimal control solution.

In subsequent discussion with the Air Force program officer the suggested piecemeal trajectory generator approach was not implemented because it did not satisfy the intent of the program and it is not significantly different from the classical trajectory generation technique already developed on the IFTC program.

Instead, the program content was modified to use the existing classical trajectory generation technique for the simulation, but increasing the capabilities of these algorithms for the survivability of military transport, bomber vehicles in the presence of SAM and AAA site ground threats.

The general task, as described in Section 3.3, was assigned to SCI as part of their analytic support contract. SCI was qualified for this task because of their previous development of minimum exposure profile generators on the Navy-funded Advanced Weapons Management System program.

3.2 OPTIMAL CONTROLLER ALGORITHM DEVELOPMENT

The general procedure of developing the linear quadratic optimal control algorithm included the following steps:

- a. Simplification of the aerodynamic coefficients for the KC-135 aircraft.
- b. Generation and simplification of the aircraft state equations using the developed coefficients of step a.
- c. Linearization of the state equations in order to apply the linear quadratic estimator.
- d. Design of the linear quadratic estimator by selection of the state and control vectors of the cost functional and analysis of the system response to deterministic inputs and sensitivity to aircraft flight dynamics.
- e. Investigation of mechanization requirements.

3.2.1 Simplified Aerodynamic Coefficients

A primary objective in developing the state model for the (LQ) regulator is to obtain the simplest aircraft model that still retains an adequate description of the airplane dynamics. In order to achieve this objective, the following assumptions were made:

- The aircraft is rigid body so that aeroelastic effects were not modeled.
- The aircraft mass, moment and products of inertia, and center of gravity are constant.
- Ground effect and landing gear coefficients were not modeled since landings were not simulated.
- Refuel boom coefficients are negligible.
- Spoilers and flaps are not deployed.

- Stabilizer angle is fixed at -6° .
- Ice doesn't form on wings.

In addition, engineering judgement was used to simplify the remaining significant dimensionless aerodynamic force and moment coefficients. In most cases the resulting coefficient is within an order of magnitude of the actual value.

Appendix A of this report contains the KC-135 aerodynamic force and moment coefficients as they appear in Boeing Document No. D3-9781-2. Many of the components of the force and moment coefficients are eliminated as a consequence of the preceding simplifying assumptions.

The simplified dimensionless aerodynamic coefficients (C_D , C_Y , C_L , C_ℓ , C_m , C_n) are then defined as,

$$\begin{aligned}
 C_L &= C_{L_0} + C_{L_\alpha} \alpha_{WCP} + C_{L_\dot{\alpha}} \left(\frac{\dot{\alpha} c}{2V_T} \right) + C_{L_q} \left(\frac{q c}{2V_T} \right) + C_{L_{\delta_e}} \delta_e \\
 C_D &= C_{D_0} + K(C_L - .15)^2 \\
 C_m &= C_{m_0} + C_{m_\alpha} \alpha_{WCP} + C_{m_\dot{\alpha}} \left(\frac{\dot{\alpha} c}{2V_T} \right) + C_{m_q} \left(\frac{q_s c}{2V_T} \right) + C_{m_{\delta_e}} \delta_e \\
 C_Y &= C_{Y_\beta} \beta + C_{Y_{\delta_R}} \delta_R \\
 C_n &= C_{n_\beta} \beta + C_{n_{\dot{\beta}}} \left(\frac{\dot{\beta} b}{2V_T} \right) + C_{n_p} \left(\frac{p_s b}{2V_T} \right) + C_{n_r} \left(\frac{r_s b}{2V_T} \right) + C_{n_{\delta_R}} \delta_R \\
 C_\ell &= C_{\ell_\beta} \beta + C_{\ell_p} \left(\frac{p_s b}{2V_T} \right) + C_{\ell_r} \left(\frac{r_s b}{2V_T} \right) + C_{\ell_{\delta_a}} \delta_a + C_{\ell_{\delta_R}} \delta_R
 \end{aligned} \quad \{48\}$$

where C_L , C_D , C_m , C_ℓ , C_n , and C_Y are the aerodynamic coefficients of list, drag, pitch-moment, roll-moment, yaw-moment, and side forces, respectively. For these coefficient equations, the term definitions are:

β	=	airplane sideslip angle (deg)
δ_R	=	rudder deflection angle (deg)
$\dot{\beta}$	=	airplane sideslip angle rate (rad/sec)
α_{wcp}	=	airplane angle of attack relative to the wing chord plane (deg)
P	=	roll rate about the stability axis (rad/sec)
r	=	yaw rate about the stability axis (rad/sec)
δ_a	=	aileron deflection angle (deg)
q	=	pitch rate about the stability axis (rad/sec)
$\dot{\alpha}$	=	airplane angle-of-attack rate (rad/sec)
δ_e	=	elevator deflection angle (deg)
M	=	Mach number
b	=	wing span = 130.83 feet for the KC-135 aircraft
V	=	true airspeed (ft/sec)
\bar{c}	=	wing mean aerodynamic chord = 20.16 feet for the KC-135 aircraft

Additional simplifications to these coefficients can be made by considering the dynamics of the lateral and longitudinal modes of an airframe.³ The approximate damping factor and natural frequency for the quadratic modes and time constants for the first order modes are

$$\omega_{\text{short period}} \approx \frac{1}{\tau} \left(\frac{\bar{c}}{2K_{yy}} \right) \left[\frac{-C_m q}{2} (C_{L\alpha} + C_D) - 2u_c C_m \alpha \right]^{\frac{1}{2}} \quad (49)$$

³Dynamics of Airplane, Northrup Corporation, Aircraft Division, Document number AE-61-4-11.

$$\zeta_{\text{short period}} \approx \frac{-1}{2\omega_{\text{short period}}} \left(\frac{1}{\tau} \right) \left(\frac{\bar{c}}{2K_{yy}} \right)^2 \left[C_{m_\alpha} + C_{m_q} - \frac{C_{L_\alpha} + C_D}{2 \left(\frac{\bar{c}}{2K_{yy}} \right)^2} \right] \quad (50)$$

$$\omega_{\text{phugoid}} \approx \frac{1}{\omega_{\text{short period}}} \left(\frac{g}{2K_{yy}} \right)^{\frac{1}{2}} \left(\frac{1}{\tau} \right) \left[(C_{m_U} + C_m)(C_{L_\alpha} + C_L) - C_{m_\alpha}(C_{L_U} + C_L) \right]^{\frac{1}{2}} \quad (51)$$

$$\zeta_{\text{phugoid}} \approx \frac{C_{D_U} + C_D}{2\tau\omega_{\text{phugoid}}} \quad (52)$$

$$\frac{1}{T} \approx \left(\frac{g}{\tau} \right) \frac{C_{n_\beta} C_{\ell_r} - C_{\ell_\beta} C_{n_r}}{\left(\frac{1}{4u_b} \right) C_Y C_{\ell_p} C_{n_r} + C_{\ell_p} C_{n_\beta} + \left(\frac{g}{U_0} \right) (4\tau) \left(\frac{k_{zz}}{b} \right)^2 C_{\ell_\beta}} \quad (53)$$

$$\frac{1}{T_{\text{rolling}}} \approx \frac{1}{4\tau} \left(\frac{b}{K_{xx}} \right)^2 \frac{\left[\frac{1}{4u_b} C_Y C_{\ell_p} C_{n_r} + C_{\ell_p} C_{n_\beta} + \left(\frac{g}{U_0} \right) (4\tau) \left(\frac{k_{zz}}{b} \right)^2 C_{\ell_p} \right]}{C_{n_\beta}} \quad (54)$$

$$\omega_{\text{Dutch Roll}} \approx \frac{1}{\tau} \left(\frac{b}{K_{zz}} \right) \sqrt{\frac{u_b}{2}} C_{n_\beta} \quad (55)$$

$$\zeta_{\text{Dutch Roll}} \approx \frac{1}{8} \left(\frac{b}{K_{zz}} \right) \frac{C_{n_r}}{\sqrt{\frac{u_b}{2}} C_{n_\beta}} \quad (56)$$

where

$$u_b = \frac{m}{\rho S b}, \quad u_c = \frac{m}{\rho S c}, \quad \tau = \frac{m}{\rho S V_T}$$

$$k_{xx} = \sqrt{\frac{I_{xx}}{m}}, k_{yy} = \sqrt{\frac{I_{yy}}{m}}, k_{zz} = \sqrt{\frac{I_{zz}}{m}}$$

Examination of equations 49 through 56 reveals that the following coefficients do not appear.

$$C_{L\dot{\alpha}}, C_{Lq}, C_{n\dot{\beta}}, \text{ and } C_{n\dot{p}}$$

These coefficients were eliminated because they were not deemed significant to longitudinal or lateral mode characteristics. The effects of

$$C_{L\dot{\delta}_e}, C_{Y\dot{\delta}_R}, \text{ and } C_{\ell\dot{\delta}_R}$$

are small ($\approx 0.004/\text{degree}$) and were also eliminated. If the resulting dimensionless aero force and moment equations are used in the state mode, the term

$$C_{m\dot{\alpha}} \left(\frac{\dot{\alpha}c}{2V_T} \right)$$

in the dimensionless pitching moment equation couples the state derivatives $\dot{\alpha}$ and q_s . This term cannot be neglected as it contributes roughly 20% of the short period mode damping. It can be shown, however that modifying the term

$$C_m \left(\frac{q\bar{c}}{2V_T} \right) \text{ to } (C_{m\dot{\alpha}} + C_{m\dot{q}}) \frac{q\bar{c}}{2V_T}$$

and deleting the term

$$C_{m\dot{\alpha}} \left(\frac{\dot{\alpha}c}{2V_T} \right)$$

will decouple the state derivatives and not alter the short period mode damping. These further simplifications, with C_L substituted into the C_D equation, reduce the dimensionless force and moment coefficients of equation 48 to,

$$\begin{aligned}
 C_L &= C_{L_0} + C_{L_\alpha} \alpha_{WCP} \\
 C_D &= C_{D_0} + K[(C_{L_\alpha} - .15)^2 + 2C_{L_0} - .015) \alpha_{WCP} + C_{L_\alpha}^2 \alpha_{WCP}^2] \\
 C_m &= C_{m_0} + C_{m_\alpha} \alpha_{WCP} + (C_{m_\alpha} + C_{m_q}) \left(\frac{q_c}{2V_T} \right) + C_{m_\delta_e} \delta_e \\
 C_Y &= C_{Y_\beta} \beta \\
 C_n &= C_{n_\beta} \beta + C_{n_r} \left(\frac{r_s b}{2V_T} \right) + C_{n_\delta_R} \delta_R \\
 C_\ell &= C_{\ell_\beta} \beta + C_{\ell_p} \left(\frac{p_s b}{2V_T} \right) + C_{\ell_r} \left(\frac{r_s b}{2V_T} \right) + C_{\ell_\delta_\alpha} \delta_\alpha
 \end{aligned} \tag{57}$$

From the graphs in Appendix A, the simplified values of terms in these coefficients for the KC-135 aircraft are:

$$\begin{aligned}
 C_{L_0} &= .05 \\
 C_{L_\alpha} &= .0796 \text{ (1/deg)} \\
 C_{m_\alpha} &= .0191 \text{ (1/deg)} \\
 C_{m_\alpha} &= -5. \text{ (1/rad)} \\
 C_{D_0} &= .0164 \\
 K &= .088 \\
 C_{m_0} &= .122
 \end{aligned}$$

$$\begin{aligned}
c_{m_q} &= -15.65 \text{ (1/rad)} \\
c_{m_{\delta_e}} &= .013 \text{ (1/deg)} \\
c_{n_{\beta}} &= -0.12 \text{ (1/deg)} \\
c_{n_r} &= -.16 \text{ (1/rad)} \\
c_{n_{\delta_R}} &= -.0017 \text{ (1/deg)} \\
c_{\lambda_{\beta}} &= c_{\lambda_{\beta_0}} + c_{\lambda_{\beta_1}} (M-.3) + c_{\lambda_{\beta_2}} \alpha_{WPC} \\
c_{\lambda_{\beta_0}} &= -.00205 \text{ (1/deg)} \\
c_{\lambda_{\beta_1}} &= -.003 \text{ (1/deg)} \\
c_{\lambda_{\beta_2}} &= -.00156 \text{ (1/deg)}^2 \\
c_{\lambda_p} &= -.408 \text{ (1/rad)} \\
c_{\lambda_r} &= c_{\lambda_{r_0}} + c_{\lambda_{r_1}} \alpha_{WPC} \\
c_{\lambda_{r_0}} &= .088 \text{ (1/rad)} \\
c_{\lambda_{r_1}} &= .0132 \text{ (1/deg)} \\
c_{\lambda_{\delta_A}} &= .0005 \text{ (1/deg)}
\end{aligned}$$

3.2.2 Aircraft State Model

A complete six-degree-of-freedom aircraft state model was derived, as defined in Section 3.4, Simulator Development, for closed-loop simulation of the optimal control algorithms using the transport cockpit.

These equations are,

$$\begin{bmatrix} \dot{V}_T \\ \dot{\beta} \\ \dot{\alpha} \\ \dot{p}_s \\ \dot{q}_s \\ \dot{r} \\ \dot{\phi} \\ \dot{\theta} \\ \dot{\psi} \end{bmatrix} = \begin{bmatrix} X_W/m \\ Y_W/mV_T \\ Z_W/(mV_T \cos\beta) + q_s - p_s \tan\beta \\ (I_1 r_s + I_2 p_s) q + I_3 L_s + I_4 N_s \\ I_5 r_s p_s + I_6 (r_s^2 - p_s^2) + I_7 M_s \\ (I_8 p_s + I_9 r_s) q_s + I_4 L_s + I_{10} N_s \\ p_s + q_s \sin\phi \tan\theta + r \cos\phi \tan\theta \\ q_s \cos\phi - r_s \sin\phi \\ q_s \sin\phi / \cos\theta + r_s \cos\phi / \cos\theta \end{bmatrix} \quad (58)$$

where

$$\begin{bmatrix} X_W \\ Y_W \\ Z_W \end{bmatrix} = \begin{bmatrix} \cos\beta & \sin\beta \\ -\sin\beta & \cos\beta \\ 0 & 0 \end{bmatrix} \begin{bmatrix} 0 \\ 0 \\ 1 \end{bmatrix} \begin{bmatrix} X_s \\ Y_s \\ Z_s \end{bmatrix} + \begin{bmatrix} \cos\alpha & 0 & \sin\alpha \\ 0 & 1 & 0 \\ -\sin\alpha & 0 & \cos\alpha \end{bmatrix} \begin{bmatrix} T \\ 0 \\ 0 \end{bmatrix} + W \begin{bmatrix} -\sin\theta \\ \cos\theta \sin\phi \\ \cos\theta \cos\phi \end{bmatrix} \quad (59)$$

and

$$\begin{aligned} X_s &= -1/2\rho V_T^2 S C_D, & L_s &= 1/2\rho V_T^2 S b C_L \\ Y_s &= 1/2\rho V_T^2 S C_Y, & M_s &= 1/2\rho V_T^2 S c C_m \\ Z_s &= -1/2\rho V_T^2 S C_L, & N_s &= 1/2\rho V_T^2 S b C_n \end{aligned}$$

For equations 58 and 59 the term definitions are

\dot{V}_T	=	true airspeed rate (ft/sec ²)
$\dot{\beta}$	=	sideslip angle rate (rad/sec)
$\dot{\alpha}$	=	angle-of-attack rate (rad/sec)
$\dot{p}_s, \dot{q}_s, \dot{r}_s$	=	roll, pitch, and yaw accelerations about stability axis (rad/sec ²)
p_s, q_s, r_s	=	roll, pitch, and yaw rates about stability axis (rad/sec)
V_T	=	true airspeed (ft/sec)
β	=	sideslip angle (rad)
α	=	angle of attack (rad)
$\dot{\phi}, \dot{\theta}, \dot{\psi}$	=	roll, pitch, yaw attitude rate (rad/sec)
ϕ, θ, ψ	=	roll, pitch, yaw attitude (rad)
X_W, Y_W, Z_W	=	external forces along the wind axes (lbs)
X_s, Y_s, Z_s	=	aerodynamic forces along stability axes (lbs)
L_s, M_s, N_s	=	aerodynamic moments about stability axes (ft-lbs)
T	=	engine thrust (lbs)
W	=	aircraft weight (132,146 lbs for KC-135 aircraft)
M	=	aircraft mass (4104 slugs for KC-135 aircraft)
$I_1, I_2, I_3, I_4, I_5, I_6, I_7, I_8, I_9, I_{10}$	=	inertial constants defined in Section 3.4.1.2 of the roll, pitch, yaw and product moments of inertial of the aircraft

S	=	wing reference area (ft^2)
\bar{c}	=	mean aerodynamic chord (ft)
b	=	wing span (ft)
M	=	Mach number
ρ	=	air density (slugs/ ft^3)
$C_D, C_Y, C_L, C_\ell, C_m, C_n$	=	coefficients of aircraft aerodynamics as defined in Section 3.2.1

By substitution of the aerodynamic coefficients of Section 3.2.1 and the above definition equations and noting that the angle of attack with respect to the wing chord plane is related to the angle of attack of the x body axis by the equation $\alpha_{WCP} = \alpha + 2^\circ$, the final state model equations are,

$$\begin{bmatrix}
\dot{v}_T \\
\dot{\beta} \\
\dot{\alpha} \\
\dot{p}_s \\
\dot{q}_s \\
\dot{r}_s \\
\dot{\phi} \\
\dot{\theta} \\
\dot{\psi}
\end{bmatrix} = \begin{bmatrix}
\frac{-\rho s}{2m} \{ [C_{D_0} + C(C_{L_0} + 2^\circ \cdot C_{L_\alpha} - .15)] + [2K C_{L_\alpha} (C_{L_0} + 2^\circ \cdot C_{L_\alpha} - .15)] \alpha + [K \cdot C_{L_\alpha}^2] \alpha^2 \} v_T^2 \cos \beta \\
\frac{+\rho s}{2m} [C_{Y_\beta}] v_T^2 \beta \sin \beta + [\frac{T}{m}] \cos \alpha \cos \beta + g (-\cos \beta \cos \alpha \sin \theta + \cos \beta \sin \alpha \cos \theta \cos \phi + \sin \beta \cos \theta \sin \phi) \\
\frac{\rho s}{2m} \{ [C_{D_0} + K(C_{L_0} + 2^\circ \cdot C_{L_\alpha} - .15)^2] + [2K C_{L_\alpha} (C_{L_0} + 2^\circ \cdot C_{L_\alpha} - .15)] \alpha + [K C_{L_\alpha}^2] \alpha^2 \} v_T \sin \beta + \\
\frac{\rho s}{2m} [C_{Y_\beta}] v_T \beta \cos \beta - [\frac{T}{m}] \sin \beta \cos \alpha v_T^{-1} \\
+ g (\sin \beta \cos \alpha \sin \theta - \sin \beta \sin \alpha \cos \theta \cos \phi + \cos \beta \cos \theta \sin \phi) v_T^{-1} r_s \\
\frac{-\rho s}{2m} [(C_{L_0} + 2^\circ C_{L_\alpha}) + C_{L_\alpha} \alpha] v_T (\cos \beta)^{-1} - [\frac{T}{m}] v_T^{-1} \sin \alpha (\cos \beta)^{-1} \\
+ g (\sin \alpha \sin \theta + \cos \alpha \cos \theta \cos \phi) v_T^{-1} (\cos \beta)^{-1} + q_s - p_s \tan \beta \\
I_1 r_s q_s + I_2 p_s q_s + \frac{I_3 \rho S b}{2} \{ [(C_{L_{\beta_0}} + 2^\circ \cdot C_{L_{\beta_2}} - .3 C_{L_{\beta_1}}) + C_{L_{\beta_1}} (M + C_{L_{\beta_2}} \alpha)] \beta v_T^2 \\
+ \frac{b}{2} [C_{L_p} p_s + (C_{L_{r_0}} + 2^\circ \cdot C_{L_{r_1}} + C_{L_{r_1}} \alpha) r_s] v_T + C_{L_{\delta_a}} \delta_a v_T^2 \\
+ \frac{I_4 \rho S b}{2} [C_{n_\beta} \beta + C_{n_{\delta_R}} \delta_R] v_T^2 + (\frac{b}{2}) C_{n_r} r v_T \} \\
I_5 r_s p_s + I_6 (r_s^2 - p_s^2) + \frac{I_7 \rho S c}{2} \{ [(C_{m_0} + 2^\circ \cdot C_{m_\alpha}) + C_{m_\alpha} \alpha + C_{m_{\delta_e}} \delta_e] v_T^2 + \frac{c}{2} (C_{m_\alpha} + C_{m_q}) q v_T \} \\
I_8 p_s q_s + I_9 r_s q_s + \frac{I_4 \rho S b}{2} \{ [(C_{L_{\beta_0}} + 2^\circ \cdot C_{L_{\beta_2}} - .3 C_{L_{\beta_1}}) + (C_{L_{\beta_1}} M + C_{L_{\beta_2}} \alpha)] \beta v_T^2 \\
+ \frac{b}{2} [C_{L_p} p_s + (C_{L_{r_0}} + 2^\circ \cdot C_{L_{r_1}} + C_{L_{r_1}} \alpha) r_s] v_T + C_{L_{\delta_a}} \delta_a v_T^2 \} \\
+ \frac{I_{10} \rho S b}{2} \{ [C_{n_\beta} \beta + C_{n_{\delta_R}} \delta_R] v_T^2 + (\frac{b}{2}) C_{n_r} r v_T \} \\
p_s + q_s \sin \phi \tan \theta + r_s \cos \phi \tan \theta \\
q_s \cos \phi - r_s \sin \phi \\
q_s \sin \phi / \cos \theta + r_s \cos \phi / \cos \theta
\end{bmatrix} \quad (60)$$

To reduce the complexity of the required solution for the linear quadratic optimal controller, these six-degree-of-freedom equations were reduced to simple point mass equations of motion.

The vector equation describing the motion of the center of mass of an airplane with respect to an inertial frame is

$$\underline{F} = m \frac{d}{dt} \underline{V} \quad (61)$$

where

- \underline{F} = external force acting upon the airplane
- m = mass of airplane
- \underline{V} = velocity of the center of mass of the airplane with respect to an inertial frame

The inertial reference frame is fixed to the earth. The z axis is along the gravity vector. The x axis points true north and the y axis complete a right-handed orthogonal coordinate system. The total velocity vector (\underline{V}) of the aircraft with respect to ground is equal to the vector sum of the aircraft velocity with respect to air (\underline{V}_{AIR}) and the wind velocity (\underline{V}_W) the velocity of the air mass with respect to inertial coordinates. Rewriting equation 61

$$\underline{F} = m \left(\frac{d}{dt} \underline{V}_{AIR} + \frac{d}{dt} \underline{V}_W \right) \quad (62)$$

The equations of motion are written with respect to an Eulerian axis system. This coordinate system, called the wind axis system, is fixed to the center of mass of the airplane. The x axis is coincident with the total velocity of the airplane. The z axis lies in the aircraft plane of symmetry perpendicular to the x axis and positive downward. The y axis completes a right-handed orthogonal system. If ω is the rotational rate of the wind with respect to inertial coordinates, then by rules for differentiation of vector,

$$\underline{F} = m \left[\frac{d}{dt} \underline{V}_{AIR} + \omega \times \underline{V}_{AIR} + \underline{R}_{IW} \cdot \frac{d}{dt} \underline{V}_W \right] \quad (63)$$

and R_{IW} is the direction cosine matrix relating inertial to wind axis coordinates. The external forces acting on the airplane consist of gravity, aerodynamic forces and thrust. These forces resolved along the wind axis system are

$$\underline{F} = \begin{bmatrix} F_{x_w} \\ F_{y_w} \\ F_{z_w} \end{bmatrix} = \begin{bmatrix} -D + T \cos \alpha - mg \sin \gamma \\ T \sin \alpha \sin \phi + L \sin \phi \\ -T \sin \alpha \cos \phi + mg \cos \gamma - L \cos \phi \end{bmatrix} \quad (64)$$

The term definitions of equation 64 are

- D = drag
- g = acceleration of gravity constant
- T = thrust
- α = angle between thrust vector and velocity vector
- γ = flight path angle
- ϕ = bank angle
- L = lift
- ψ = heading angle

The wind axis angular velocity vector

$$\underline{\omega} = \begin{bmatrix} \omega_{x_w} \\ \omega_{y_w} \\ \omega_{z_w} \end{bmatrix} = \begin{bmatrix} -\dot{\psi} \sin \gamma \\ \dot{\gamma} \\ \dot{\psi} \cos \gamma \end{bmatrix} \quad (65)$$

The wind axis velocity components of the airspeed vector

$$\underline{v}_{AIK} = [v \ 0 \ 0]^T \quad (66)$$

Considering only the horizontal component of wind in the ground frame

$$\underline{V}_W = [V_W \cos \psi_W \quad V_W \sin \psi_W \quad 0]^T \quad (67)$$

where V_W is the magnitude of the horizontal wind and ψ_W is the wind direction in inertial coordinates. The direction cosine matrix

$$R_{IW} = \begin{bmatrix} \cos \gamma \cos \psi & \cos \gamma \sin \psi & -\sin \gamma \\ \cos \psi \sin \gamma \sin \phi & \cos \psi \cos \phi & \cos \gamma \sin \phi \\ -\sin \psi \cos \phi & +\sin \psi \sin \gamma \sin \phi & \\ \cos \psi \sin \gamma \cos \phi & \sin \psi \sin \gamma \cos \phi & \cos \gamma \cos \phi \\ +\sin \psi \sin \phi & -\cos \psi \sin \phi & \end{bmatrix} \quad (68)$$

is used to transform the time derivative of wind vector $\frac{d}{dt} \underline{V}_W$ from the inertial reference frame to the wind axis frame. Substituting equations 64 through 68 into equation 63,

$$\begin{bmatrix} \dot{v} \\ \dot{\psi} \\ \dot{\gamma} \end{bmatrix} = \begin{bmatrix} \frac{1}{m}(-D+T\cos\alpha)-g\sin\gamma-\cos\gamma\cos(\psi-\psi_W)\dot{V}_W-V_W\cos\gamma\sin(\psi-\psi_W)\dot{\psi}_W \\ -\frac{1}{V\cos\gamma}\{(T\sin\alpha+L)(\frac{\sin\phi}{m})-[s\sin\gamma\sin\phi\cos(\psi-\psi_W)-\cos\phi\sin(\psi-\psi_W)]\dot{V}_W \\ -V_W[s\sin\gamma\sin\phi\sin(\psi-\psi_W)+\cos\phi\cos(\psi-\psi_W)]\dot{\psi}_W \\ (\frac{1}{mV})(T\sin\alpha+L)\cos\phi-(\frac{g}{V})\cos\gamma+(\frac{1}{V})\{[s\sin\gamma\cos\phi\cos(\psi-\psi_W)+\sin\phi\sin(\psi-\psi_W)]\dot{V}_W \\ +V[s\sin\gamma\cos\phi\sin(\psi-\psi_W)-\sin\phi\cos(\psi-\psi_W)]\dot{\psi}_W \end{bmatrix} \quad (69.1)$$

Lift is modeled by the relation

$$L = \frac{1}{2}\rho(h)V^2SC_L \quad (70)$$

and drag by the equation

$$D = \frac{1}{2}\rho(h)V^2SC_D \quad (71)$$

The dimensionless aerodynamic coefficients C_L and C_D were derived in Section 3.2.1 as

$$C_L = C_{L_0} + C_{L_\alpha} \alpha_{WCP} \quad (72)$$

$$C_D = C_{D_0} + K[(C_{L_0} - .15)^2 + 2C_{L_\alpha}(C_{L_0} - .15)\alpha_{WCP} + C_{L_\alpha}^2 \alpha_{WCP}^2] \quad (73)$$

where

$$\alpha_{WCP} = \alpha + 2^\circ$$

The air density $\rho(h)$ is approximated by the quadratic

$$\rho(h) = \rho_0 [1. - 1.835(\frac{h}{65536}) + (\frac{h}{65536})^2] \quad (74)$$

where ρ_0 is the air density at sea level.

The aircraft position relative to earth is obtained by resolving the aircraft velocity vector along the inertial reference frame axis.

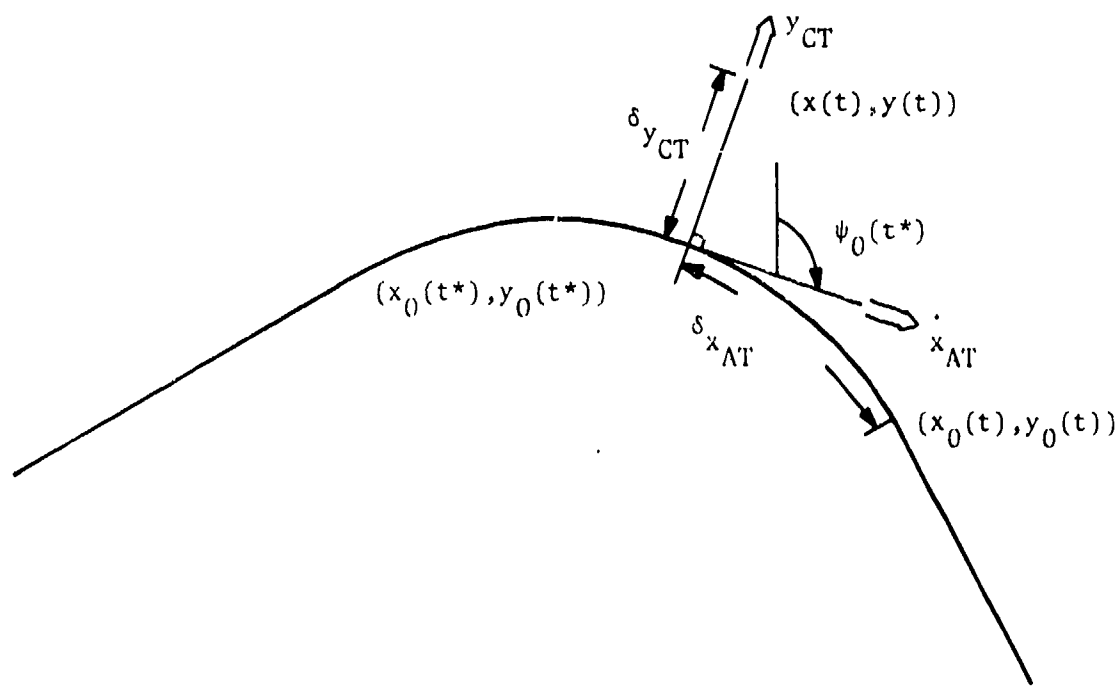
$$\begin{bmatrix} \dot{x} \\ \dot{y} \\ \dot{h} \end{bmatrix} = \begin{bmatrix} V \cos \gamma \cos \psi + V_w \cos \psi_w \\ V \cos \gamma \sin \psi + V_w \sin \psi_w \\ V \sin \gamma \end{bmatrix} \quad (75)$$

To steer the aircraft in the horizontal plane, it is desirable to have along-track and cross-track distances available as state variables. Referring to Figure 2, a coordinate frame is defined with its origin at a reference position on the nominal horizontal trajectory such that the distance between the reference and aircraft position is minimized. Defining the reference position in this manner ensures that the control corrections will always be steering the aircraft in order to maintain the smallest spatial errors possible. Along-track and cross-track rates are obtained from x and y using the relation

$$\begin{bmatrix} \dot{x}_{AT} \\ \dot{y}_{CT} \end{bmatrix} = \begin{bmatrix} \cos \psi_0 & \sin \psi_0 \\ -\sin \psi_0 & \cos \psi_0 \end{bmatrix} \begin{bmatrix} \dot{x} \\ \dot{y} \end{bmatrix} \quad (76)$$

Modifying equation 74

$$\begin{bmatrix} \dot{x}_{AT} \\ \dot{y}_{CT} \\ \dot{h} \end{bmatrix} = \begin{bmatrix} v \cos \gamma \cos(\psi - \psi_0) + v_w \cos(\psi_w - \psi_0) \\ v \cos \gamma \sin(\psi - \psi_0) + v_w \sin(\psi_w - \psi_0) \\ v \sin \gamma \end{bmatrix} \quad (77)$$



MOVING TARGET COORDINATE SYSTEM
FIGURE 2

The horizontal wind magnitude (v_w) and wind direction (ψ_w) will be modeled as deterministic disturbances. The disturbance dynamics are in the form of

$$\dot{\underline{z}}(t) = \underline{F}\underline{z}(t) \quad (78)$$

where

$$\underline{z}(t) = \begin{bmatrix} v_w \\ \psi_w \end{bmatrix}, \quad \underline{F} = \begin{bmatrix} -\omega_w & 0 \\ 0 & -\omega_\psi \end{bmatrix}$$

ω_w and ω_ψ are the break frequencies for first order disturbances v_w and ψ_w . The combined dynamic model is obtained by appending the two additional disturbance states to the aircraft states. Combining equations 69, 70, 71, 72, 73, 77, and 78.

$$\begin{bmatrix} \dot{v} \\ \dot{\psi} \\ \dot{\gamma} \\ \dot{x}_{AT} \\ \dot{y}_{CT} \\ \dot{h} \\ \dot{v}_w \\ \dot{\psi}_w \end{bmatrix} = \begin{bmatrix} -\left(\frac{1}{2m}\rho(h)V^2S[C_{D_0} + K((C_{L_0} - .15)^2 + 2C_{L_\alpha}(C_{L_0} - .15)(\alpha + 2^\circ) + C_{L_\alpha}^2(\alpha + 2^\circ)^2)]\right) \\ +\left(\frac{T}{m}\right)\cos\alpha - g\sin\gamma + \cos\gamma\cos(\psi_o - \psi_w)\omega_w v_w + v_w \cos\gamma\sin(\psi_o - \psi_w)\omega_\psi \psi_w \\ \left(\frac{1}{V\cos\gamma}\right)\{(T\sin\alpha + \frac{1}{2}\rho(h)V^2S[C_{L_0} + C_{L_\alpha}(\alpha + 2^\circ)])\left(\frac{\sin\phi}{m}\right) \\ + [\sin\gamma\sin\phi\cos(\psi - \psi_w) - \cos\phi\sin(\psi - \psi_w)]\omega_v v_w \\ + v_w [\sin\gamma\sin\phi\sin(\psi - \psi_w) + \cos\phi\cos(\psi - \psi_w)]\omega_\psi \psi_w \} \\ \left(\frac{1}{mV}\right)(T\sin\alpha + \frac{1}{2}\rho(h)V^2S[C_{L_0} + C_{L_\alpha}(\alpha + 2^\circ)])\cos\phi - \frac{g}{V}\cos\gamma \\ + \left(\frac{1}{V}\right)\{-[\sin\gamma\cos\phi\cos(\psi - \psi_w) + \sin\phi\sin(\psi - \psi_w)]\omega_v v_w \\ - v_w [\sin\gamma\cos\phi\sin(\psi - \psi_w) - \sin\phi\cos(\psi - \psi_w)]\omega_\psi \psi_w \} \\ V\cos\gamma\cos(\psi - \psi_o) + v_w \cos(\psi_w - \psi_o) \\ V\cos\gamma\sin(\psi - \psi_o) + v_w \sin(\psi_w - \psi_o) \\ V\sin\gamma \\ -\omega_v v_w \\ -\omega_\psi \psi_w \end{bmatrix} \quad (79)$$

The degree of simplification obtained by using point mass equations of motion can be readily seen by comparing the above equations to the full six-degree-of-freedom equation 60.

3.2.3 Dynamic Linearization of State Model Equations

The general form of the aircraft state equations, with input disturbances as developed in Section 3.2.2, may be written

$$\dot{\underline{x}}(t) = \underline{f}(\underline{x}(t), \underline{U}(t)) \quad (80)$$

where

$$\underline{x}(t) = \begin{bmatrix} v \\ \psi \\ \gamma \\ \dot{\gamma} \\ x_{AT} \\ y_{CT} \\ h \\ v_w \\ \psi_w \end{bmatrix}$$

the state vector, and a control vector.

$$\underline{U}(t) = \begin{bmatrix} \alpha \\ \phi \\ T \end{bmatrix}$$

To apply Linear Quadratic Optimal Control Theory, equation 79 must be linearized.

Define

$$\underline{x} = \underline{x}_0 + \delta \underline{x} \quad (81)$$

$$\underline{U} = \underline{U}_0 + \delta \underline{U} \quad (82)$$

where \underline{x} consists of a nominal state vector (\underline{x}_0) and a state perturbation vector ($\delta \underline{x}$) and \underline{U} consists of a nominal control vector (\underline{U}_0) and a control correction vector ($\delta \underline{U}$).

Expanding in a Taylor Series about the nominal

$$\dot{\underline{x}}_0 + \delta \dot{\underline{x}} = \underline{f}(\underline{x}_0, \underline{U}_0) + \left. \frac{\partial \underline{f}}{\partial \underline{x}} \right|_{\substack{\underline{x}=\underline{x}_0 \\ \underline{U}=\underline{U}_0}} \cdot \delta \underline{x} + \left. \frac{\partial \underline{f}}{\partial \underline{U}} \right|_{\substack{\underline{x}=\underline{x}_0 \\ \underline{U}=\underline{U}_0}} \cdot \delta \underline{U} + \text{higher order terms} \quad (83)$$

Since

$$\dot{\underline{x}}_0 = \underline{f}(\underline{x}_0, \underline{U}_0)$$

and neglecting higher order terms

$$\dot{\delta \underline{x}} = \left. \frac{\partial \underline{f}}{\partial \underline{x}} \right|_{\substack{\underline{x}=\underline{x}_0 \\ \underline{U}=\underline{U}_0}} \cdot \delta \underline{x} + \left. \frac{\partial \underline{f}}{\partial \underline{U}} \right|_{\substack{\underline{x}=\underline{x}_0 \\ \underline{U}=\underline{U}_0}} \cdot \delta \underline{U} \quad (84)$$

Defining

$$\underline{A} = \left. \frac{\partial \underline{f}}{\partial \underline{x}} \right|_0 = \left. \frac{\partial \underline{f}}{\partial \underline{x}} \right|_{\substack{\underline{x}=\underline{x}_0 \\ \underline{U}=\underline{U}_0}} \quad \text{and} \quad \underline{B} = \left. \frac{\partial \underline{f}}{\partial \underline{U}} \right|_0 = \left. \frac{\partial \underline{f}}{\partial \underline{U}} \right|_{\substack{\underline{x}=\underline{x}_0 \\ \underline{U}=\underline{U}_0}}$$

we have

$$\dot{\delta \underline{x}} = \underline{A} \delta \underline{x} + \underline{B} \delta \underline{U} \quad (85)$$

where, in the general form

$$\underline{A} = \begin{bmatrix}
 \frac{\partial \dot{v}}{\partial v} \Big|_0 & \frac{\partial \dot{v}}{\partial \psi} \Big|_0 & \frac{\partial \dot{v}}{\partial \gamma} \Big|_0 & \frac{\partial \dot{v}}{\partial x_{AT}} \Big|_0 & \frac{\partial \dot{v}}{\partial y_{CT}} \Big|_0 & \frac{\partial \dot{v}}{\partial h} \Big|_0 & \frac{\partial \dot{v}}{\partial v_w} \Big|_0 & \frac{\partial \dot{v}}{\partial \psi_w} \Big|_0 \\
 \frac{\partial \dot{\psi}}{\partial v} \Big|_0 & \frac{\partial \dot{\psi}}{\partial \psi} \Big|_0 & \frac{\partial \dot{\psi}}{\partial \gamma} \Big|_0 & \frac{\partial \dot{\psi}}{\partial x_{AT}} \Big|_0 & \frac{\partial \dot{\psi}}{\partial y_{CT}} \Big|_0 & \frac{\partial \dot{\psi}}{\partial h} \Big|_0 & \frac{\partial \dot{\psi}}{\partial v_w} \Big|_0 & \frac{\partial \dot{\psi}}{\partial \psi_w} \Big|_0 \\
 \frac{\partial \dot{\gamma}}{\partial v} \Big|_0 & \frac{\partial \dot{\gamma}}{\partial \psi} \Big|_0 & \frac{\partial \dot{\gamma}}{\partial \gamma} \Big|_0 & \frac{\partial \dot{\gamma}}{\partial x_{AT}} \Big|_0 & \frac{\partial \dot{\gamma}}{\partial y_{CT}} \Big|_0 & \frac{\partial \dot{\gamma}}{\partial h} \Big|_0 & \frac{\partial \dot{\gamma}}{\partial v_w} \Big|_0 & \frac{\partial \dot{\gamma}}{\partial \psi_w} \Big|_0 \\
 \frac{\partial \dot{x}_{AT}}{\partial v} \Big|_0 & \frac{\partial \dot{x}_{AT}}{\partial x} \Big|_0 & \frac{\partial \dot{x}_{AT}}{\partial \gamma} \Big|_0 & \frac{\partial \dot{x}_{AT}}{\partial x_{AT}} \Big|_0 & \frac{\partial \dot{x}_{AT}}{\partial y_{CT}} \Big|_0 & \frac{\partial \dot{x}_{AT}}{\partial h} \Big|_0 & \frac{\partial \dot{x}_{AT}}{\partial v_w} \Big|_0 & \frac{\partial \dot{x}_{AT}}{\partial \psi_w} \Big|_0 \\
 \frac{\partial \dot{y}_{CT}}{\partial v} \Big|_0 & \frac{\partial \dot{y}_{CT}}{\partial x} \Big|_0 & \frac{\partial \dot{y}_{CT}}{\partial \gamma} \Big|_0 & \frac{\partial \dot{y}_{CT}}{\partial x_{AT}} \Big|_0 & \frac{\partial \dot{y}_{CT}}{\partial y_{CT}} \Big|_0 & \frac{\partial \dot{y}_{CT}}{\partial h} \Big|_0 & \frac{\partial \dot{y}_{CT}}{\partial v_w} \Big|_0 & \frac{\partial \dot{y}_{CT}}{\partial \psi_w} \Big|_0 \\
 \frac{\partial \dot{h}}{\partial v} \Big|_0 & \frac{\partial \dot{h}}{\partial \psi} \Big|_0 & \frac{\partial \dot{h}}{\partial \gamma} \Big|_0 & \frac{\partial \dot{h}}{\partial x_{AT}} \Big|_0 & \frac{\partial \dot{h}}{\partial y_{CT}} \Big|_0 & \frac{\partial \dot{h}}{\partial h} \Big|_0 & \frac{\partial \dot{h}}{\partial v_w} \Big|_0 & \frac{\partial \dot{h}}{\partial \psi_w} \Big|_0 \\
 \frac{\partial \dot{v}_w}{\partial v} \Big|_0 & \frac{\partial \dot{v}_w}{\partial \psi} \Big|_0 & \frac{\partial \dot{v}_w}{\partial \gamma} \Big|_0 & \frac{\partial \dot{v}_w}{\partial x_{AT}} \Big|_0 & \frac{\partial \dot{v}_w}{\partial y_{CT}} \Big|_0 & \frac{\partial \dot{v}_w}{\partial h} \Big|_0 & \frac{\partial \dot{v}_w}{\partial v_w} \Big|_0 & \frac{\partial \dot{v}_w}{\partial \psi_w} \Big|_0 \\
 \frac{\partial \dot{\psi}_w}{\partial v} \Big|_0 & \frac{\partial \dot{\psi}_w}{\partial \psi} \Big|_0 & \frac{\partial \dot{\psi}_w}{\partial \gamma} \Big|_0 & \frac{\partial \dot{\psi}_w}{\partial x_{AT}} \Big|_0 & \frac{\partial \dot{\psi}_w}{\partial y_{CT}} \Big|_0 & \frac{\partial \dot{\psi}_w}{\partial h} \Big|_0 & \frac{\partial \dot{\psi}_w}{\partial v_w} \Big|_0 & \frac{\partial \dot{\psi}_w}{\partial \psi_w} \Big|_0
 \end{bmatrix} \quad (86)$$

and

$$\underline{B} = \begin{bmatrix} \frac{\partial \dot{v}}{\partial \alpha} \Big|_0 & \frac{\partial \dot{v}}{\partial \phi} \Big|_0 & \frac{\partial \dot{v}}{\partial T} \Big|_0 \\ \frac{\partial \dot{\psi}}{\partial \alpha} \Big|_0 & \frac{\partial \dot{\psi}}{\partial \phi} \Big|_0 & \frac{\partial \dot{\psi}}{\partial T} \Big|_0 \\ \frac{\partial \dot{y}}{\partial \alpha} \Big|_0 & \frac{\partial \dot{y}}{\partial \phi} \Big|_0 & \frac{\partial \dot{y}}{\partial T} \Big|_0 \\ \frac{\partial \dot{x}_{AT}}{\partial \alpha} \Big|_0 & \frac{\partial \dot{x}_{AT}}{\partial \phi} \Big|_0 & \frac{\partial \dot{x}_{AT}}{\partial T} \Big|_0 \\ \frac{\partial \dot{y}_{CT}}{\partial \alpha} \Big|_0 & \frac{\partial \dot{y}_{CT}}{\partial \phi} \Big|_0 & \frac{\partial \dot{y}_{CT}}{\partial T} \Big|_0 \\ \frac{\partial \dot{h}}{\partial \alpha} \Big|_0 & \frac{\partial \dot{h}}{\partial \phi} \Big|_0 & \frac{\partial \dot{h}}{\partial T} \Big|_0 \\ \frac{\partial \dot{v}_W}{\partial \alpha} \Big|_0 & \frac{\partial \dot{v}_W}{\partial \phi} \Big|_0 & \frac{\partial \dot{v}_W}{\partial T} \Big|_0 \\ \frac{\partial \dot{\psi}_W}{\partial \alpha} \Big|_0 & \frac{\partial \dot{\psi}_W}{\partial \phi} \Big|_0 & \frac{\partial \dot{\psi}_W}{\partial T} \Big|_0 \end{bmatrix} \quad (87)$$

The partial derivatives that comprise the non-zero elements of the matrices \underline{A} and \underline{B} are obtained by performing the indicated operation on equation 79 and evaluating at $x=x_0$, $u=u_0$. Then,

$$a_{11} = \frac{\partial \dot{v}}{\partial v} \Big|_0 = -\left(\frac{1}{m}\right)\rho(h_0)v_0 s c_D \Big|_0$$

$$a_{13} = \left. \frac{\partial \dot{v}}{\partial \gamma} \right|_0 = -g \cos \gamma_0$$

$$a_{16} = \left. \frac{\partial \dot{v}}{\partial h} \right|_0 = -\left(\frac{\rho_0}{2m} \right) (v_0^2 \text{SC}_{D_0}) \left(\frac{-1.835}{65536.} + \frac{2h_0}{(65536.)^2} \right)$$

$$a_{17} = \left. \frac{\partial \dot{v}}{\partial v_w} \right|_0 = \omega_w \cos \gamma_0 \cos(\psi_0 - \psi_{w_0})$$

$$a_{18} = \left. \frac{\partial \dot{v}}{\partial \psi_w} \right|_0 = \omega_w v_{w_0} \cos \gamma_0 \sin(\psi_0 - \psi_w)$$

$$a_{21} = \left. \frac{\partial \dot{\psi}}{\partial v} \right|_0 = \left(\frac{\sin \phi_0}{m \cos \gamma_0} \right) \left[\frac{1}{2} \rho(h_0) \text{SC}_L \right]_0 - \left(\frac{T_0}{V_0^2} \right) \sin \alpha_0$$

$$a_{23} = \left. \frac{\partial \dot{\psi}}{\partial \gamma} \right|_0 = - \left(\frac{\sin \phi_0}{m V_0 \sqrt{1 - \gamma_0^2}} \right) (T_0 \sin \alpha_0 + \frac{1}{2} \rho(h_0) v_0^2 \text{SC}_L)_0$$

$$a_{26} = \left. \frac{\partial \dot{\psi}}{\partial h} \right|_0 = \left(\frac{\rho_0 \sin \phi_0}{2m \cos \gamma_0} \right) (v_0 \text{SC}_L)_0 \left(\frac{-1.835}{65536.} + \frac{2h_0}{(65536.)^2} \right)$$

$$a_{27} = \left. \frac{\partial \dot{\psi}}{\partial v_w} \right|_0 = \frac{\omega_v}{V_0 \cos j_0} \left[\sin \gamma_0 \sin \phi_0 \cos(\psi_0 - \psi_{w_0}) - \cos \phi_0 \sin(\psi_0 - \psi_{w_0}) \right]$$

$$a_{28} = \left. \frac{\partial \dot{\psi}}{\partial \psi_w} \right|_0 = \frac{\omega_w v_{w_0}}{V_0 \cos j_0} \left[\sin \gamma_0 \sin \phi_0 \sin(\psi_0 - \psi_{w_0}) + \cos \phi_0 \cos(\psi_0 - \psi_{w_0}) \right]$$

$$a_{31} = \left. \frac{\partial \dot{\gamma}}{\partial v} \right|_0 = -\left(\frac{1}{V_0^2} \right) \left[\left(\frac{T_0}{m} \right) \sin \alpha_0 \cos \phi_0 - g \cos \gamma_0 \right] + \left(\frac{\cos \phi_0}{2m} \right) \rho(h_0) \text{SC}_L)_0$$

$$a_{33} = \left. \frac{\partial \dot{\gamma}}{\partial \gamma} \right|_0 = \left(\frac{g}{V_0^2} \right) \sin \gamma_0$$

$$a_{36} = \frac{\partial \dot{\gamma}}{\partial h} \Big|_0 = \left(\frac{\rho_0 \cos \phi_0}{2m} \right) (v_0 \sin \psi_L \Big|_0) \left(\frac{-1.835}{65536.} + \frac{2h_0}{(65536.)^2} \right)$$

$$a_{37} = \frac{\partial \dot{\gamma}}{\partial v_w} \Big|_0 = - \left(\frac{1}{v_0} \right) [\sin \gamma_0 \cos \phi_0 \cos(\psi_0 - \psi_w) + \sin \phi_0 \sin(\psi_0 - \psi_w) \omega_v]$$

$$a_{38} = \frac{\partial \dot{\gamma}}{\partial \psi_w} \Big|_0 = - \left(\frac{1}{v_0} \right) \omega_v v_w [\sin \gamma_0 \cos \phi_0 \sin(\psi_0 - \psi_w) - \sin \phi_0 \cos(\psi_0 - \psi_w)]$$

$$a_{41} = \frac{\partial \dot{x}_{AT}}{\partial v} \Big|_0 = \cos \gamma_0$$

$$a_{43} = \frac{\partial \dot{x}_{AT}}{\partial \gamma} \Big|_0 = -v_0 \sin \gamma_0$$

$$a_{47} = \frac{\partial \dot{x}_{AT}}{\partial v_w} \Big|_0 = \cos(\psi_w - \psi_0)$$

$$a_{48} = \frac{\partial \dot{x}_{AT}}{\partial \psi_w} \Big|_0 = -v_w \sin(\psi_w - \psi_0)$$

$$a_{52} = \frac{\delta \dot{y}_{CT}}{\partial \psi} \Big|_0 = +v_0 \cos \gamma_0$$

$$a_{57} = \frac{\delta \dot{y}_{CT}}{\partial v_w} \Big|_0 = \sin(\psi_w - \psi_0)$$

$$a_{58} = \frac{\delta \dot{y}_{CT}}{\partial \psi_w} \Big|_0 = v_w \cos(\psi_w - \psi_0)$$

$$\begin{aligned}
a_{61} &= \frac{\partial \dot{h}}{\partial v} \Big|_0 = \sin \gamma_0 \\
a_{63} &= \frac{\partial \dot{h}}{\partial \gamma} \Big|_0 = +v_0 \cos \gamma_0 \\
a_{77} &= \frac{\partial \dot{v}_w}{\partial v_w} \Big|_0 = -\omega_v \\
a_{88} &= \frac{\partial \dot{\psi}_w}{\partial \psi_w} \Big|_0 = -\omega_\psi \\
b_{11} &= \frac{\partial \dot{v}}{\partial \alpha} \Big|_0 = -\left(\frac{1}{2m}\right)\rho(h_0)v_0^2 S[2(57.3)C_{L\alpha}(C_{L0} - .15) + 2(57.3)C_{L\alpha}^2(\alpha + 2^\circ)] - \left(\frac{T_0}{m}\right) \sin \alpha_0 \\
b_{13} &= \frac{\partial \dot{v}}{\partial T} \Big|_0 = \frac{\cos \alpha_0}{m} \\
b_{21} &= \frac{\partial \dot{\psi}}{\partial \alpha} \Big|_0 = \left(\frac{\sin \phi_0}{m v_0 \cos \gamma_0}\right) [T_0 \cos \alpha_0 + \frac{1}{2}\rho(h_0)v_0^2 S(57.3)C_{L\alpha}] \\
b_{22} &= \frac{\partial \dot{\psi}}{\partial \phi} \Big|_0 = \left(\frac{\cos \phi_0}{m v_0 \cos \gamma_0}\right) [T_0 \sin \alpha_0 + \frac{1}{2}\rho(h_0)v_0^2 S C_L] \\
b_{23} &= \frac{\partial \dot{\psi}}{\partial T} \Big|_0 = \left(\frac{\sin \alpha_0 \sin \phi_0}{m v_0 \cos \gamma_0}\right) \\
b_{31} &= \frac{\partial \dot{\gamma}}{\partial \alpha} \Big|_0 = \left(\frac{\cos \phi_0}{m v_0}\right) [T_0 \cos \alpha_0 + \frac{1}{2}\rho(h_0)v_0^2 S(57.3)C_{L\alpha}] \\
b_{32} &= \frac{\partial \dot{\gamma}}{\partial \phi} \Big|_0 = -\left(\frac{\sin \phi_0}{m v_0}\right) [T_0 \sin \alpha_0 + \frac{1}{2}\rho(h_0)v_0^2 S C_L]
\end{aligned}$$

$$b_{33} = \left. \frac{\partial \dot{y}}{\partial T} \right|_0 = \left(\frac{1}{mV_0} \right) \sin \alpha_0 \cos \phi_0$$

Nominal horizontal wind magnitude and direction gradients were assumed to be equal to zero.

3.2.4 Design of Linear Quadratic Regulator

The state model developed in this previous section may be written in the form,

$$\frac{d}{dt} \begin{bmatrix} \underline{x}(t) \\ \underline{z}(t) \end{bmatrix} = \begin{bmatrix} \underline{A}(t) & \underline{B}(t) \\ 0 & \underline{F}(t) \end{bmatrix} \begin{bmatrix} \underline{x}(t) \\ \underline{z}(t) \end{bmatrix} + \begin{bmatrix} \underline{B}(t) \\ 0 \end{bmatrix} \underline{u}(t) \quad (88)$$

where

$$\underline{x}(t) = [\delta V \quad \delta \psi \quad \delta \gamma \quad \delta x_{AT} \quad \delta y_{CT} \quad \delta h]^T$$

δV = velocity error (ft/sec)

$\delta \psi$ = heading error (rad)

$\delta \gamma$ = flight path angle error (rad)

δx_{AT} = along-track distance error (ft)

δy_{CT} = cross-track distance error (ft)

δh = altitude error (ft)

$$\underline{z}(t) = [\delta V_W \quad \delta \psi_W]^T$$

δV_W = difference between measured and nominal wind velocity (ft/sec)

$\delta \psi_W$ = difference between measured and nominal wind direction (rad)

$$\underline{u}(t) = [\delta \alpha \quad \delta \phi \quad \delta T]^T$$

$\delta\alpha$ = difference between measured and nominal angle-of-attack (rad)
 $\delta\phi$ = difference between measured and nominal bank angle (rad)
 δT = difference between measured nominal thrust (lbs)
 $\underline{A}(t)$ = 6x6 plant system matrix
 $\underline{H}(t)$ = 6x2 disturbance input matrix
 $\underline{F}(t)$ = 2x2 disturbance system matrix
 $\underline{B}(t)$ = 6x3 plant input matrix

The form of these matrices is

$$\underline{A} = \begin{bmatrix} a_{11} & 0 & a_{13} & 0 & 0 & a_{16} \\ a_{21} & 0 & a_{23} & 0 & 0 & a_{26} \\ a_{31} & 0 & a_{33} & 0 & 0 & a_{36} \\ a_{41} & 0 & a_{43} & 0 & 0 & 0 \\ 0 & a_{52} & 0 & 0 & 0 & 0 \\ a_{61} & 0 & a & 0 & 0 & 0 \end{bmatrix} \quad \underline{B} = \begin{bmatrix} b_{11} & 0 & b_{13} \\ b_{21} & b_{22} & b_{23} \\ b_{31} & b_{32} & b_{33} \\ 0 & 0 & 0 \\ 0 & 0 & 0 \\ 0 & 0 & 0 \end{bmatrix}$$

$$\underline{H} = \begin{bmatrix} a_{17} & a_{18} \\ a_{27} & a_{28} \\ a_{37} & a_{38} \\ a_{47} & a_{48} \\ a_{57} & a_{58} \\ 0 & 0 \end{bmatrix} \quad \text{and } \underline{F} = \begin{bmatrix} a_{77} & 0 \\ 0 & a_{99} \end{bmatrix}$$

and the explicit form of the non-zero elements are the partial derivatives of the state equations, evaluated at x_0, U_0 , as shown in the previous section.

The quadratic cost functional to be minimized is

$$J(t) = \int_0^{\infty} \{ [\underline{x}(t)^T \underline{z}(t)^T] \begin{bmatrix} \underline{Q}(t) & \underline{0} \\ \underline{0} & \underline{0} \end{bmatrix} \begin{bmatrix} \underline{x}(t) \\ \underline{z}(t) \end{bmatrix} + \underline{u}^T(t) \underline{R}(t) \underline{u}(t) \} dt \quad (89)$$

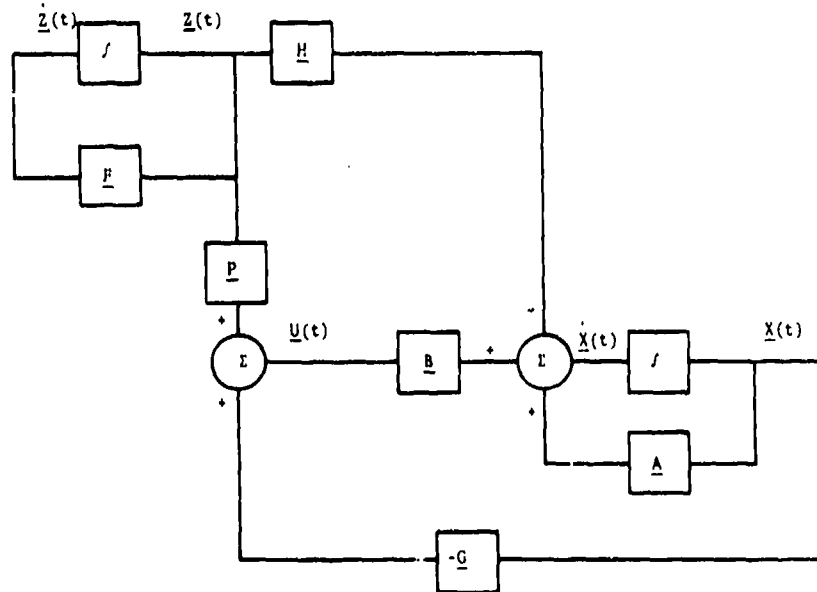
Note that, since the control correction vector cannot influence disturbances $\underline{z}(t)$, these disturbances are not included in the cost function.

This steady-state linear quadratic problem has a solution provided (1) $[\underline{A}, \underline{B}]$ is controllable, and (2) \underline{F} is strictly stable (eigenvalues in left half plane).

The optimal control law consists of plant state feedbacks and disturbance state feedbacks, i.e.,

$$\underline{u}(t) = -\underline{G}\underline{x}(t) - \underline{P}\underline{z}(t) \quad (90)$$

This is shown in block diagram form in Figure 3.



LINEAR QUADRATIC CONTROLLER BLOCK DIAGRAM
FIGURE 3

In this diagram,

G is a 3x6 constant plant state gain matrix and is given by

$$\underline{G} = \underline{R}^{-1} \underline{B}^T \underline{K} \quad (91)$$

where K is 6x6 and is the solution to the algebraic Riccati equation

$$\underline{0} = -\underline{K}\underline{A} - \underline{A}^T \underline{K} - \underline{Q} + \underline{K}\underline{B}\underline{R}^{-1} \underline{B}^T \underline{K} \quad (92)$$

Observe that the gain matrix G is independent of the disturbance dynamics.

P is a 3x2 constant disturbance state gain matrix and is given by

$$\underline{P} = \underline{R}^{-1} \underline{B}^T \underline{M} \quad (93)$$

where M is 6x2 and is the solution to

$$\underline{0} = -\underline{K}\underline{H} - \underline{A}^T \underline{M} - \underline{M}\underline{F} + \underline{K}\underline{B}\underline{R}^{-1} \underline{B}^T \underline{M} \quad (94)$$

The solution of these equations is dependent on the values of Q(t) and R(5). Assume that

$$\begin{aligned} \underline{Q}(t) &= \text{diag}[\underline{Q}_{11}(t) \ \underline{Q}_{22}(t) \ \underline{Q}_{33}(t) \ \underline{Q}_{44}(t) \ \underline{Q}_{55}(t) \ \underline{Q}_{66}(t)] \\ \underline{R}(t) &= \text{diag}[\underline{R}_{11}(t) \ \underline{R}_{22}(t) \ \underline{R}_{33}(t)] \end{aligned} \quad (95)$$

The weighting matrices were chosen to be diagonal since this allows the states and controls to be penalized individually.

Selection of the weighting matrices Q and R was accomplished in four steps.

- Step 1: Obtain a good first guess of the weighting matrices Q and R for a specific flight condition.
- Step 2: Assuming the same flight condition as in step 1, individually vary the components of the weighting matrices to determine the effect on the resulting closed loop system eigenvalues.
- Step 3: Using the weighting matrices selected in step 1, study the locus of the closed loop system eigenvalues as a function of flight condition.

Step 4: Use the results of steps 2 and 3 to schedule the weighting matrices \underline{Q} and \underline{R} such that critically damped eigenvalues are obtained for varying flight conditions.

3.2.4.1 LQ Design - Step 1

A common method of initially selecting the \underline{Q} and \underline{R} matrices is to assign maximum values to the plant states and maximum allowable controls corresponding to those values. This information is communicated to the mathematics by restructuring the cost functional in the form

$$J = \int_0^{\infty} \left[\left(\frac{\delta V}{\delta V_{\max}} \right)^2 + \left(\frac{\delta \psi}{\delta \psi_{\max}} \right)^2 + \left(\frac{\delta y}{\delta y_{\max}} \right)^2 + \left(\frac{\delta x_{AT}}{\delta x_{AT_{\max}}} \right)^2 + \left(\frac{\delta y_{CT}}{\delta y_{CT_{\max}}} \right)^2 + \left(\frac{\delta h}{\delta h_{\max}} \right)^2 + \left(\frac{\delta \phi}{\delta \phi_{\max}} \right)^2 + \left(\frac{\delta T}{\delta T_{\max}} \right)^2 \right] dt \quad (96)$$

where

$$\begin{aligned} \underline{Q} &= \text{diag} \left[\left(\frac{1}{\delta V_{\max}} \right) \left(\frac{1}{\delta \psi_{\max}} \right) \left(\frac{1}{\delta y_{\max}} \right) \left(\frac{1}{\delta x_{AT_{\max}}} \right) \left(\frac{1}{\delta y_{CT_{\max}}} \right) \left(\frac{1}{\delta h_{\max}} \right) \right] \\ \underline{R} &= \text{diag} \left[\left(\frac{1}{\delta \alpha_{\max}} \right) \left(\frac{1}{\delta \phi_{\max}} \right) \left(\frac{1}{\delta T_{\max}} \right) \right] \end{aligned} \quad (97)$$

The maximum values assigned to the state and control perturbations are shown in Table I for a wings level aircraft flight condition having a low dynamic pressure q corresponding to an altitude of 5000 feet and a velocity of 274.8 feet per second.

The structure of the optimal feedback control corresponding to the solution of several different steady-state linear quadratic problem formulations is given in Table II. For wings level and no wind disturbances the lateral control $\delta\phi(t)$ is independent of the vertical ($\delta y(t)$, $\delta h(t)$) and longitudinal ($\delta V(t)$, $\delta x_{AT}(t)$) mode state feedbacks. The lateral mode is, therefore, decoupled from the longitudinal and vertical modes. Coupling exists, however, between the longitudinal and vertical modes. For a nominal aircraft bank angle of 45° , all three path modes are coupled. When wind disturbances are included, the disturbance states begin to appear in the control equations. For a 50 ft/sec tailwind, the wind magnitude perturbation contributes to the perturbed angle-of-attack and thrust commands. The wind direction perturbation contributes to the perturbed bank angle command. For a 50 ft/sec cross-

TABLE I
INITIAL Q AND R SELECTION

$\delta V_{\max} = 50 \text{ ft/sec}$	$\delta x_{AT_{\max}} = 2000 \text{ ft}$	$\delta \alpha_{\max} = 5^\circ$
$\delta \psi_{\max} = 7.5^\circ$	$\delta y_{CT_{\max}} = 1000 \text{ ft}$	$\delta \phi_{\max} = 7.5^\circ$
$\delta \gamma_{\max} = 5^\circ$	$\delta h_{\max} = 100 \text{ ft}$	$\delta T_{\max} = 12000 \text{ lbs}$

TABLE II
SOLUTION OF STEADY STATE LQ PROBLEM

• NO WIND DISTURBANCES - LOW \bar{q} FLIGHT CONDITION WITH NOMINAL PERFORMANCE INDEX

• WINGS LEVEL

$$\begin{aligned}\delta u(t) &= .000409\delta V(t) + 1.236\gamma(t) - .000013\delta x_{AT}(t) + .000827\delta h(t) \\ \delta \phi(t) &= 1.274\psi(t) + .000131\delta y_{CT}(t) \\ \delta T(t) &= 379.6V(t) + 15302.6\gamma(t) + 5.716\delta x_{AT}(t) + 36.46h(t)\end{aligned}$$

• 45° ROLL ATTITUDE

$$\begin{aligned}\delta u(t) &= .0003176V(t) + .3126\psi(t) + 1.0436\gamma(t) - .00001428\delta x_{AT}(t) \\ &\quad + .0000368\delta y_{CT}(t) + .0007326h(t) \\ \delta \phi(t) &= -.00129\delta V(t) + 1.0528\psi(t) - 1.48\delta \gamma(t) + .00000855\delta x_{AT}(t) \\ &\quad + .0001196\delta y_{CT}(t) - .0005266h(t) \\ \delta T(t) &= 41.86V(t) + 316.46\psi(t) + 28346.8\gamma(t) + 5.628\delta x_{AT}(t) \\ &\quad + .252\delta y_{CT}(t) + 41.66h(t)\end{aligned}$$

• WITH WIND DISTURBANCES - LOW \bar{q} FLIGHT CONDITION WITH NOMINAL PERFORMANCE INDEX AND WINGS LEVEL

• 50 FT/SEC TAILWIND

$$\begin{aligned}\delta u(t) &= .000409\delta V(t) + 1.236\gamma(t) - .000013\delta x_{AT}(t) + .000827\delta h(t) \\ &\quad - .0002946V_W(t) \\ \delta \phi(t) &= 1.274\psi(t) + .000131\delta y_{CT}(t) + .1735\psi_W(t) \\ \delta T(t) &= 379.6V(t) + 15302.6\gamma(t) + 5.716\delta x_{AT}(t) + 36.46h(t) \\ &\quad + 304.5V_W(t)\end{aligned}$$

• 50 FT/SEC CROSSWIND

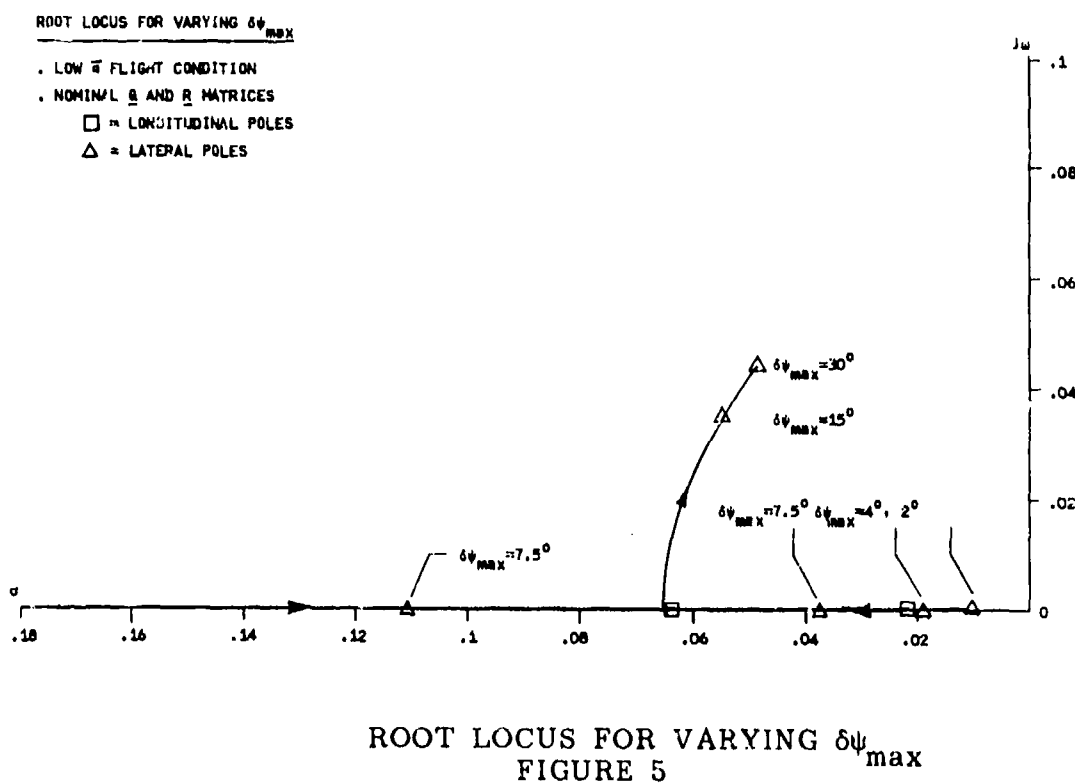
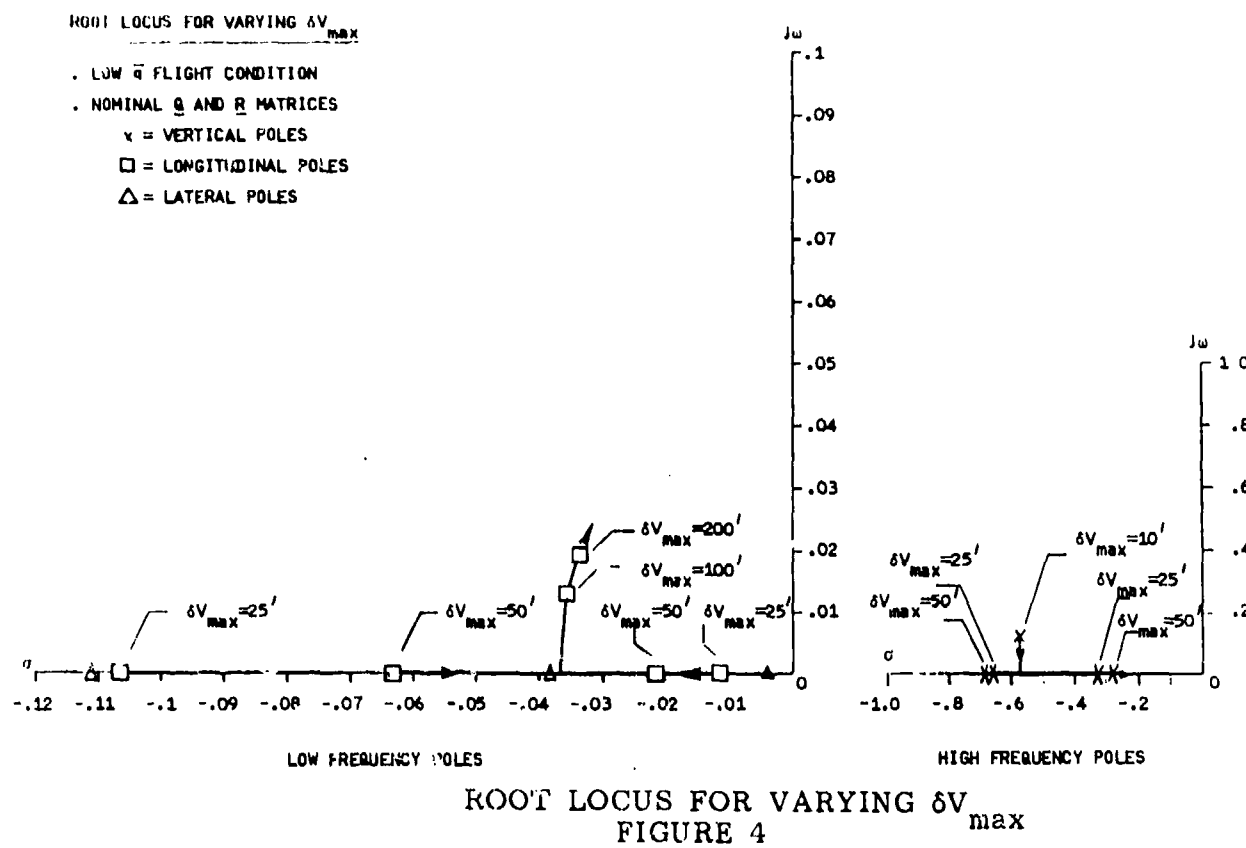
$$\begin{aligned}\delta u(t) &= .000409\delta V(t) + 1.236\gamma(t) - .000013\delta x_{AT}(t) + .000827\delta h(t) \\ &\quad - .0000000346V_W(t) + .00846\psi_W(t) \\ \delta \phi(t) &= 1.274\psi(t) + .000131\delta y_{CT}(t) + .002236V_W(t) + .000026\psi_W(t) \\ \delta T(t) &= 379.6V(t) + 15302.6\gamma(t) + 5.716\delta x_{AT}(t) + 36.46h(t) \\ &\quad + .03516V_W(t) - 12400.8\psi_W(t)\end{aligned}$$

wind, the disturbance state feedback gains change so that the wind magnitude perturbation affects mainly the perturbed bank angle command while the wind direction perturbation affects mainly the perturbed angle-of-attack and thrust commands

3.2.4.2 LQ Design - Step 2

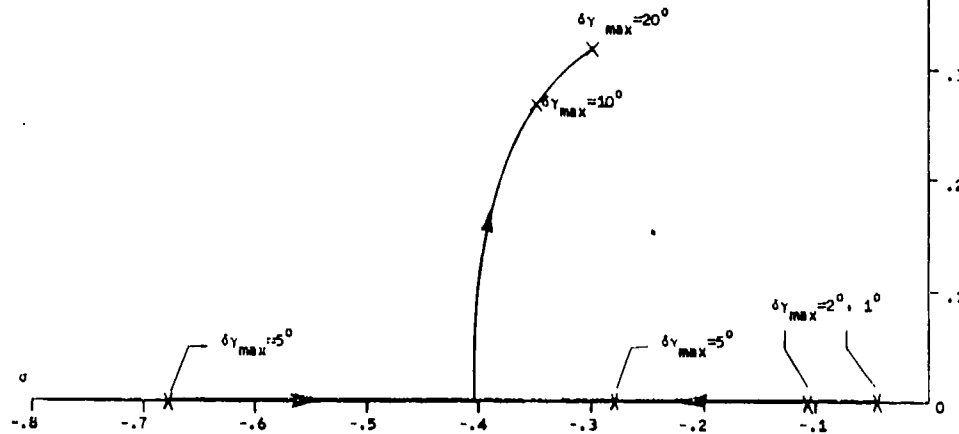
An eigenvalue analysis was made to determine the effects varying individual components of the Q and R matrices had on the stability of the optimal controller. Figures 4 through 12 are root locus type diagrams which illustrate these effects. The following conclusions can be drawn from these figures.

- Three sets of eigenvalues can be identified as corresponding to the longitudinal, lateral, and vertical path modes.
 - Longitudinal path mode has a bandwidth of the order of .035 rad/sec.
 - Lateral path mode has a bandwidth of the order of .06 rad/sec.
 - Vertical path mode has a bandwidth of the order of .5 rad/sec.
- Decreasing δV_{\max} decreases the longitudinal mode bandwidth and also effects the vertical mode bandwidth.
- Decreasing $\delta \psi_{\max}$ decreases the lateral mode bandwidth.
- Decreasing δy_{\max} decreases the vertical mode bandwidth.
- Increasing $\delta x_{AT\max}$ decreases the longitudinal mode bandwidth.
- Increasing $\delta y_{CT\max}$ decreases the lateral mode bandwidth.
- Increasing δh_{\max} decreases the vertical mode bandwidth.
- Increasing $\delta \alpha_{\max}$ decreases the vertical mode bandwidth and also effects the longitudinal mode bandwidth.
- Increasing $\delta \phi_{\max}$ decreases the lateral mode bandwidth.
- Increasing δT_{\max} decreases the longitudinal mode bandwidth.



ROOT LOCUS FOR VARYING δy_{max}

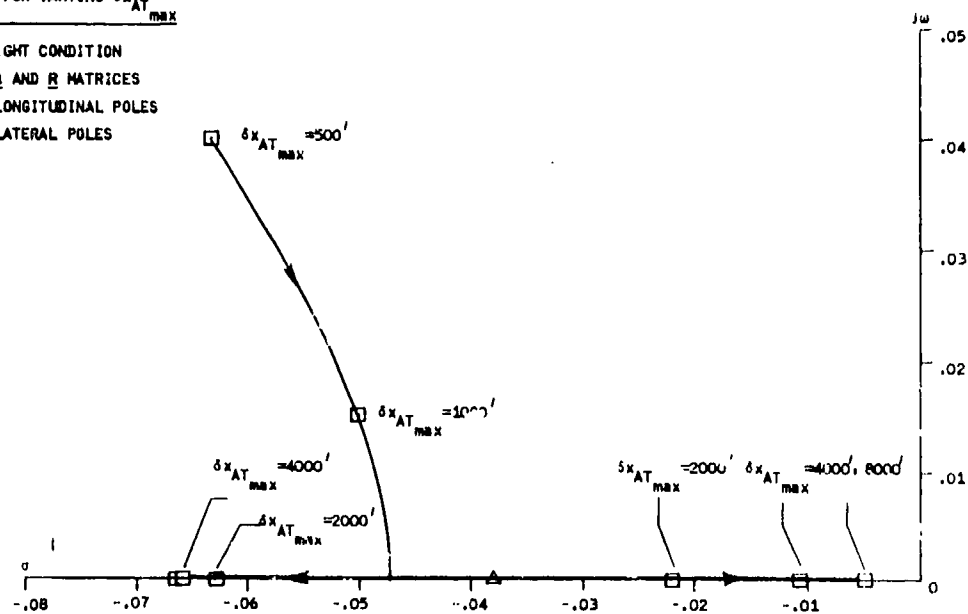
- LOW \bar{q} FLIGHT CONDITION
- NOMINAL \underline{Q} AND \underline{R} MATRICES
- x = VERTICAL POLES



ROOT LOCUS FOR VARYING δy_{max}
FIGURE 6

ROOT LOCUS FOR VARYING $\delta x_{AT_{max}}$

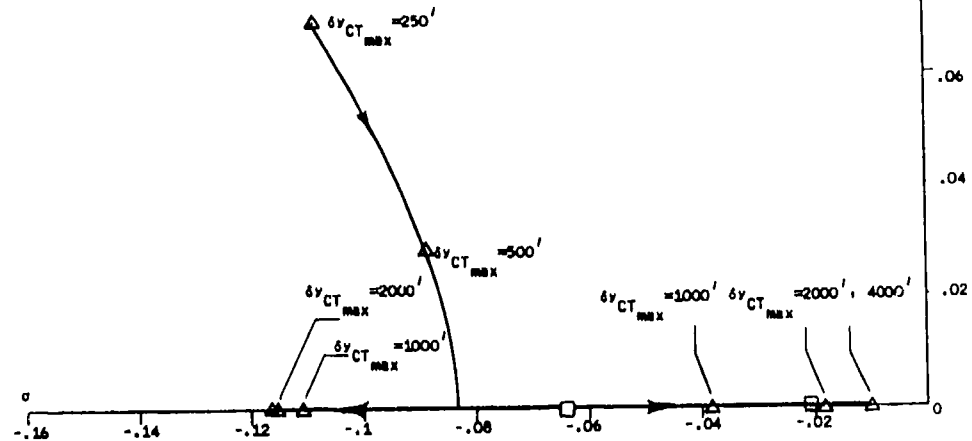
- LOW \bar{q} FLIGHT CONDITION
- NOMINAL \underline{Q} AND \underline{R} MATRICES
- \square = LONGITUDINAL POLES
- \triangle = LATERAL POLES



ROOT LOCUS FOR VARYING $\delta x_{AT_{max}}$
FIGURE 7

ROOT LOCUS FOR VARYING $\delta y_{CT_{\max}}$

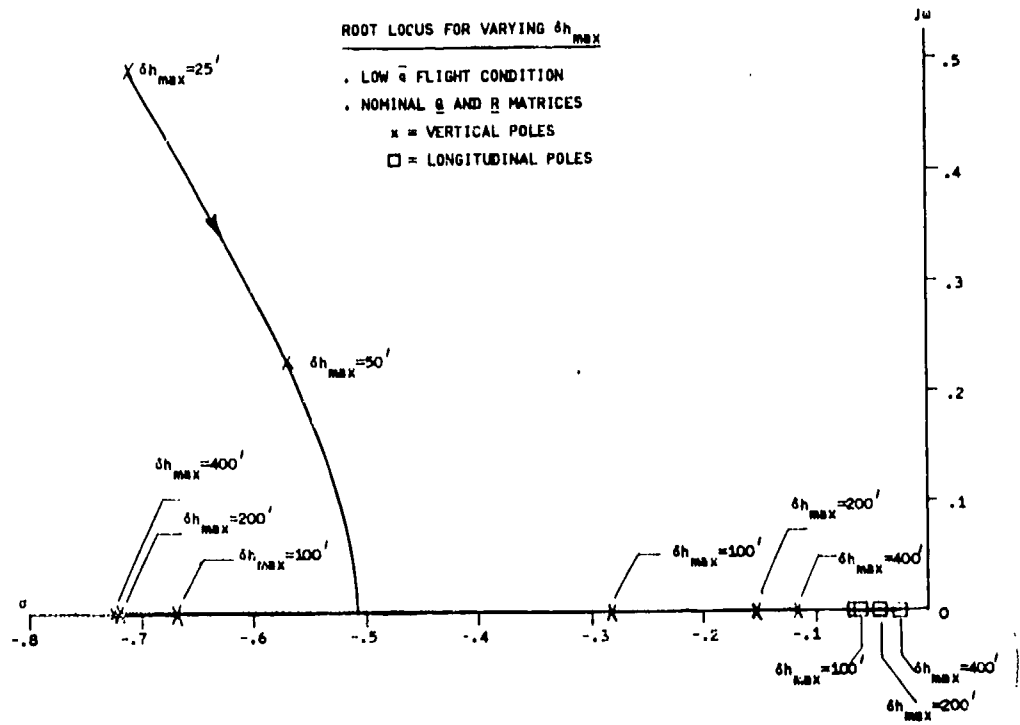
- LOW \bar{q} FLIGHT CONDITION
- NOMINAL \mathbf{Q} AND \mathbf{R} MATRICES
- = LONGITUDINAL POLES
- △ = LATERAL POLES



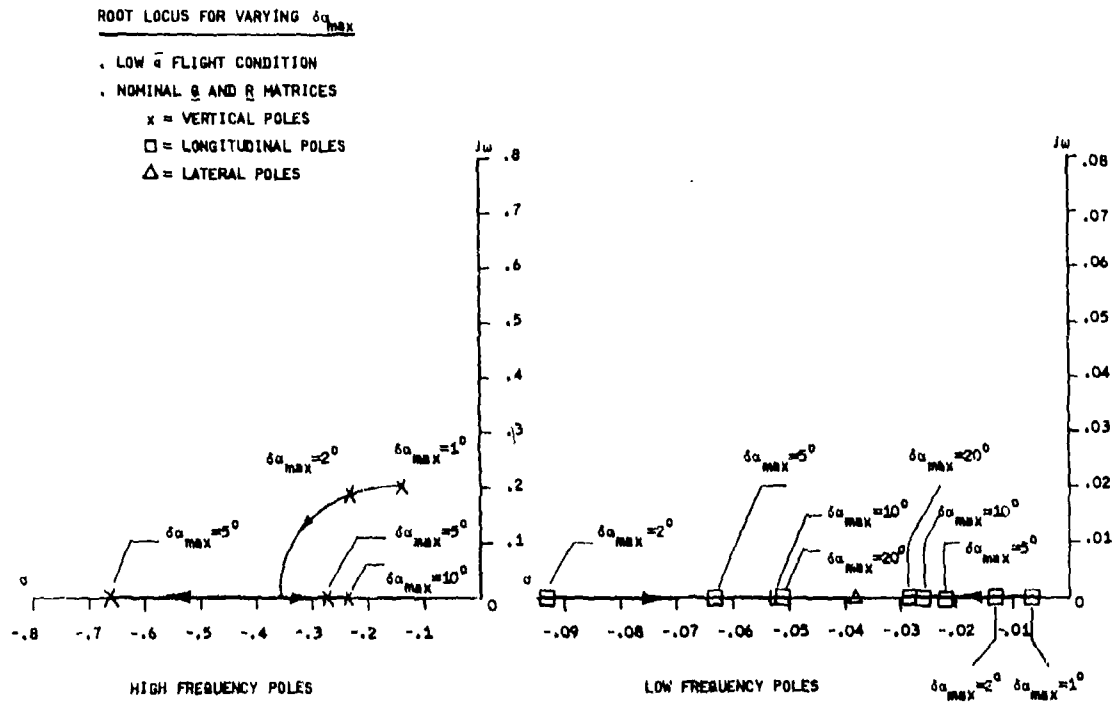
ROOT LOCUS FOR VARYING $\delta y_{CT_{\max}}$
FIGURE 8

ROOT LOCUS FOR VARYING δh_{\max}

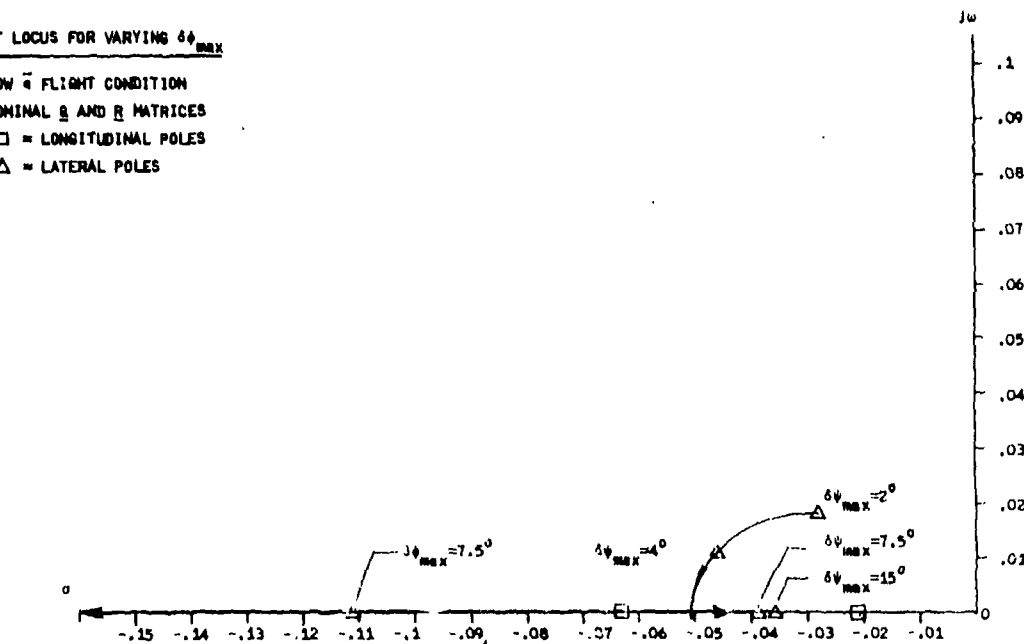
- LOW \bar{q} FLIGHT CONDITION
- NOMINAL \mathbf{Q} AND \mathbf{R} MATRICES
- ✗ = VERTICAL POLES
- = LONGITUDINAL POLES



ROOT LOCUS FOR VARYING δh_{\max}
FIGURE 9



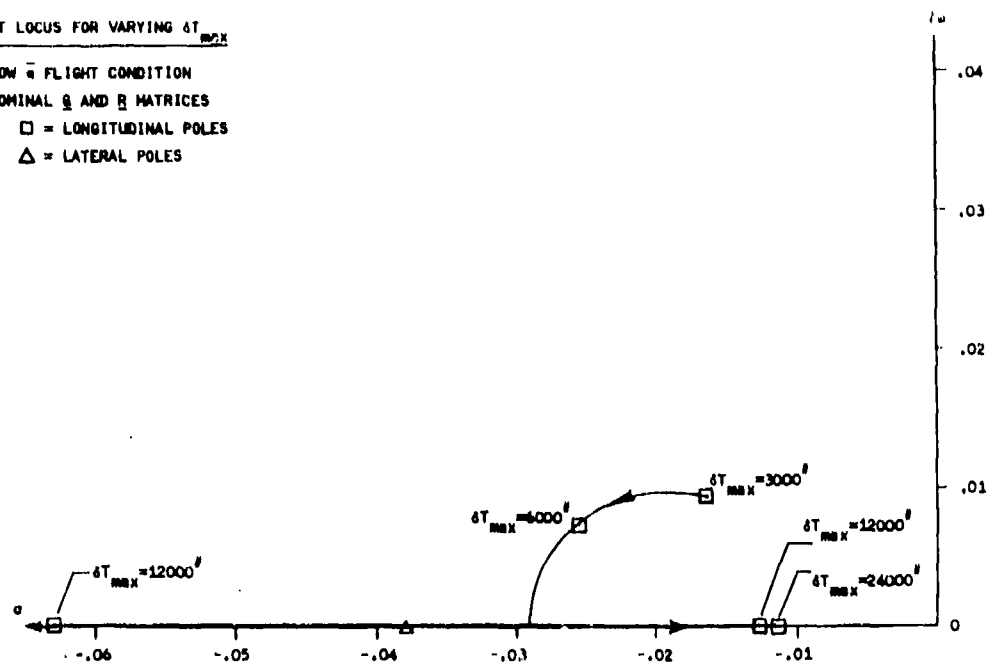
ROOT LOCUS FOR VARYING $\delta\alpha_{\max}$
FIGURE 10



ROOT LOCUS FOR VARYING $\delta\phi_{\max}$
FIGURE 11

ROOT LOCUS FOR VARYING δT_{max}

- LOW \bar{a} FLIGHT CONDITION
- NOMINAL \mathbf{Q} AND \mathbf{R} MATRICES
- \square = LONGITUDINAL POLES
- Δ = LATERAL POLES



ROOT LOCUS FOR VARYING δT_{max}
FIGURE 12

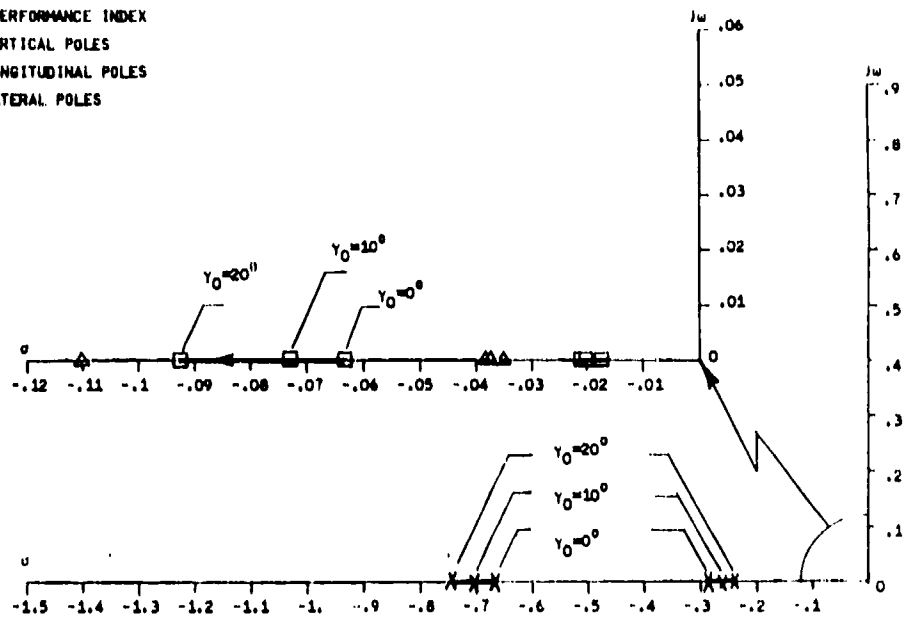
3.2.4.3 LQ Design - Step 3

A sensitivity analysis was performed to study the variation of the closed-loop eigenvalues as the nominal flight path angle (γ_0), nominal bank angle (ϕ_0), nominal altitude (h_0), or nominal velocity (V_0) varies. Nominal thrust (T_0) and angle-of-attack (α_0) were adjusted so that the aircraft is trimmed. Root locus type plots illustrating the results of this analysis are shown in Figures 13 through 16. The following observations can be made:

- \square Varying the nominal flight path angle has negligible effect on path mode dynamics.
- \square The vertical path mode dynamics are strongly influenced by varying nominal altitude and to a lesser extent by varying nominal velocity.
- \square The lateral path mode dynamics are strongly affected by varying nominal velocity.
- \square The longitudinal path mode dynamics are only slightly affected by varying nominal altitude, velocity, and bank angle.

ROOT LOCUS FOR NOMINAL FLIGHT PATH ANGLE VARIATION

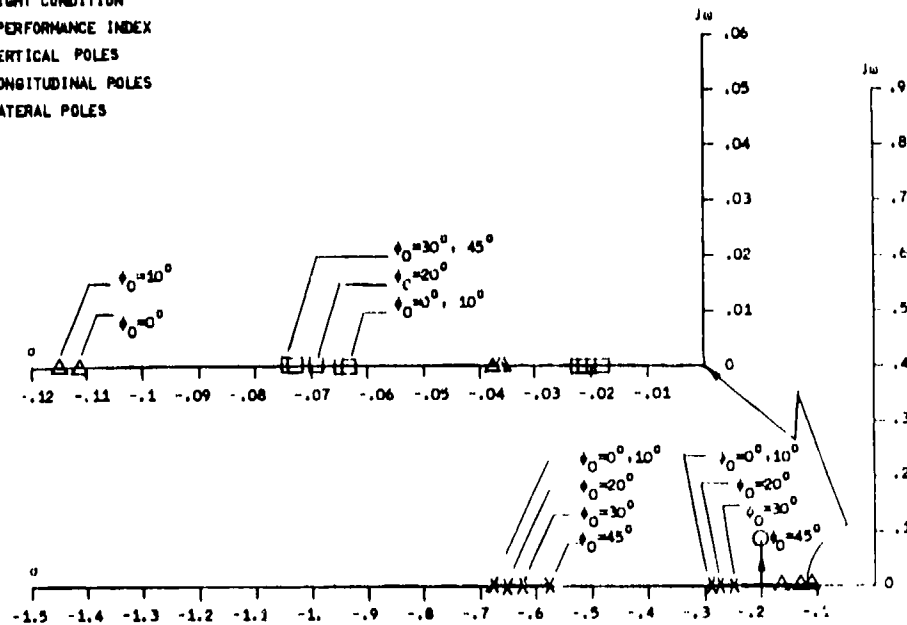
- LOW \bar{v} FLIGHT CONDITION
- NOMINAL PERFORMANCE INDEX
- \times = VERTICAL POLES
- \square = LONGITUDINAL POLES
- \triangle = LATERAL POLES



ROOT LOCUS FOR NOMINAL FLIGHT PATH ANGLE VARIATION
FIGURE 13

ROOT LOCUS FOR NOMINAL BANK ANGLE VARIATION

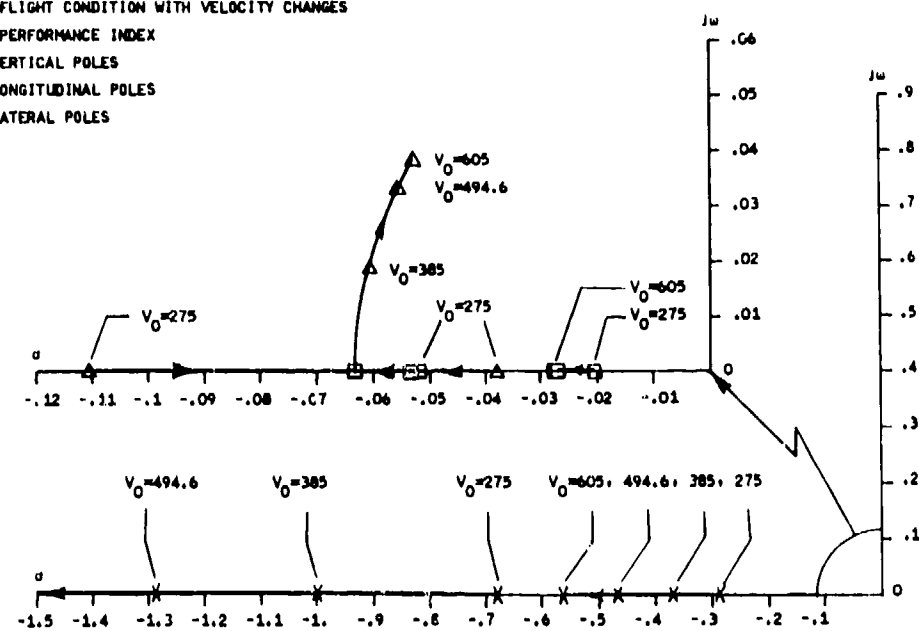
- LOW \bar{v} FLIGHT CONDITION
- NOMINAL PERFORMANCE INDEX
- \times = VERTICAL POLES
- \square = LONGITUDINAL POLES
- \triangle = LATERAL POLES



ROOT LOCUS FOR NOMINAL BANK ANGLE VARIATION
FIGURE 14

ROOT LOCUS FOR NOMINAL VELOCITY VARIATION

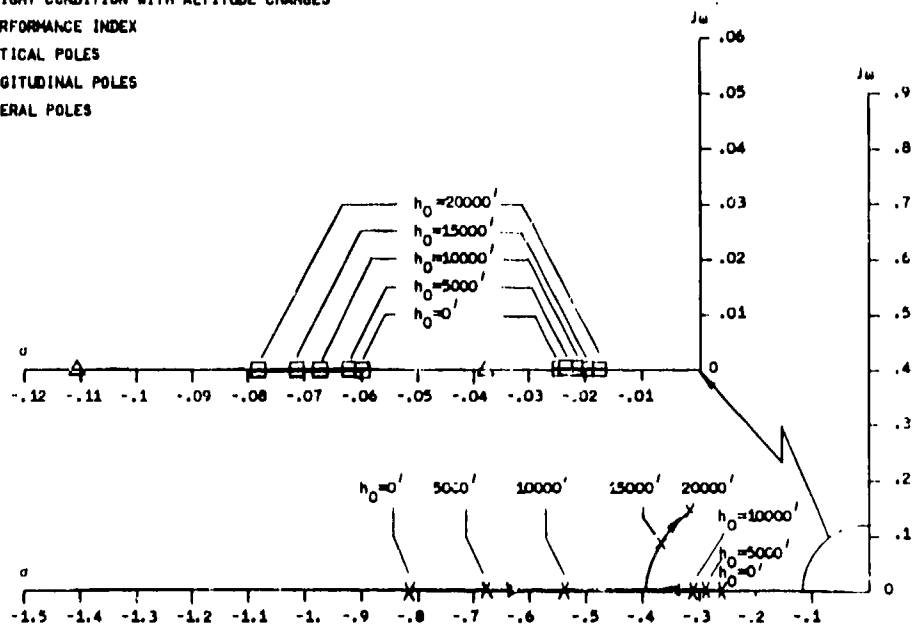
- NOMINAL FLIGHT CONDITION WITH VELOCITY CHANGES
- NOMINAL PERFORMANCE INDEX
- VERTICAL POLES
- = LONGITUDINAL POLES
- △ = LATERAL POLES



ROOT LOCUS FOR NOMINAL ALTITUDE VARIATION
FIGURE 15

ROOT LOCUS FOR NOMINAL ALTITUDE VARIATION

- NOMINAL FLIGHT CONDITION WITH ALTITUDE CHANGES
- NOMINAL PERFORMANCE INDEX
- VERTICAL POLES
- = LONGITUDINAL POLES
- △ = LATERAL POLES



ROOT LOCUS FOR NOMINAL VELOCITY VARIATION
FIGURE 16

3.2.4.4 LQ Design - Step 4

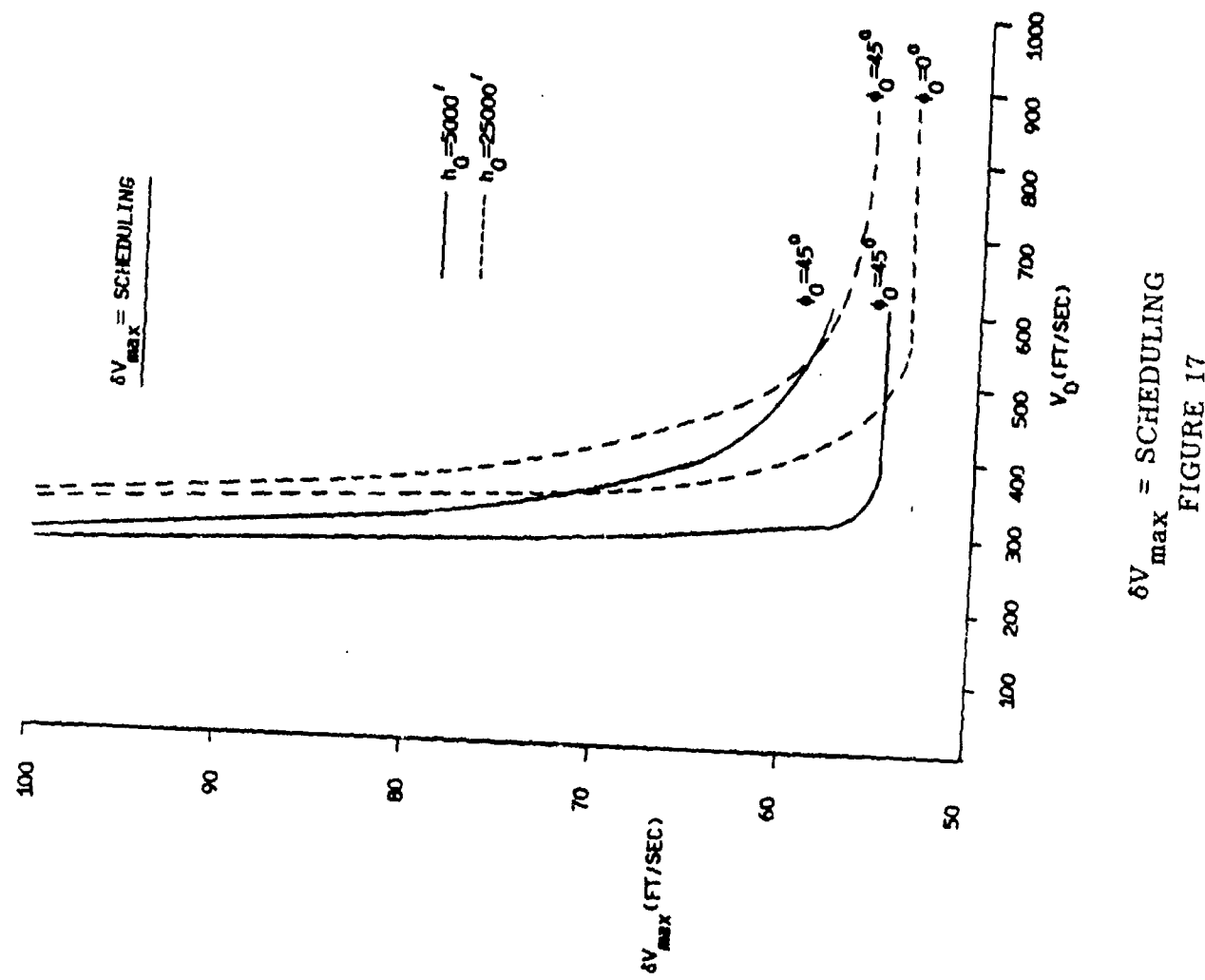
The weighting matrices Q and R are scheduled as a function of flight condition by selecting a performance index for a sample of representative flight conditions that yielded eigenvalues that are approximately critically damped. The rationale for critically damped eigenvalues is to minimize overshoots which are undesirable in path guidance. The performance index was modified by changing the maximum velocity error (δV_{\max}), heading error ($\delta \psi_{\max}$), and flight path angle error ($\delta \gamma_{\max}$) terms. Figures 17, 18, and 19 show the error scheduling as a function of velocity, altitude, and bank angle. Table III presents the final weighting matrix selection illustrating the actual implementation of the δV_{\max} , $\delta \psi_{\max}$, and $\delta \gamma_{\max}$ scheduling.

3.2.4.5 Mechanization Requirements

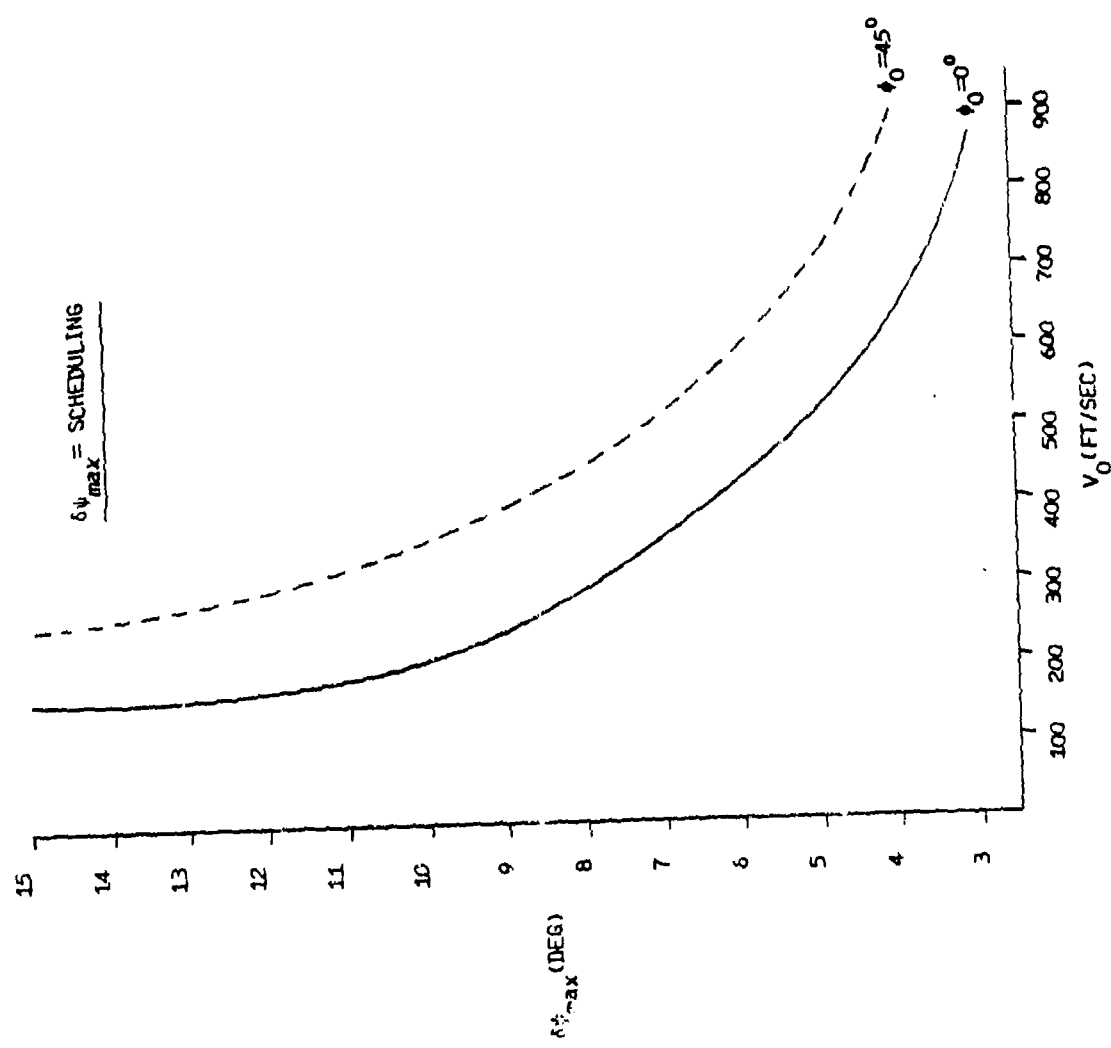
The design of the optimal controller, as defined, incorporates two principal approximations to keep the requirement for airborne processing capability within reason. These restrictions were (a) the use of a point mass aircraft model, and (b) the implementation of a proportional control system that excluded integral terms. These simplified models require the scheduling of the weighting matrices, Q and R , as a function of aircraft flight condition (as previously shown) and analysis of the inner loop gains of the normal Stability Augmentation System (SAS) of the KC-135 aircraft.

In addition, simplified aircraft control systems required either angle-of-attack or normal acceleration control signals for the outer loop pitch axis. This type of control system is considerably more difficult to implement than a conventional pitch attitude control system. In fact, without the integral terms in the control system, the angle of attack or normal acceleration control signals in the outer loop would also have to be scheduled in gain, as a function of flight mode, to maintain desired stability.

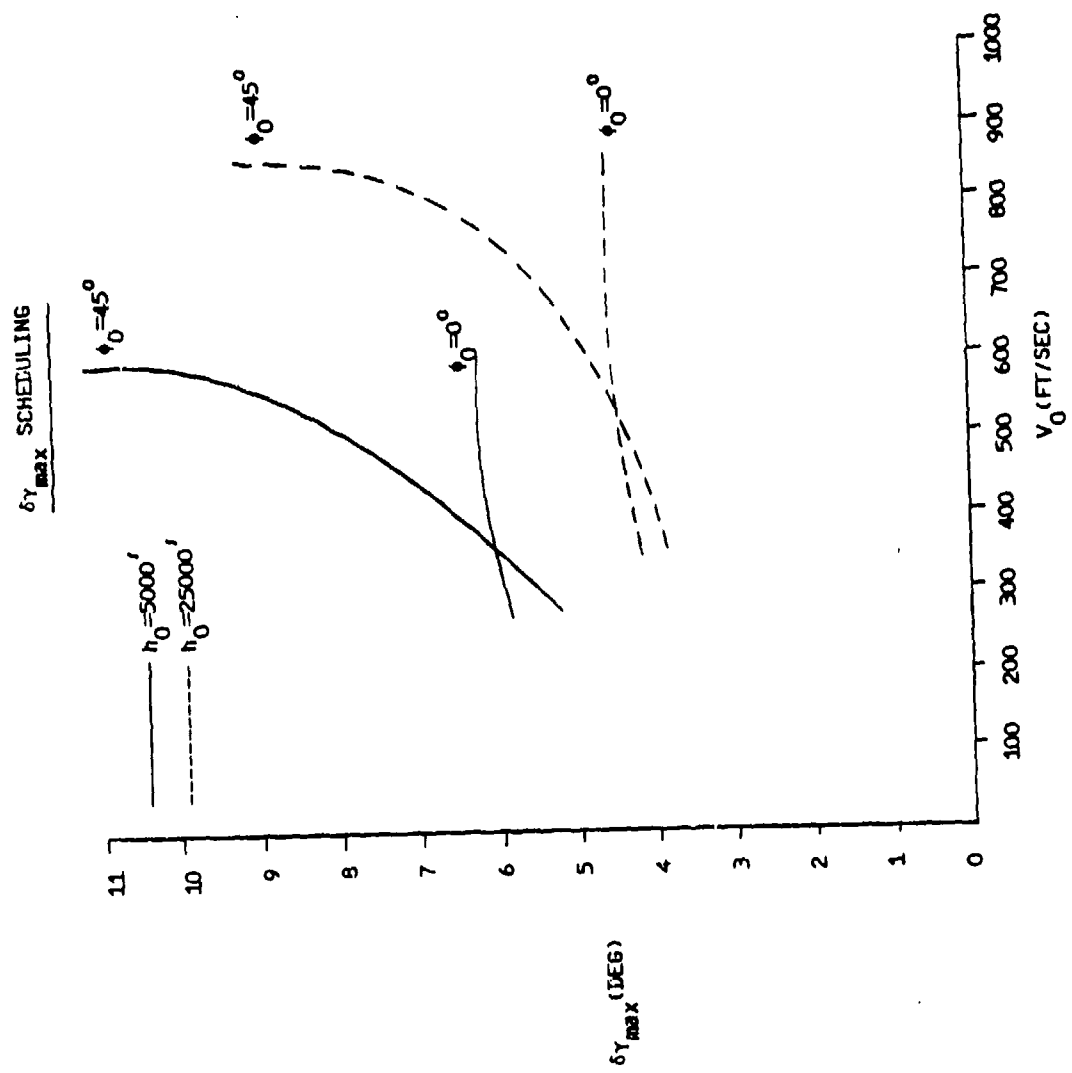
Performance improvements of an optimal control system compared to a conventional control system on a KC-135 aircraft would be difficult to measure if the only criteria were the arrival at a rendezvous point or CARP at a given time. However, some of the negative comparisons may be more apparent to the air crew. The crossfeed terms derived by the optimal control system would undoubtedly provide smaller profile errors, but the transient responses to pilot overrides and at profile boundaries when new gains were generated may be very disconcerting to pilots. Also, the crossfeed terms to the throttle would probably cause an excessive amount of throttle activity.



$\delta V_{\max} = \text{SCHEDULING}$
FIGURE 17



$\delta\psi_{\max} = \text{SCHEDULING}$
FIGURE 18



$\delta\gamma_{\max}$ SCHEDULING
FIGURE 19

TABLE III
FINAL Q AND R SELECTION

$\Delta V_{\max}(\bar{q}, \phi) = \delta V_{\max}(\bar{q}, \phi=0^\circ) + K_{\delta V}(\phi) [\delta V_{\max}(\bar{q}, \phi=45^\circ) - \delta V_{\max}(\bar{q}, \phi=0^\circ)]$	
$\delta V_{\max}(\bar{q}, \phi=0^\circ) = 100.$	$\bar{q} < 55$
$= -.25(\bar{q}-55.) + 67.$	$55 < \bar{q} < 107$
$= 54.$	$\bar{q} \geq 107$
$K_{\delta V}(\phi) = 0$	$ \phi < 13^\circ$
$= .03125(\phi - 13^\circ)$	$ \phi \geq 13^\circ$
$\delta V_{\max}(\bar{q}, \phi=45^\circ) = 100.$	$\bar{q} < 72.5$
$= -.25(\bar{q}-80.) + 72.5$	$72.5 \leq \bar{q} < 145.$
$= 56.$	$\bar{q} \geq 145.$
$\delta \psi_{\max}(V, \phi) = K_{\delta \psi}(\phi) \delta \psi_{\max}(V, \phi=0^\circ)$	
$K_{\delta \psi}(\phi) = 0$	$ \phi < 17^\circ$
$= .00917(\phi - 17^\circ)$	$17^\circ \leq \phi < 35^\circ$
$= .0215(\phi - 35^\circ) + .165$	$ \phi \geq 35^\circ$
$\delta \psi_{\max}(V, \phi=0^\circ) = 15.$	$V < 170$
$= -.0173(V - 170) + 10.3$	$170 \leq V < 480$
$= -.0065(V - 480) + 5.$	$V \geq 480$
$\delta \gamma_{\max}(h, \phi, \bar{q}) = [1 + K_{\delta \gamma}(\bar{q}, \phi=45^\circ) K_{\delta \gamma}(\phi)] \delta \gamma_{\max}(h, \phi=0^\circ)$	
$K_{\delta \gamma}(\bar{q}, \phi=45^\circ) = .00203\bar{q} - .33$	$\bar{q} < 310$
$= .007(\bar{q} - .33)$	$\bar{q} \geq 310$
$K_{\delta \gamma}(\phi) = 0.$	$ \phi < 10^\circ$
$= .0164(\phi - 10^\circ)$	$10^\circ \leq \phi < 29.5^\circ$
$= .0438(\phi - 29.5^\circ) + .32$	$ \phi \geq 29.5^\circ$
$\delta \gamma_{\max}(h, \phi=0^\circ) = (-9.74 \times 10^{-5})h + 6.25$	
$\delta x_{AT_{\max}} = 2000 \text{ ft}$	$\delta \alpha_{\max} \approx 5^\circ$
$\delta y_{CT_{\max}} = 1000 \text{ ft}$	$\delta \phi_{\max} \approx 7.5^\circ$
$\delta h_{\max} = 100 \text{ ft}$	$\delta T_{\max} = 12000 \text{ lbs}$

These mechanization problems resulted in a decision by the AFFDL program manager to terminate the optimal controller development task and proceed with the effort of demonstrating the improved threat avoidance conventional algorithms and specifying a preferred method to demonstrate the integrated flight trajectory system in a future flight test demonstration program.

3.3 THREAT AVOIDANCE ALGORITHM

As defined in Section 3.1.7, the task of defining an optimal trajectory generator, because of the complexity involved, was deferred in favor of upgrading the existing conventional algorithm trajectory generator to include threat avoidance capability. Specifically, the function of the algorithms is to compute mission trajectory modifications for avoiding or minimizing the aircraft exposure to ground threats (SAMs or AAA) during tactical airlift or transport/bomber missions. A secondary objective is to develop threat evasion algorithms which compute guidance/control cues or commands for evasive maneuvers after a threat has been launched, detected, and identified.

These algorithms will be simulated and evaluated with a cockpit, and hybrid computer simulator that includes a KC-135 cockpit and aerodynamic model plus a tactical flight management system. This flight management system consists of a tactical situation display, an alphanumeric display, and keyboard installed in the cockpit, and a 4-D trajectory generator for path guidance implemented in the hybrid's digital computer. In the simulation, the increased survivability algorithms will be integrated with the existing 4-D trajectory generation algorithms, which have been developed on the USAF Integrated Flight Trajectory Control (IFTC) program.

3.3.1 Task Definition

The specific scope of the revised task included in analytical characterization of the ground-located threats and definition of increased survivability trajectory generator algorithms.

As a background for the algorithm definition task, a realistic ground threat environment for tactical airlift or bomber missions in the 1980-1990 European theatre was requested. The ground threat would then be analytically modeled with equations that could be used to adequately represent the threats on a tactical situation display. The threat avoidance, minimum exposure, and threat evasion algorithms that are developed would be compatible with the IFTC trajectory generator equations and the flight control system capabilities of the simulated KC-135 aircraft.

The final engineering report on this task, as generated by SCI (Vt), is contained in Sections 3.3.2 through 3.3.4. This report briefly reviews the concept of resource management for aircraft survival, threat modeling, and threat avoidance algorithms.

3.3.2 Resource Management Concepts

The problem of threat avoidance is best considered in the more comprehensive framework of resource management. By normalizing the current military value of an aircraft in terms of aircraft (e.g., 2.7 aircraft) as a function of the vector of allocable resources, \underline{R} , for multiple objectives, it can be shown that

$$V(\underline{R}) = T_1 \prod_{j=1}^{m_1-1} S_j M_1 + \dots + T_i \prod_{j=1}^{m_i-1} S_j M_i + \dots + T_N \prod_{j=1}^{m_{N-1}} S_j M_N + \prod_{j=1}^{m_{N+1}} S_j \quad (98)$$

where

T_i = value of the i th objective ($i = 1, 2, \dots, N$)

M_i = probability of accomplishing i th objective conditioned upon arriving at i th objective

m_i = index of interval incorporating i th objective

S_j = probability of surviving j th interval

$(\prod_{j=1}^{m_{N-1}} S_j)$ = the probability of survival to the aircraft return base)

The primary resources available to an aircraft fall into three categories. The aircraft maneuvers, specified by the three-dimensional position and velocity as a function of time, comprise the first. The second is non-expendable resources, which can be allocated at each time of mission without "using up" the resource. For example, ECM RF power, fire control, and surveillance sensors, radar cross section presented to

threats (which is a function of relative altitude), and computer capacity. The third resource category includes expendable resources which, once used, are no longer available. These include flares, decoys, guns, defensive/offensive missiles, etc.

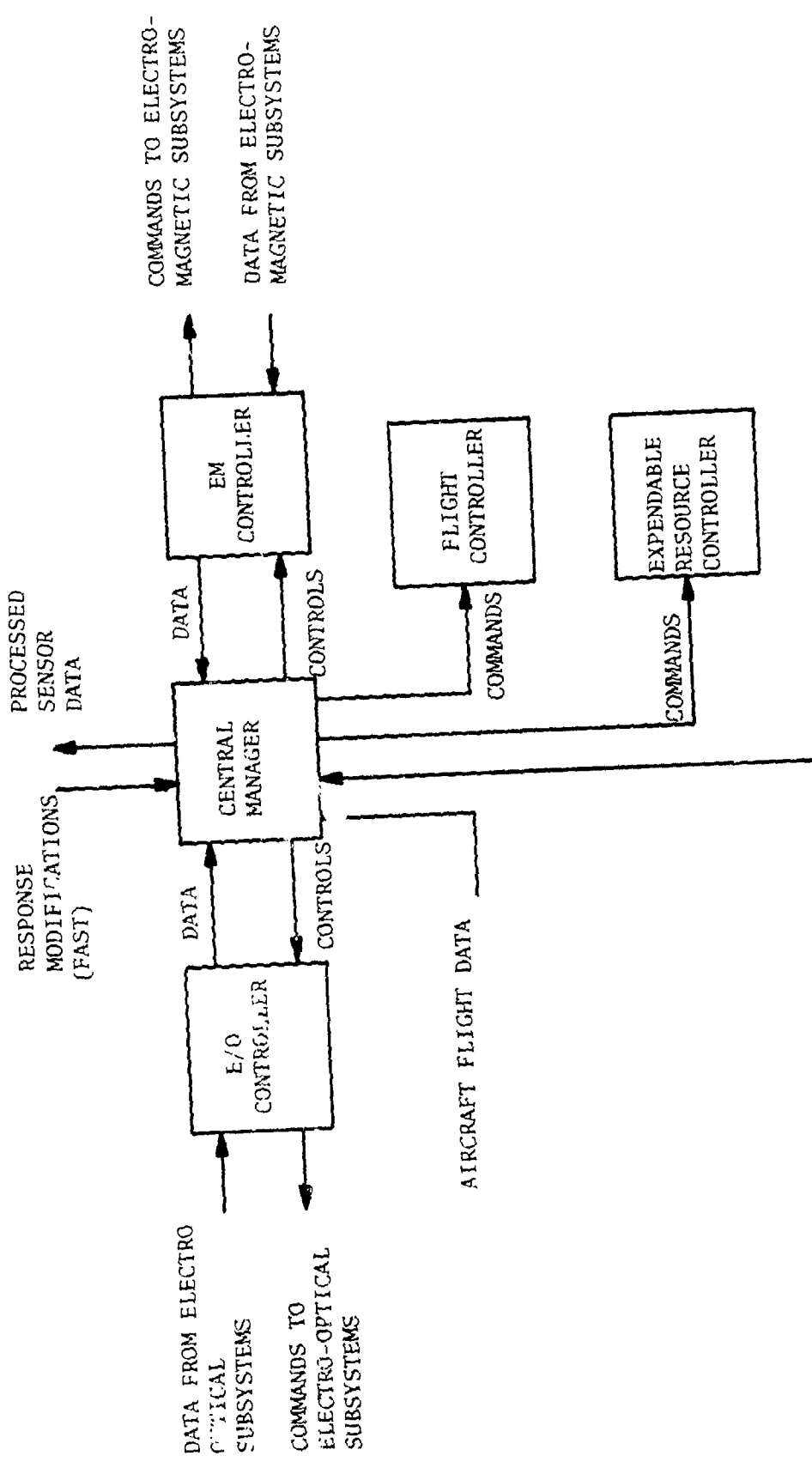
The resource management approach, block diagrammed in Figure 20, is to formulate the problem in recursive form and maximize the index formulated in equation 98 over the allowable flight control subject to fuel constraints.

Radar cross section is controlled by considering the effect of aspect angle and, hence, cross section, on the probability of detection by various radars along the flight path. These probabilities are then mapped into the probability of aircraft survival at each grid point in a three-dimensional position/velocity space. A similar approach is used to model the effects of terrain masking. Parts of the space that are masked from threat radars by terrain are assigned a unity probability of survival, while portions of space below ground level are given a probability of survival of zero.

As can be envisioned, the objective is to maximize the probability of survival along all possible flight paths to and returning from the objectives, match the resulting solutions to boundary conditions, and then choose the one flight path giving the highest current military value of the aircraft using models that describe the effect on the performance measure of allocating a particular resource to a given threat. An important issue in the optimal allocation of resources is the time-line trade-off between an allocation of resources at a current time during a mission and the allocation of the remaining resources at later times during that mission. The algorithm must include the capability for real-time allocation of resources as threats actually materialize (e.g., 10 seconds) while still reserving the necessary resources for allocation in later mission phases. The allocation for later phases of the mission usually can be carried out on a slower time scale. These two "fast" and "slow" allocation regimes are not independent, and a consistent global optimization must be performed; the expendables are allocated globally, while the nonexpendables may be allocated locally.

One possible approach to the problem taken by SCI⁴ is a modification of the dynamic programming procedure for solving multistage decision processes to make the procedure suitable for airborne computation.

⁴J. P. March and M. Grossberg, "Advanced Weapons Management Systems", Pacific Missile Test Center, April 1978.



INCREMENTAL ALLOCATIONS

REAL-TIME RESOURCE CONTROLLER
FIGURE 20

3.3.3 Threat Avoidance Review

The implementation of threat-avoidance algorithms can be performed at various levels of sophistication. The algorithm selected is directly related to the quality of the threat models.

Using a cylindrical threat volume around a known threat size, algorithms developed by LSI on the IFTC simulation skirt around the periphery of the threat volume using a trajectory-generation technique linking a set of dynamically generated waypoints. However, the approach is not satisfactory in multi-threat environments where the threat volumes are overlapping and the deployment of expendable resources is not accounted for.

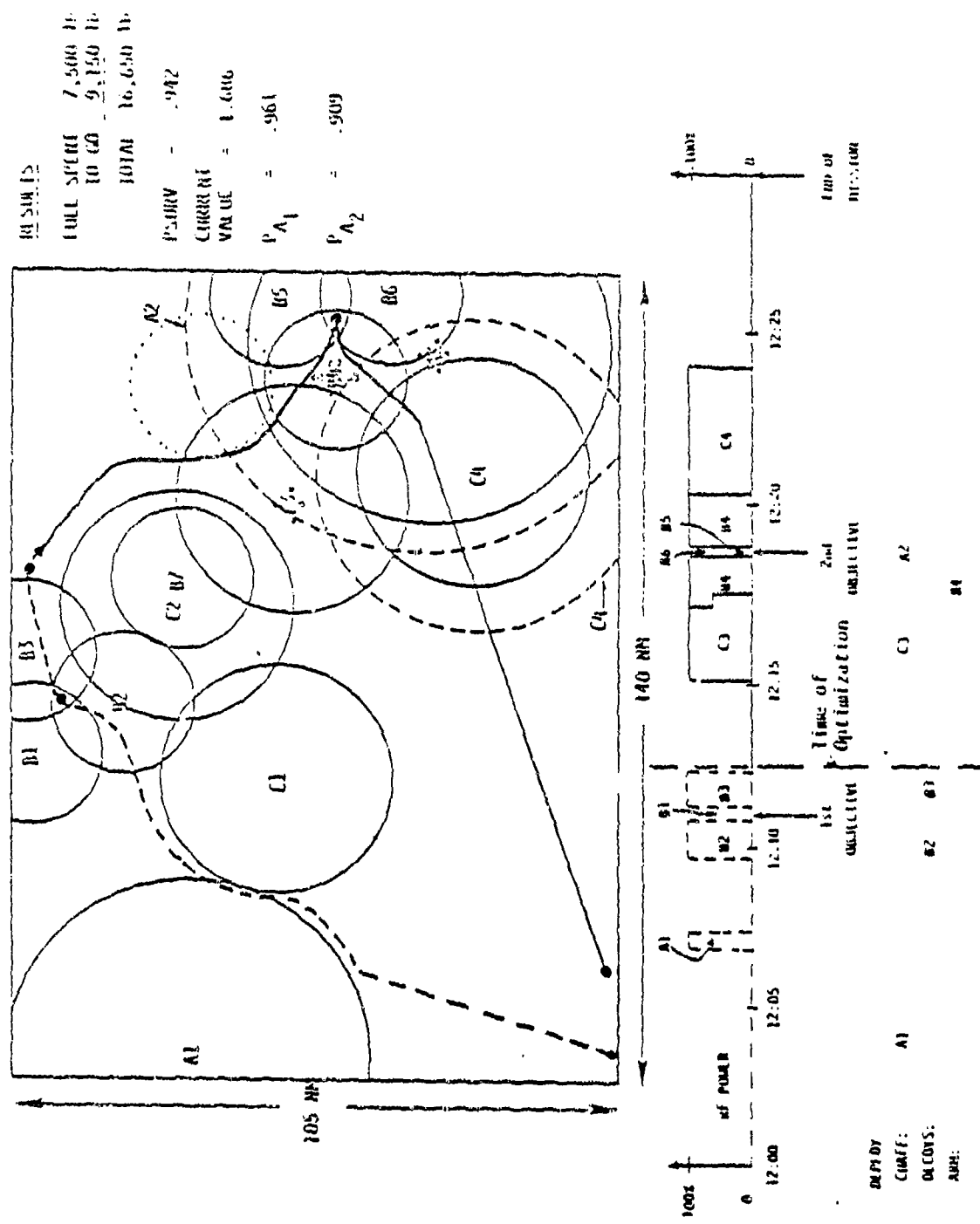
To provide an illustration for the nature of the operational problem and the type of solution sought, consider the mission trajectory of Figure 21. The "A", "B", and "C" threat categories describe three types of threats. The end of the dotted line shows the current location of the aircraft. At this point, a pop-up threat A2 is detected. The algorithm generates the solid trajectory in real time to accommodate this event. Note that besides generating the horizontal (shown in the figure) and vertical (not shown) plane trajectories, the algorithm also suggests an expendable and nonexpendable resource deployment schedule, depicted in the lower portion of the figure. On the upper right the fuel used is shown; the probability of survival, and the probability of achieving objectives 1 and 2 are also shown. The algorithms developed by SCI (Vt) entail the use of dynamic programming methods implemented on an array processor.⁵ Modifications to these algorithms would be required if a serial processor is used. However, Figure 21 does show the nature of the output that ought to be generated by a meaningful operational algorithm.

3.3.4 Threat Modeling Survey

This section surveys some state-of-the-art techniques of threat modeling. Generally speaking, no validated threat models are available at this time. However, it is useful to review the modeling methods currently used. As noted earlier the threat must be described in terms of spatial elements wherein the probability of surviving transition from one cell to the next is specified as a function of aircraft position and velocity with respect to the threat; either tabular storage or curves could be used for this.

One approach to model development for the slow-allocation mode for a SAM site is to perform off-line Monte Carlo runs simulating fly-past at different offsets and relative heading using available SAM data on each Monte Carlo run. The A/C cross section (radar/optical) history, ECM effectiveness, and missile effectiveness must be chosen independently.

⁵Ibid



OPTIMUM FLIGHT PATH ASSUMING FIRST OBJECTIVE IS COMPLETED AND A POP-UP THREAD IS DETECTED BY ON-BOARD SENSORS
FIGURE 21

In this way the unconditioned probability of surviving can be quantified probabilistically. Models generated by these techniques are not available at this time and are the subject of on-going research studies. In lieu of these validated models, a stochastic threat model can be developed as detailed in Appendix B. It is suggested that this stochastic model might be a satisfactory means of tuning up the threat-avoidance algorithm by using a range of numerical values for the threat lethality parameters.

3.3.5 Conclusions

Threat avoidance and threat modeling literature, particularly SCI work, was surveyed to determine the following:

- a. No validated threat-survival models exists.
- b. A generalized stochastic threat model has been formulated (Appendix B).
- c. Operational threat-avoidance algorithms should provide resource allocation capability.
- d. A dynamic programming approach on an array processor can be used to implement a real-time threat-avoidance algorithm.

Finally, it is noted that a more detailed analysis of threat avoidance is beyond the scope of this advisory study and substantial additional work remains to be performed before a realistic modification of the existing trajectory generator algorithms can be implemented.

3.4 SIMULATOR DEVELOPMENT

The major areas of simulator development were the following.

- a. Applying the developed six-degree-of-freedom KC-135 aerodynamics and the Stability Augmentation System models to the closed loop simulation.
- b. Converting the Integrated Flight Trajectory Control (IFTC) program from the IBM-370 computer to a PDP-11/70.
- c. Modifying the control-display hardware for the transport cockpit.

The latter two tasks were accomplished under in-house funding.

3.4.1 Aerodynamics and Stability Augmentation System

The F-4 aerodynamics in the existing IFTC closed-loop hybrid simulation were replaced with the KC-135 aerodynamics.

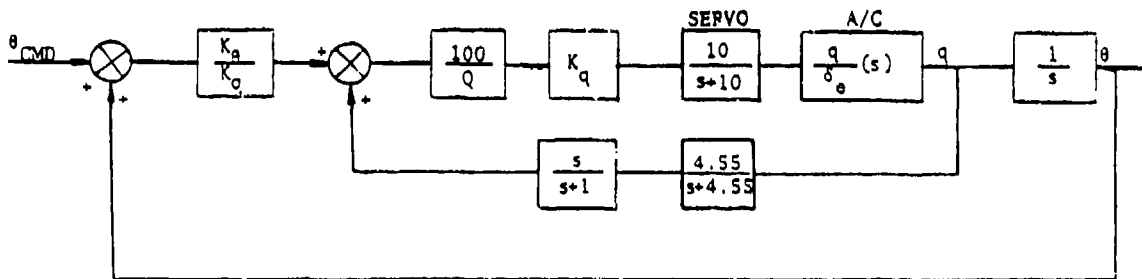
The Stability Augmentation System (SAS) was developed and checked out with the aircraft model. The mechanization and characteristics of the SAS are similar to existing functions of the digital flight control system presently installed on the Speckled Trout.⁶

3.4.1.1 SAS Design

The SAS structure, as defined in Boeing Aircraft Company report, "KC/E/RC-135 System Characteristics Missions Simulator", consists of a pitch axis, roll axis, and yaw damper.

The pitch axis feedbacks are pitch attitude and washed-out pitch rate. The lateral axis feedbacks are roll attitude and roll rate. The yaw damper feedback is washed-out yaw rate. Gains for these loops are obtained using a standard root locus analysis program that is resident in the PDP-11/70 laboratory computer.

The pitch axis block diagram is shown in Figure 22.



SAS PITCH AXIS BLOCK DIAGRAM
FIGURE 22

⁶Speckled Trout Software Documents, Specification #5710, Sperry Flight Systems, Phoenix, Arizona.

In this diagram

K_θ = pitch attitude feedback gain
 K_q = pitch rate feedback gain
 Q = dynamic pressure
 $\frac{q}{\delta_e} (s)$ = aircraft short period mode transfer function

Selection of K_θ and K_q depends on the flight condition. The block $\frac{100}{Q}$ was inserted into the pitch axis control in order to adapt the gains to varying flight conditions. The pitch SAS will be evaluated for both a high Q and low Q flight condition. The flight conditions selected are summarized in Table IV.

TABLE IV
SUMMARY OF A/C FLIGHT CONDITIONS

Aircraft Parameter	Flight Condition	
	Low Q	High Q
h	5000'	25000'
M	.25	.75
ρ	.002049	.001065
V	274.8 ft/sec	763.4 ft/sec
Q	77.4 lbs/ft ²	310.3 lb/sec
α_{trim}	7.19°	-.36°
$s_{WCP_{trim}}$	-7.13°	-2.27°
T_{trim}	7711 lbs	12728 lbs

The short period mode transfer functions are derived in Appendix A.

For the low Q flight condition:

$$\frac{q}{\delta_e} (s) = \frac{-0.921(s + 0.717)}{s^2 + 1.75s + 2.05} \quad (99)$$

For the high Q flight condition:

$$\frac{q}{\delta_e} (s) = \frac{-2.6(s + 0.83)}{s^2 + 2.45 + 8.17} \quad (100)$$

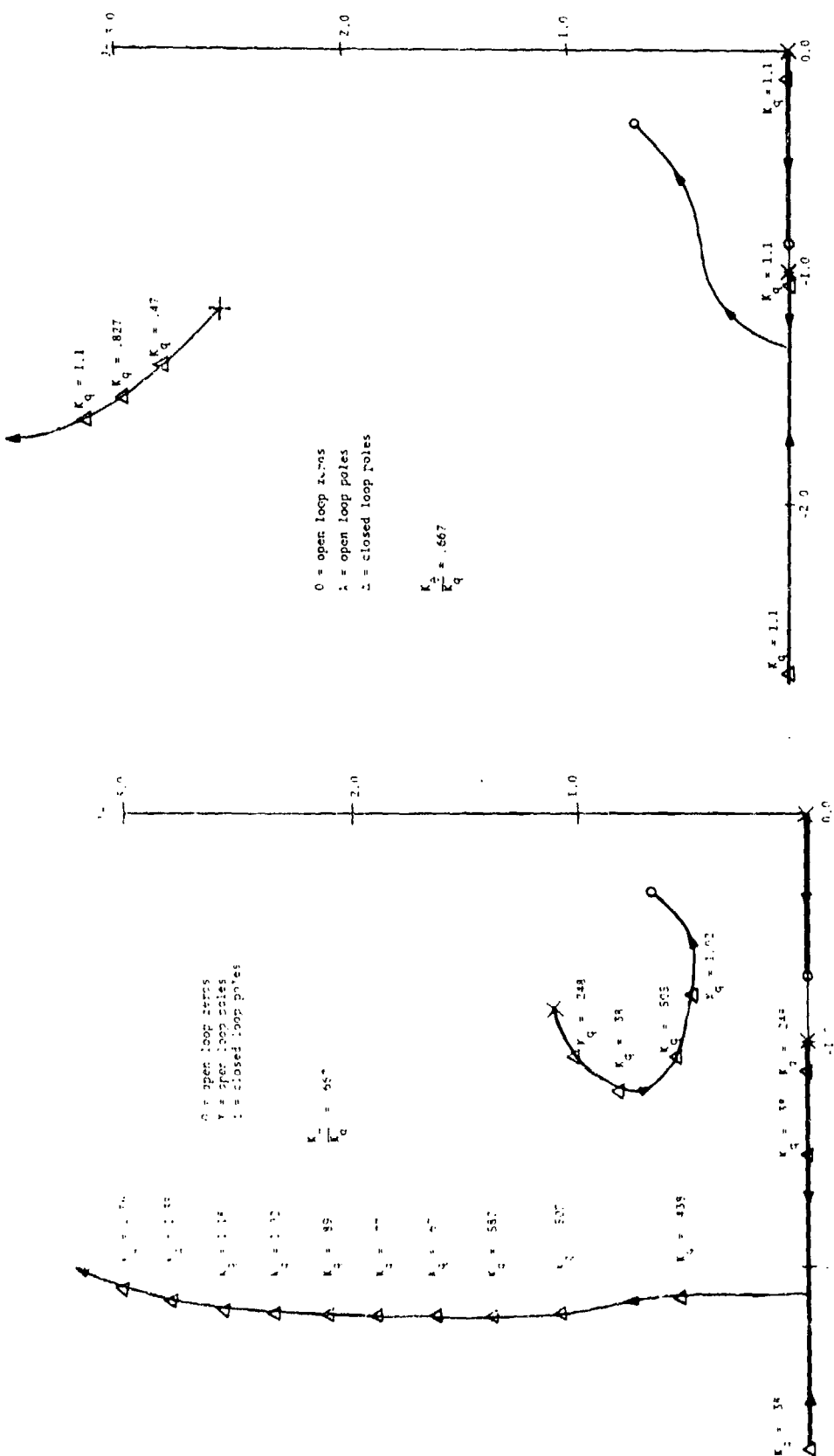
The root loci for both flight conditions were obtained by breaking the innermost loop and are shown in Figure 23 for

$$\frac{K_\theta}{K_q} = .677$$

Selecting $K_q = 1$ results in good transient response characteristics. The characteristics of the dominant complex poles are summarized in Table V.

TABLE V
PITCH SAS RESPONSE CHARACTERISTICS

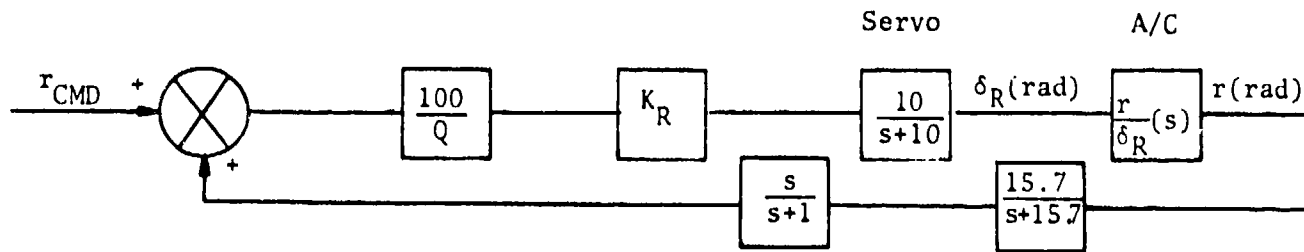
Flight Condition	Damping Ratio (ξ)	Natural Frequency (ω_n)
Low Q	.79	3.15 rad/sec
High Q	.49	3.47 rad/sec



HIGH Q FLIGHT CONDITION

PITCH AXIS ROOT LOCI - DOMINANT POLES
FIGURE 23

The yaw damper block diagram is shown in Figure 24.



SAS YAW DAMPER BLOCK DIAGRAM
FIGURE 24

Derivation of the aircraft transfer function $\frac{r}{\delta_R}$ (s) is shown in Appendix A

For the low Q flight condition

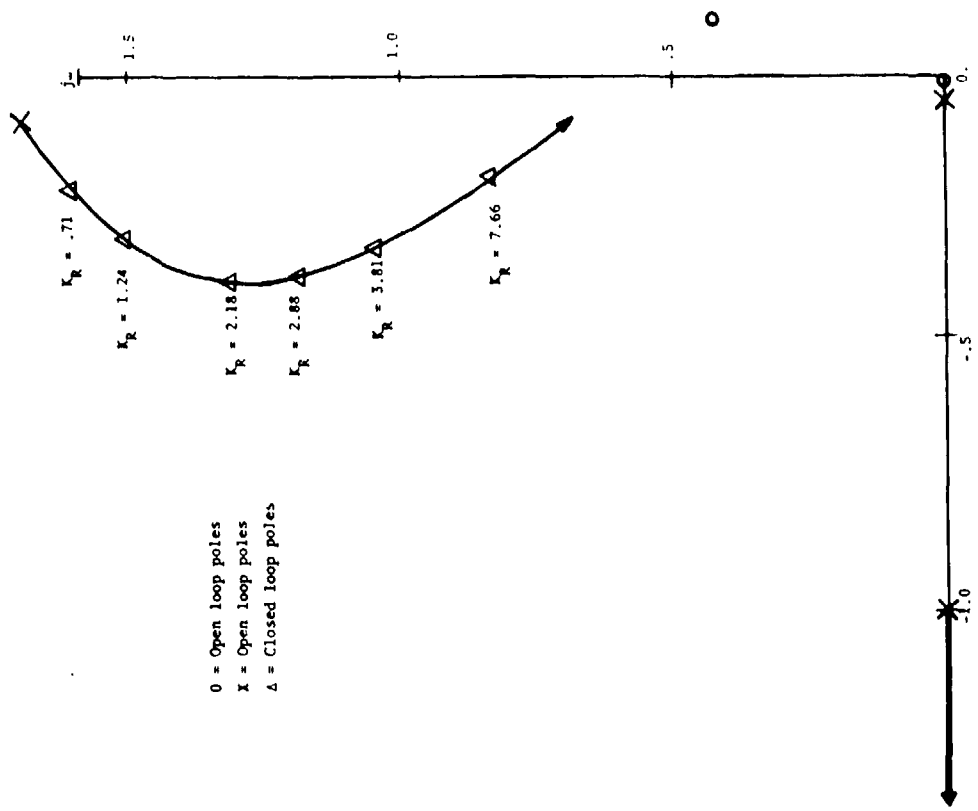
$$\frac{r}{\delta_R} (s) = \frac{-0.447(s+1.25)[(s-0.0934)^2 + (0.437)^2]}{(s+1.26)(s+0.00589)[(s+0.00586)^2 + (0.934)^2]} \quad (101)$$

For the high Q flight condition

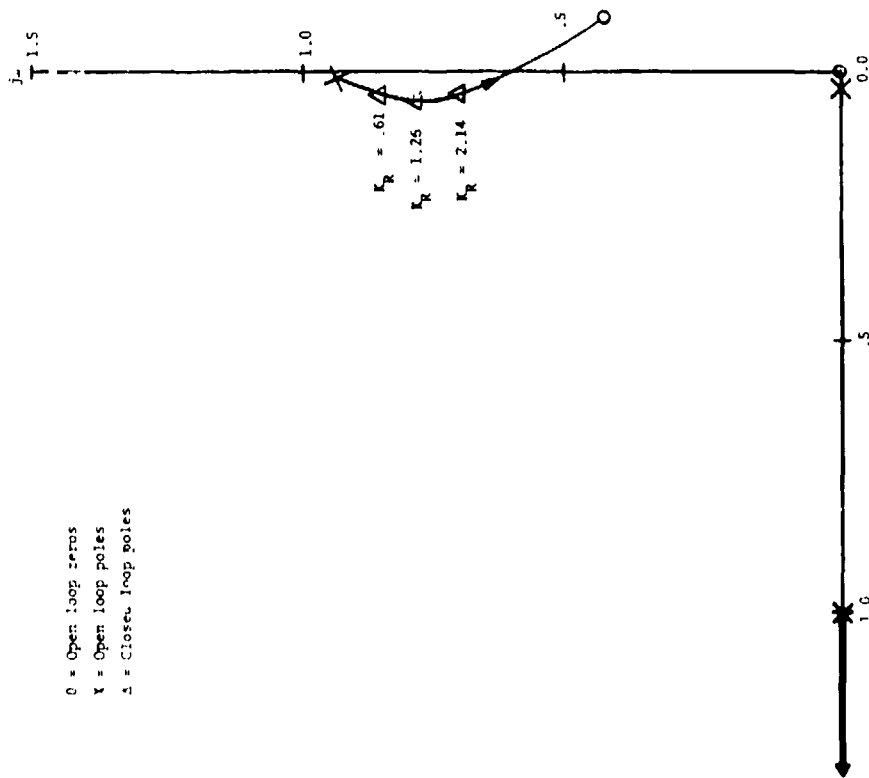
$$\frac{r}{\delta_R} (s) = \frac{-1.54(s+1.44)[(s-0.0976)^2 + (0.436)^2]}{(s+1.49)(s+0.00668)[(s+0.0913)^2 + (1.69)^2]} \quad (102)$$

The root loci for both conditions are shown in Figure 25. $K_R = 2$ was chosen for maximum damping of the dominant complex poles.

The roll axis SAS is shown in block diagram form in Figure 26.

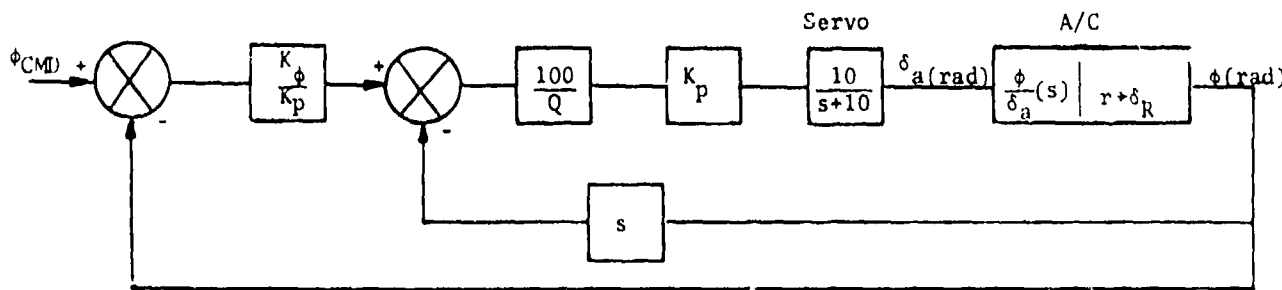


HIGH Q FLIGHT CONDITION



LOW Q FLIGHT CONDITION

YAW DAMPER ROOT LOCI - DOMINANT POLES
FIGURE 25



ROLL AXIS BLOCK DIAGRAM
FIGURE 26

In Figure 26,

K_ϕ = roll attitude feedback gain

K_p = roll rate feedback gain

$$\left. \frac{\phi}{\delta_a} (s) \right|_{r+\delta_R}$$

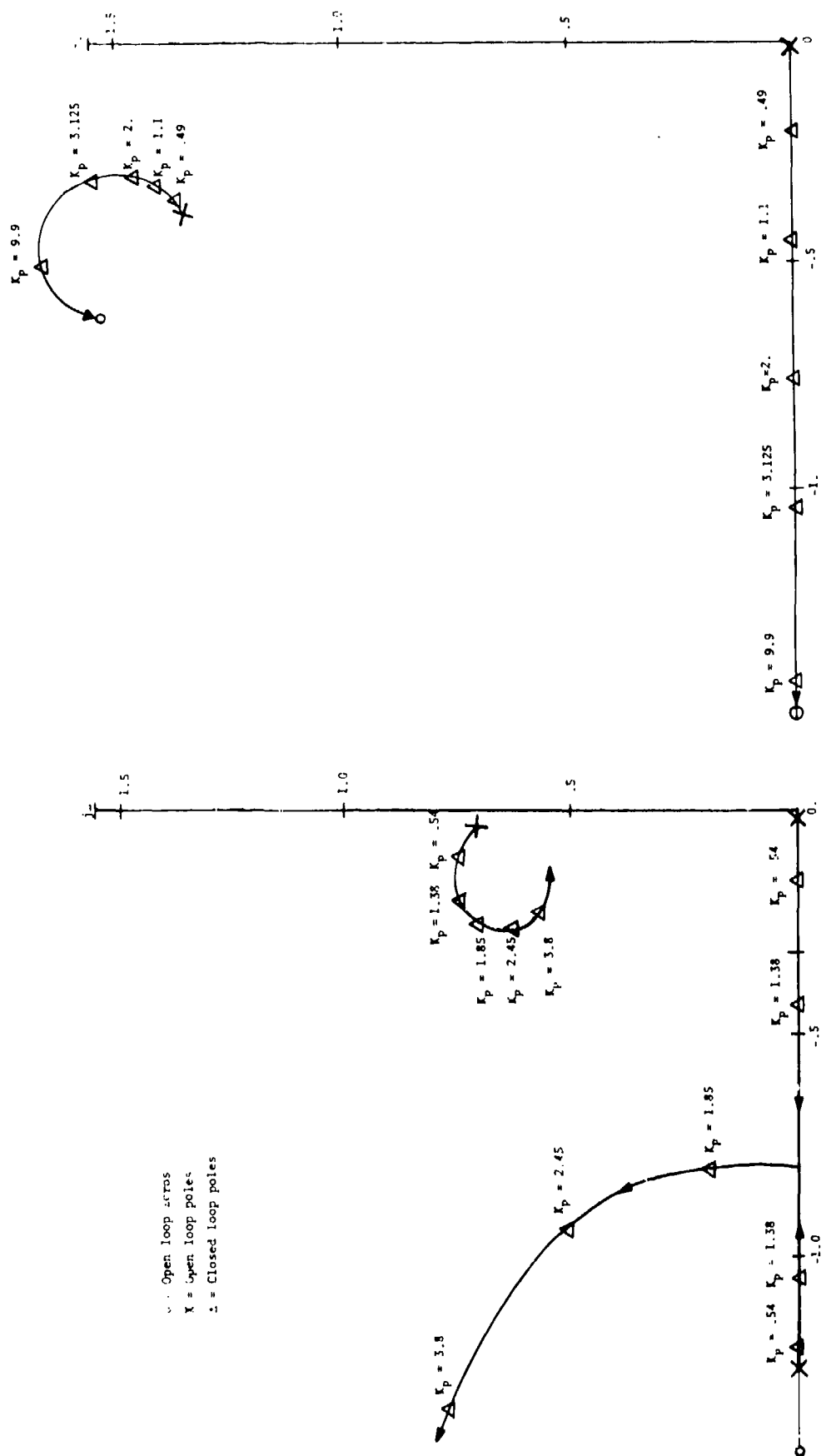
is the roll attitude to aileron transfer function with the yaw loop closed and is derived in Appendix A. The root locus for the lateral SAS was obtained by breaking the innermost loop and setting

$$\frac{K_\phi}{K_p} = 1.5$$

The root loci for both flight conditions are shown in Figure 27. A value of $K_p = 2.5$ was chosen for the roll rate gain. The characteristics of the dominant complex poles are summarized in Table VI.

TABLE VI
LATERAL SAS RESPONSE CHARACTERISTICS

Flight Condition	Damping Ratio (ξ)	Natural Frequency (ω_n)
Low Q	.4	.695 rad/sec
High Q	.2	1.53 rad/sec



HIGH Q FLIGHT CONDITION

ROLL SAS ROOT LOCI
FIGURE 27

LOW Q FLIGHT CONDITION

3.4.1.2 SAS Mechanization

The SAS dynamics were simulated on the laboratory analog computer with several of the gains computed digitally and set on the appropriate pots. The SAS block diagrams written in equation form become

$$\left[q \left(\frac{s}{s+1} \right) \left(\frac{4.55}{s+4.55} \right) + (\theta_{CMD} + \theta) \frac{K_\theta}{K_q} \right] \left(\frac{100}{Q} \right) k_q \left(\frac{10}{s+10} \right) = \delta_e \quad (103)$$

$$r \left(\frac{s}{s+1} \right) \left(\frac{15.7}{s+15.7} \right) \left(\frac{100}{Q} \right) K_R \left(\frac{10}{s+10} \right) = \delta_R \quad (104)$$

$$\left[(\phi_{CMD} - \phi) \frac{K_\phi}{K_p} - p \right] \left(\frac{100}{Q} \right) K_p \left(\frac{10}{s+10} \right) = \delta_a \quad (105)$$

Definitions of the terms used in equations 99 through 105 are given in Table VII.

These equations are scaled by redefining the problem variables as the ratios of the original variables divided by their maximum magnitude. For a 100-volt analog machine, a scaled variable with value 1 is equivalent to 100 volts. Maximum magnitudes assigned to the problem variables are shown in Table VIII.

Rewriting the SAS equations

$$\begin{aligned} \left[1.835 \left(\frac{s}{s+1} \right) \left(\frac{4.55}{s+4.55} \right) q' + 2.3375 \frac{K_\theta}{K_q} (\theta_{CMD} + \theta) \right] \frac{100K_q}{Q} \left(\frac{10}{s+10} \right) &= \delta_e' \\ .8K_R r' \left(\frac{s}{s+1} \right) \left(\frac{15.7}{s+15.7} \right) \left(\frac{100}{Q} \right) \left(\frac{10}{s+10} \right) &= \delta_R' \quad (106) \\ [K_\phi(\phi_{CMD} - \phi) - K_p p] \left(\frac{100}{Q} \right) 2.865 \left(\frac{10}{s+10} \right) &= \delta_a' \end{aligned}$$

The analog implementation of these equations is shown in Figure 28.

3.4.1.3 SAS Performance

The SAS design and mechanization was verified by recording the longitudinal and lateral SAS responses to pulse elevator and aileron deflections, respectively. Figures 29 and 30 show these responses. Table IX compares the recordings with the calculated SAS transient response characteristics.

TABLE VII
TERM DEFINITION, EQUATIONS 99 through 105

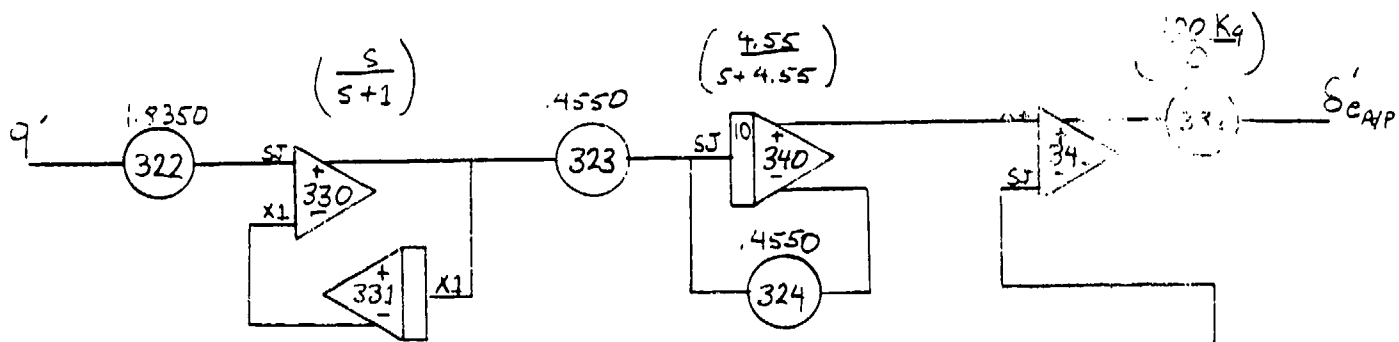
K_θ	=	pitch attitude feedback gain (rad/rad)
K_q	=	pitch rate feedback gain (rad/rad/sec)
K_R	=	yaw rate feedback gain (rad/rad/sec)
K_ϕ	=	roll attitude feedback gain (rad/rad/sec)
K_p	=	roll rate feedback gain (rad/rad/sec)
δ_e	=	elevator deflection angle (rad)
δ_R	=	rudder deflection angle (rad)
δ_a	=	aileron deflection angle (rad)
s	=	laplace transform operator
Q	=	dynamic pressure (lbs/ft ²)
h	=	altitude (ft)
M	=	Mach number
ρ	=	air density (slugs/ft ³)
V_T	=	total linear velocity (ft/sec)
α	=	angle of attack (deg)
s_{WCP}	=	stabilizer deflection angle (deg)
T	=	engine thrust (lbs)
r	=	yaw rate (rad/sec)
p	=	roll rate (rad/sec)
q	=	pitch rate (rad/sec)
ϕ	=	pitch attitude (rad)
ξ	=	damping ratio

TABLE VII
TERM DEFINITION, EQUATIONS 99 through 105 (Continued)

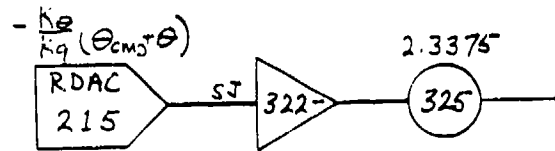
w_n	=	natural frequency (rad/sec)
\bar{c}	=	wing chord (20.16 ft/)
S	=	wing reference area (24.33 ft ²)
I_{YY}	=	pitch moment of inertia (slug-ft ²)
m	=	aircraft mass (4204 slugs)
g	=	gravity constant (32.2 ft/sec ²)
b	=	wing span (130.83 ft)
I_{XX}	=	roll moment of inertial (1.985x10 ⁶ slug-ft ²)
I_{ZZ}	=	yaw momemt of inertia (4.608x10 ⁶ slug-ft ²)
I_{XZ}	=	product of inertia (.147x10 ⁶ slug-ft ²)

TABLE VIII. PROBLEM VARIABLE SCALING

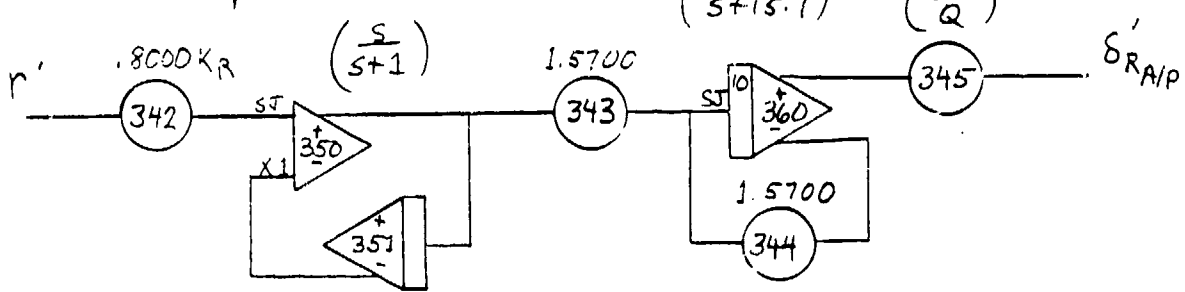
Symbol	Maximum Value	Scaled Variable
q	.785 rad/sec	$q' = \left[\frac{q}{.785} \right]$
δ_e	.4278 rad	$\delta_e' = \left[\frac{\delta_e}{.4278} \right]$
r	.349 rad/sec	$r' = \left[\frac{r}{.349} \right]$
δ_R	436	$\delta_R' = \left[\frac{\delta_R}{436} \right]$
δ_a	.349 rad	$\delta_a' = \left[\frac{\delta_a}{.349} \right]$



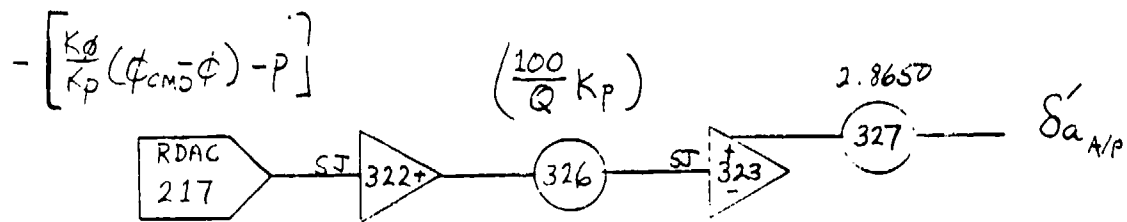
Longitudinal Autopilot



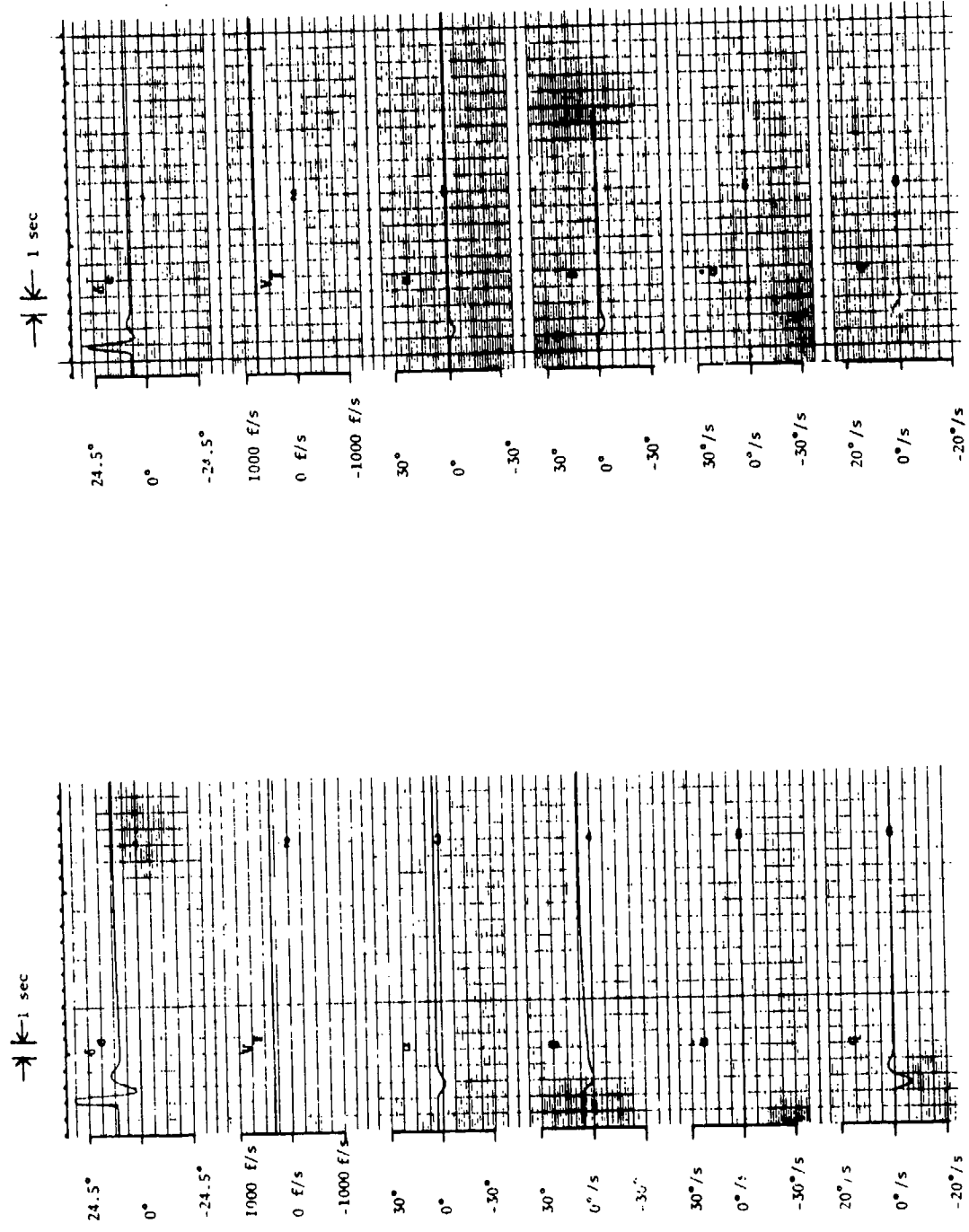
Yaw Damper



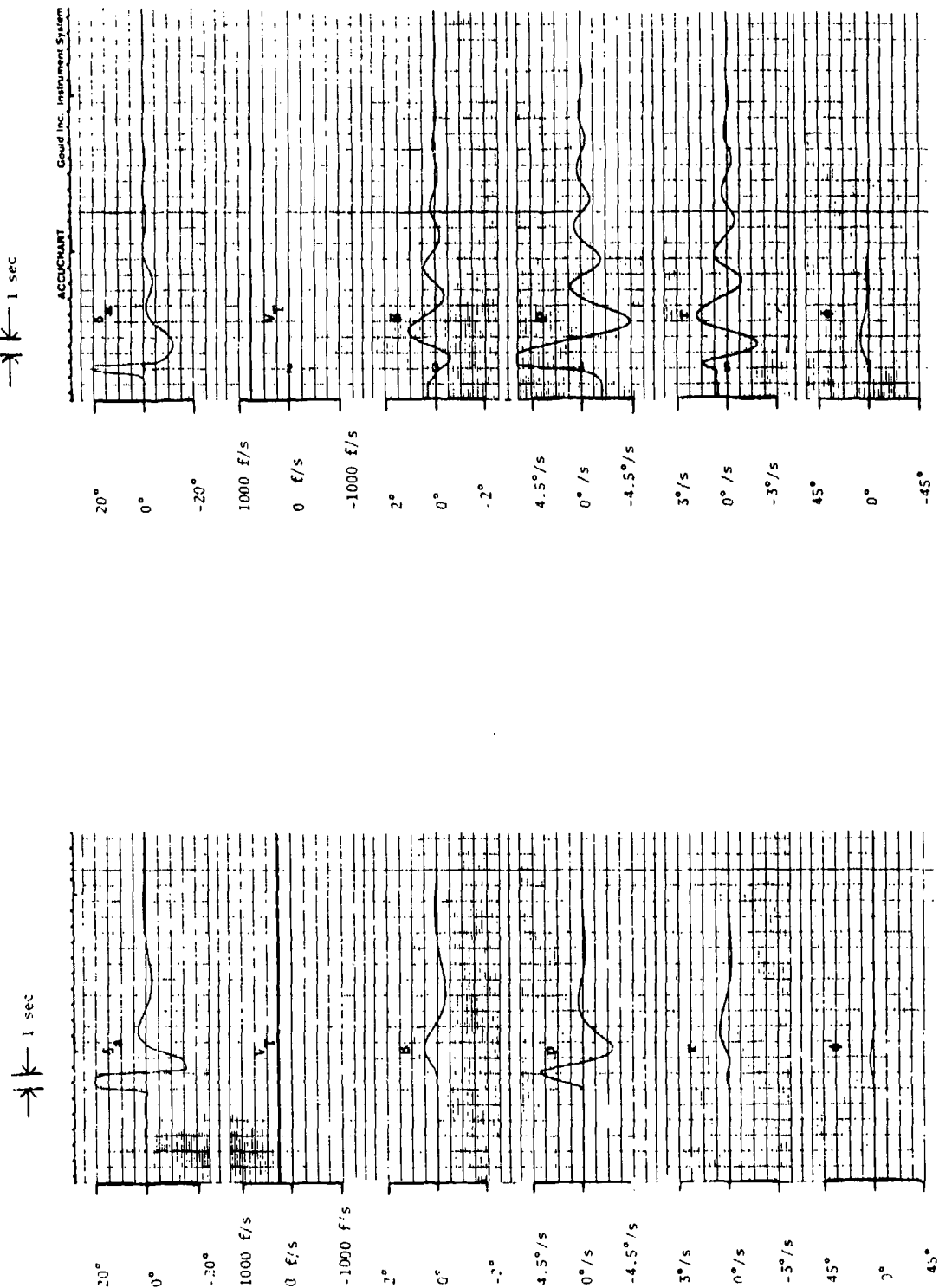
Lateral Autopilot



STABILITY AUGMENTATION SYSTEM CIRCUIT DIAGRAMS
FIGURE 28



HIGH Q FLIGHT CONDITION
 LOW Q FLIGHT CONDITION
 LONGITUDINAL SAS RESPONSE TO PULSE ELEVATOR DEFLECTION
 FIGURE 29



HIGH Q FLIGHT CONDITION
LOW Q FLIGHT CONDITION
LATERAL SAS RESPONSE TO PULSE AILERON DEFLECTION
FIGURE 30

TABLE IX
SAS DESIGN VERIFICATION

Axis	Flight Condition	Measured SAS Response		Calculated SAS Response	
		ξ	w_n (rad/sec)	ξ	w_n (rad/sec)
Longitudinal	Low Q	.8	3.14	.79	3.15
	High Q	.5	3.3	.49	3.47
Lateral/Directional	Low Q	.4	.698	.4	.695
	High Q	.14	1.57	.2	1.53

3.4.1.4 KC-135 Aerodynamics

Six-degree-of-freedom aircraft equations of motion were derived to simulate the KC-135 aircraft aerodynamics.

The equations of motion of an airframe referred to Eulerian axes are:

$$\begin{bmatrix} \dot{U} \\ \dot{V} \\ \dot{W} \end{bmatrix} = \frac{1}{\text{mass}} \begin{bmatrix} \Sigma F_X \\ \Sigma F_Y \\ \Sigma F_Z \end{bmatrix} + \begin{bmatrix} 0 & r & -q \\ -r & 0 & p \\ q & -p & 0 \end{bmatrix} \begin{bmatrix} U \\ V \\ W \end{bmatrix} \quad (107)$$

$$\begin{bmatrix} \dot{p} \\ \dot{q} \\ \dot{r} \end{bmatrix} = \begin{bmatrix} I_{XX} & 0 & -I_{XZ}^{-1} \\ 0 & I_{YY} & 0 \\ -I_{XZ} & 0 & I_{ZZ} \end{bmatrix} \begin{bmatrix} \Sigma L \\ \Sigma M \\ \Sigma N \end{bmatrix} \begin{bmatrix} 0 & r & -q \\ -r & 0 & p \\ q & -p & 0 \end{bmatrix} \begin{bmatrix} I_{XX} & 0 & -I_{XZ} \\ 0 & I_{YY} & 0 \\ -I_{XZ} & 0 & I_{ZZ} \end{bmatrix} \begin{bmatrix} p \\ q \\ r \end{bmatrix} \quad (108)$$

The Euler angle rates

$$\begin{bmatrix} \dot{\phi} \\ \dot{\theta} \\ \dot{\psi} \end{bmatrix} = \begin{bmatrix} 1 & \sin\phi\tan\theta & \cos\phi\tan\theta \\ 0 & \cos\phi & -\sin\phi \\ 0 & \sin\phi/\cos\theta & \cos\phi/\cos\theta \end{bmatrix} \begin{bmatrix} p \\ q \\ r \end{bmatrix} \quad (109)$$

The external forces and moments acting on the aircraft consist of aerodynamic, propulsion, and gravity components. The translational equations are solved using the wind axis system since it is well known that much lower accuracy and speed demands are made on computer mechanization than a body axis solution.⁷ The aerodynamic forces defined in the stability axis system and the gravity and propulsion forces defined in the body axis system are transformed into the wind axis coordinate system as shown below.

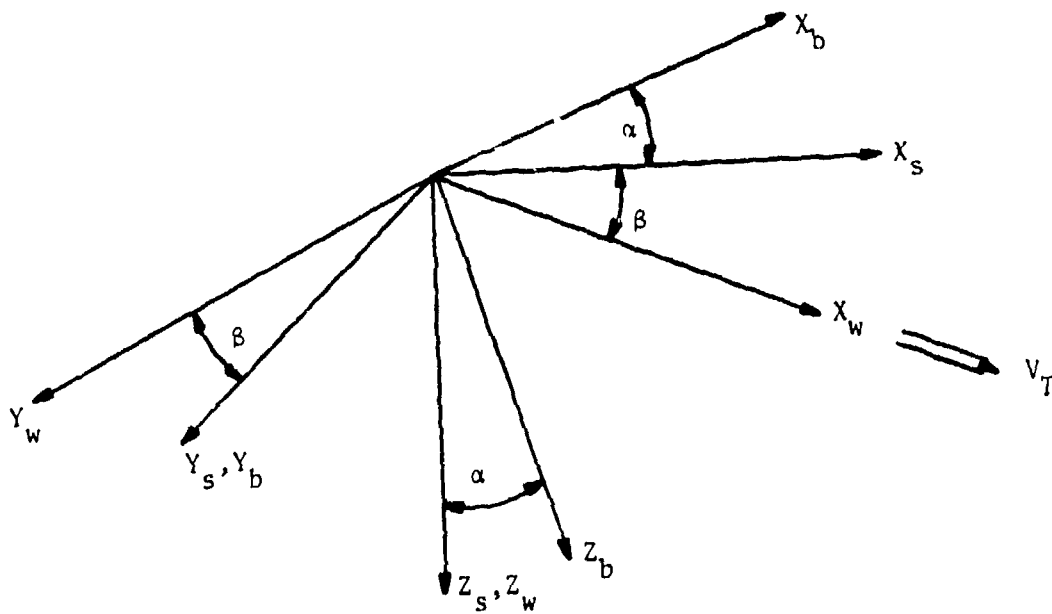
$$\begin{bmatrix} X_w \\ Y_w \\ Z_w \end{bmatrix} = \begin{bmatrix} \Sigma F_X \\ \Sigma F_Y \\ \Sigma F_Z \end{bmatrix} = \begin{bmatrix} \cos\beta & \sin\beta & 0 \\ -\sin\beta & \cos\beta & 0 \\ 0 & 0 & 1 \end{bmatrix} \begin{bmatrix} X_s \\ Y_s \\ Z_s \end{bmatrix} + \begin{bmatrix} \cos\alpha & 0 & \sin\alpha \\ 0 & 1 & 0 \\ -\sin\alpha & 0 & \cos\alpha \end{bmatrix} \begin{bmatrix} T \\ 0 \\ 0 \end{bmatrix} + W \begin{bmatrix} -\sin\theta \\ \cos\theta \sin\phi \\ \cos\theta \cos\phi \end{bmatrix} \quad (110)$$

By definition, the velocity vector of the aircraft (V_T) is along the X_w axis and, therefore, $\dot{W}_w = W_w = \dot{V}_w = V_w = 0$. We have then

$$\begin{aligned} m\dot{V}_T &= X \\ mV_T r_w &= Y_w \quad \text{or} \quad r_w = Y_w / mV_T \\ mV_T q_w &= Z_w \quad \text{or} \quad q_w = -Z_w / mV_T \end{aligned} \quad (111)$$

where r_w and q_w are flight path axis angular rates about the Z_w and X_w axes, respectively. Equations for $\dot{\alpha}$ and $\dot{\beta}$ are derived⁷ from the geometrical relationships between axis systems (Figure 31).

⁷Feasibility Study for Integrated Flight Trajectory Control (Airlift). LSI Report # GRR-008-0177A, AFFDL-TR-77-120, contract F33615-74-C-3083.



BODY, STABILITY, AND WIND AXIS SYSTEM GEOMETRIES
FIGURE 31

$$\dot{\alpha} = \left(\frac{1}{\cos\beta} \right) \left\{ [q_s \cos\beta - p_s \sin\beta] + \frac{z_w}{mV_T} \right\} \quad (112)$$

$$\dot{\beta} = \frac{y_w}{mV_s} - r_s$$

After expanding and simplifying, the following translational equations result:

$$\begin{aligned} \dot{V}_T &= X_w/m \\ \dot{\beta} &= Y_w/mV_T - r \\ \dot{\alpha} &= Z_w/(mV_T \cos\beta) + q_s - p_s \tan\beta \end{aligned} \quad (113)$$

The rotational equations of motion are computed in the stability axis. After simplification we have

$$\begin{bmatrix} \dot{p}_b \\ \dot{q}_b \\ \dot{r}_b \end{bmatrix} = \begin{bmatrix} (I_1 r_b + I_2 p_b) q_b + I_3 L_b + I_4 N_b \\ I_5 r_b p_b + I_6 (r_b^2 - p_b^2) + I_7 M_b \\ (I_8 p_b + I_9 r_b) q_b + I_4 L_b + I_{10} N_b \end{bmatrix} \quad (114)$$

where

$$\begin{aligned} I_1 &= \frac{(I_{YY} - I_{ZZ}) I_{ZZ} - I_{XZ}^2}{I_{XX} I_{ZZ} - I_{XZ}^2} & I_2 &= \frac{(I_{XX} - I_{YY} + I_{ZZ}) I_{XZ}}{I_{XX} I_{ZZ} - I_{XZ}^2} \\ I_3 &= \frac{I_{ZZ}}{I_{XX} I_{ZZ} - I_{XZ}^2} & I_4 &= \frac{I_{XZ}}{I_{XX} I_{ZZ} - I_{XZ}^2} \\ I_5 &= \frac{I_{ZZ} - I_{XX}}{I_{YY}} & I_6 &= \frac{I_{XZ}}{I_{YY}} \\ I_7 &= \frac{1}{I_{YY}} & I_8 &= \frac{(I_{XX} - I_{YY}) I_{XX} + I_{XZ}^2}{I_{XX} I_{ZZ} - I_{XZ}^2} \\ I_9 &= \frac{(I_{YY} - I_{ZZ} - I_{XX}) I_{XZ}}{I_{XX} I_{ZZ} - I_{XZ}^2} & I_{10} &= \frac{I_{XX}}{I_{XX} I_{ZZ} - I_{XZ}^2} \end{aligned} \quad (115)$$

The aerodynamic forces and moments are defined below.

$$\begin{aligned} X_s &= -\frac{1}{2} \rho V_T^2 S C_D & L_s &= \frac{1}{2} \rho V_T^2 S b C_\ell \\ Y_s &= \frac{1}{2} \rho V_T^2 S C_Y & M_s &= \frac{1}{2} \rho V_T^2 S c C_m \\ Z_s &= -\frac{1}{2} \rho V_T^2 S C_L & N_s &= \frac{1}{2} \rho V_T^2 S b C_n \end{aligned} \quad (116)$$

The dimensionless aerodynamic coefficients (C_D , C_Y , C_L , C_ℓ , C_m , C_n) were obtained with assumptions defined in Section 3.2.1.

With reference to Appendix A, the Aerodynamic coefficient equations for simulation requirements, reduce to the following:

$$\begin{aligned}
C_D &= C_{D_{\text{BASIC}}} \\
C_Y &= \left(\frac{dC_Y}{d\beta} \right)_{M=0} \cdot \frac{(C_Y)_{\beta M}}{(C_Y)_{\beta M=0}} \cdot \beta + \frac{b}{2V_T} \left[\frac{dC_Y}{dp_s} \cdot p_s + \left(\frac{dC_Y}{dr_s} \right)_{M=0} \cdot \frac{(C_Y)_{r M}}{(C_Y)_{r M=0}} \cdot r_s \right] \\
&\quad + (\Delta C_Y)_{R M=0} \cdot \frac{(\Delta C_Y)_{R M}}{(\Delta C_Y)_{R M=0}} \\
C_L &= C_{L_{\text{BASIC}}} + (\Delta C_L)_{\alpha_{WCP}=0^\circ} + \Delta \left(\frac{dC_L}{d\alpha} \right)_{\alpha_{WCP}} + \frac{\bar{c}}{2V_T} \left[\frac{dC_L}{d\dot{\alpha}} \cdot \dot{\alpha} + \frac{dC_L}{dq_s} \cdot q_s \right] \\
&\quad + K_E \cdot \frac{dC_L}{d\delta_e} \cdot \delta_e \\
C_\ell &= \left(\frac{dC_\ell}{d\beta} \right)_{\beta=0} \cdot \frac{(C_\ell)_{\beta E}}{(C_\ell)_{\beta R}} \cdot \beta + \frac{b}{2V_T} \left[\left(\frac{dC_\ell}{dp_s} \right)_{M=0} \cdot \frac{(C_\ell)_{p M}}{(C_\ell)_{p M=0}} \cdot p_s \right. \\
&\quad \left. + \left(\frac{dC_\ell}{dr_s} \right)_{M=0} \cdot \frac{(C_\ell)_{r M}}{(C_\ell)_{r M=0}} \cdot r_s \right] + K_{\delta_{A_I}} \cdot (\Delta C_{\ell_{A_I}}) \cdot \frac{(C_{\ell_{A_I}})_{M}}{(C_{\ell_{A_I}})_{M=0}} \cdot \left(\frac{R_E}{R_R} \right) C_{\ell_{A_I}} \\
&\quad + K_{\delta_R} \cdot (\Delta C_\ell)_{\delta_R=25^\circ} \cdot \frac{(\Delta C_Y)_{M}}{(\Delta C_Y)_{M=0}} \\
C_m &= C_{m .25} + (\Delta C_{m .25})_{\alpha_{WCP}=0^\circ} + \frac{dC_m}{d\alpha} \cdot .25 \cdot \alpha_{WCP} \\
&\quad + \frac{\bar{c}}{2V_T} \left[\frac{dC_m}{d\dot{\alpha}} \cdot \dot{\alpha} + \frac{dC_m}{dq_s} \cdot q_s \right] + K_E \cdot \frac{dC_m}{d\delta_e} \cdot \delta_e \\
C_n &= \left(\frac{dC_n}{d\beta} \right)_{M=0} \cdot \frac{(C_n)_{\beta M}}{(C_n)_{\beta M=0}} + \frac{b}{2V_T} \left[\left(\frac{dC_n}{d\beta} \right)_{M=0} \cdot \frac{(C_n)_{\beta M}}{(C_n)_{\beta M=0}} \cdot \beta + \frac{dC_n}{dp_s} \cdot p_s \right. \\
&\quad \left. + \left(\frac{dC_n}{dr_s} \right)_{M=0} \cdot \frac{(C_n)_{r M}}{(C_n)_{r M=0}} \cdot r_s \right] + K_{\delta_{A_I}} \cdot (\Delta C_{n_{A_I}}) \cdot \frac{(C_{n_{A_I}})_{M}}{(C_{n_{A_I}})_{M=0}}
\end{aligned} \tag{117}$$

The terms of the aerodynamic coefficient equations are stored in computer memory in a table lookup format. Term definitions have been given previously after equation 59.

The KC-135 aerodynamics were incorporated in a complete man-in-the-loop simulation using a hybrid analog/digital computer and our two-man cockpit.

The driving function inputs to the simulation, as mechanized in the block diagram of figure 32, are the cockpit stick and throttle controls manipulated by the "pilot".

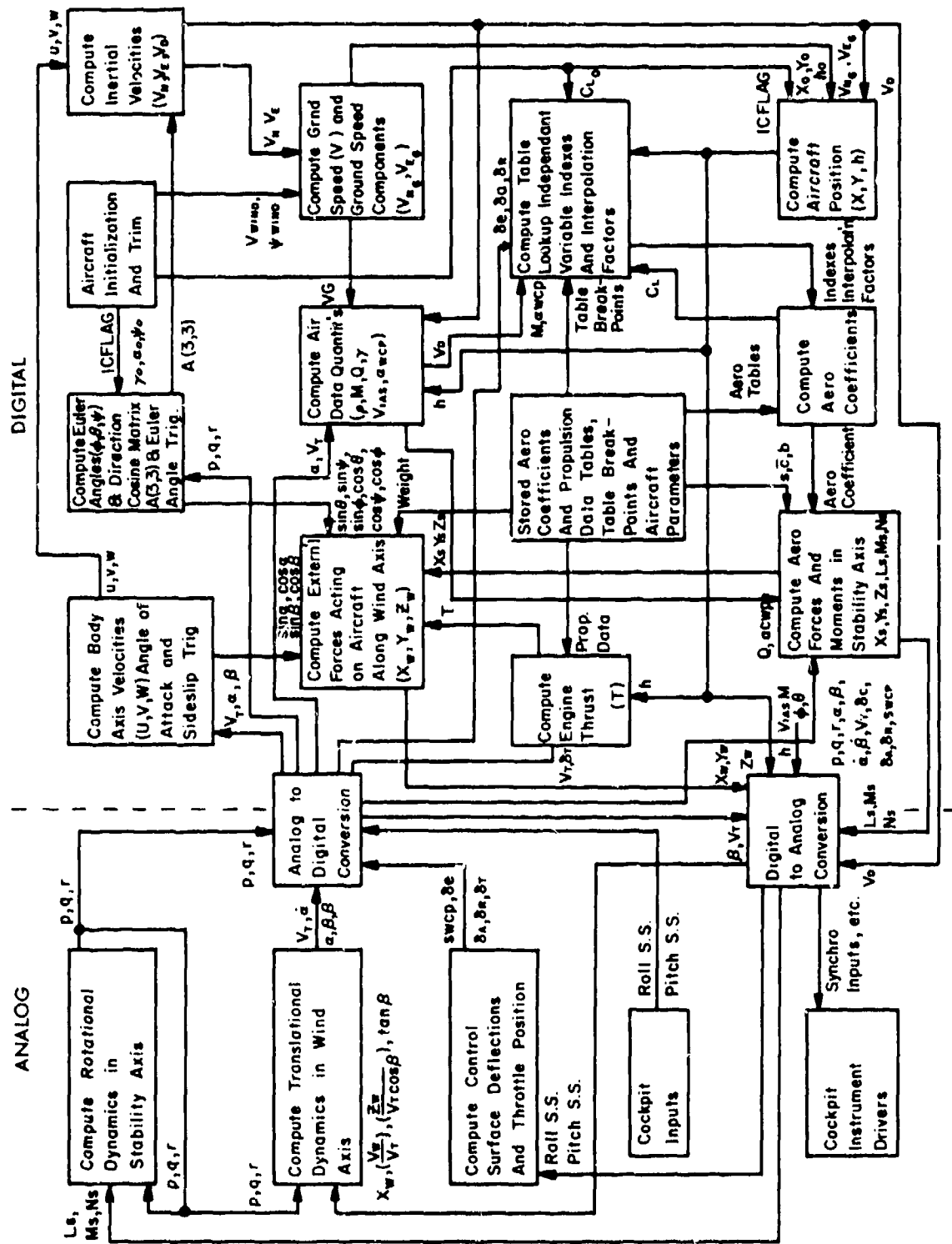
The computations performed by the blocks indicated with an asterick have been previously described. The remaining blocks perform the following computations:

□ Body Axis Velocity Computations

$$\begin{aligned} U &= V_T \cdot \cos\alpha \cos\beta \\ V &= V_T \cdot \sin\beta \\ W &= V_T \cdot \sin\alpha \cos\beta \end{aligned} \tag{118}$$

□ Euler angles and direction cosine matrix computations

$$\begin{aligned} \phi &= \int(p + \dot{\psi} \sin\theta) dt \\ \theta &= \int(q \cos\phi - r \sin\phi) dt \\ \psi &= \int[(\dot{\phi} - p) \sin\theta + (q \sin\phi + r \cos\phi) \cos\theta] dt \\ \phi &= \tan^{-1} \left(\frac{\sin\phi}{\cos\phi} \right) \\ \theta &= \tan^{-1} \left(\frac{\sin\theta}{\cos\theta} \right) \\ \psi &= \tan^{-1} \left(\frac{\sin\psi}{\cos\psi} \right) \end{aligned} \tag{119}$$



SIMULATION BLOCK DIAGRAM
FIGURE 32

$$\underline{A} = \begin{bmatrix} \cos\psi\cos\theta & \cos\theta\sin\psi & -\sin\theta \\ \cos\psi\sin\theta\sin\phi & \cos\psi\cos\phi & \cos\theta\sin\phi \\ -\sin\psi\cos\phi & +\sin\psi\sin\theta\sin\phi & \\ \cos\psi\sin\theta\cos\phi & \sin\psi\sin\theta\cos\phi & \cos\theta\cos\phi \\ +\sin\psi\sin\phi & -\cos\psi\sin\phi & \end{bmatrix} \quad (121)$$

□ Inertial velocity computations

$$\begin{bmatrix} V_N \\ V_E \\ V_D \end{bmatrix} = \underline{A}^T \begin{bmatrix} U \\ V \\ W \end{bmatrix} \quad (122)$$

□ Ground speed computations

$$\begin{aligned} V_{Ng} &= V_N + V_W \cos\psi_w \\ V_{Eg} &= V_E + V_W \sin\psi_w \end{aligned} \quad (123)$$

$$V_g = \sqrt{V_{Ng}^2 + V_{Eg}^2}$$

□ Aircraft position computations

$$\begin{aligned} x &= \int V_{Ng} dt \\ y &= \int V_{Eg} dt \\ h &= \int -V_D dt \end{aligned} \quad (124)$$

□ Air data computations

$$\begin{aligned}
 \rho &= \left[\rho_0 \cdot 1. - 1.835 \left(\frac{h}{65536} \right) + \left(\frac{h}{65536} \right)^2 \right] \\
 M &= \frac{V_T}{1116.4[1. - 3.683 \times 10^{-6}h]} \\
 Q &= .5 \rho V_T^2 \\
 \gamma &= \tan^{-1} \left(\frac{-V_D}{V_g} \right) \\
 V_{IAS} &= V_T \sqrt{\frac{\rho}{\rho_0}}
 \end{aligned} \tag{125}$$

□ EPR, thrust, and thrust transient computations

$$\begin{aligned}
 EPR_{CMD} &= EPR(\delta_t, M, h) \\
 \dot{EPR} &= (EPR_{CMD} - EPR)/1.3 \\
 T &= 4 \cdot \text{THRUST}(EPR, M)
 \end{aligned} \tag{126}$$

□ Control surface computations

$$\begin{aligned}
 \dot{\delta}_a &= (\delta_{a,CMD} - \delta_a)/.1 \\
 -20^\circ &\leq \delta_a \leq 20^\circ \\
 \dot{\delta}_e &= (\delta_{e,CMD} - \delta_e)/.1 \\
 -24.5 &\leq \delta_e \leq 15 \\
 \dot{\delta}_R &= (\delta_{R,CMD} - \delta_R)/.1 \\
 -25^\circ &\leq \delta_R \leq 25^\circ \\
 .5^\circ &\leq s_{WCP} \leq 13.7^\circ
 \end{aligned} \tag{127}$$

The translational and rotational equations of motion and the control surface dynamics programmed on the analog computer were scaled by redefining the problem variables as the ratios of the original variables divided by their maximum magnitude. For a 100-volt analog machine, a scaled variable with value 1 is equivalent to 100 volts. Maximum magnitudes assigned to the problem variables are shown in Table X.

Solving the rotational equations of motion using the redefined problem variables we have

$$\begin{aligned}\dot{p}' &= .2123 r' q' + .0320 p' q' + .6433 L'_S + .0205 N'_S \\ \dot{q}' &= .4887 r' p' + .0122 r'^2 - .0616 p'^2 + .6802 M'_S \\ \dot{r}' &= -.2075 p' q' - .0320 r' q' + .0461 L'_S + .6232 N'_S\end{aligned}\quad (128)$$

The translational equations of motion become

$$\begin{aligned}\dot{v}'_T &= 2.4266 X'_W \\ \dot{\beta}' &= .3491 \frac{Y'_W}{v'_T} - r'_S \\ \dot{\alpha}' &= .2325 \frac{Z'_W}{v'_T \cos \beta} + q' - 1.4981 p' \tan \beta\end{aligned}\quad (129)$$

and the control surface dynamics are

$$\begin{aligned}\dot{\delta}'_e &= (\delta'_{e_{CMD}} - \delta'_e) / .1 \quad -1. \leq \delta'_e \leq .6122 \\ \dot{\delta}'_a &= (\delta'_{a_{CMD}} - \delta'_a) / .1 \quad -1. \leq \delta'_a \leq 1. \\ \dot{\delta}'_R &= (\delta'_{R_{CMD}} - \delta'_R) / .1 \quad -1. \leq \delta'_R \leq 1. \\ &\quad -.0357 \leq s'_{WCP} \leq 1\end{aligned}\quad (130)$$

TABLE X
MAXIMUM VALUES

SYMBOL	MAXIMUM VALUE	SCALED VARIABLE
X_W	50000. slugs-ft/sec ²	$X'_W = \frac{X_W}{50000}$
$\frac{Y_W}{V_T}$	500 slugs/sec	$\frac{Y'_W}{V'_T} = \frac{Y_W/V_T}{500}$
$\frac{Z_W}{V_T \cos \beta}$	500 slugs/sec	$\frac{Z'_W}{V'_T \cos \beta} = \frac{Z_W/V_T \cos \beta}{500}$
L_S	1000000. ft-lbs	$L'_S = \frac{L_S}{1000000.}$
M_S	1000000. ft-lbs	$M'_S = \frac{M_S}{1000000.}$
N_S	1000000. ft-lbs	$N'_S = \frac{N_S}{1000000.}$
P	.785 rad/sec	$P' = \frac{P}{.785}$
τ	.524 rad/sec	$\tau' = \frac{\tau}{.524}$
q	.349 rad/sec	$q' = \frac{q}{.349}$
\dot{p}	.785 rad/sec ²	$\dot{p}' = \frac{\dot{p}}{.785}$
$\dot{\tau}$.524 rad/sec ²	$\dot{\tau}' = \frac{\dot{\tau}}{.524}$
\dot{q}	.349 rad/sec ²	$\dot{q}' = \frac{\dot{q}}{.349}$
$\dot{\alpha}$.524 rad/sec	$\dot{\alpha}' = \frac{\dot{\alpha}}{.524}$
$\dot{\beta}$.349 rad/sec ²	$\dot{\beta}' = \frac{\dot{\beta}}{.349}$
β	.349 rad/sec	$\beta' = \frac{\beta}{.349}$
\dot{v}_T	10 ft/sec ²	$\dot{v}'_T = \frac{\dot{v}_T}{10}$
v_T	1000 ft/sec	$v'_T = \frac{v_T}{1000}$
δ_e	24.5°	$\delta'_e = \frac{\delta_e}{24.5}$
δ_a	20°	$\delta'_a = \frac{\delta_a}{20.}$
δ_R	25°	$\delta'_R = \frac{\delta_R}{25}$
δ_{WCP}	13.75°	$\delta'_{WCP} = \frac{\delta_{WCP}}{}$

The preceding equations, together with the cockpit trunking, were implemented as shown in the analog circuit diagrams contained in Appendix C.

The digital computations are performed every 50 milliseconds. A functional flowchart of these computations is contained in Appendix C.

Aircraft response to pulse elevator and pulse aileron deflections are shown in Figures 33 and 34 for both a high Q and a low Q flight condition. Table XI compares the simulated and desired aircraft models by presenting the characteristics of the dominant lateral and longitudinal aircraft modes.

TABLE XI
AIRCRAFT DYNAMICS VERIFICATION

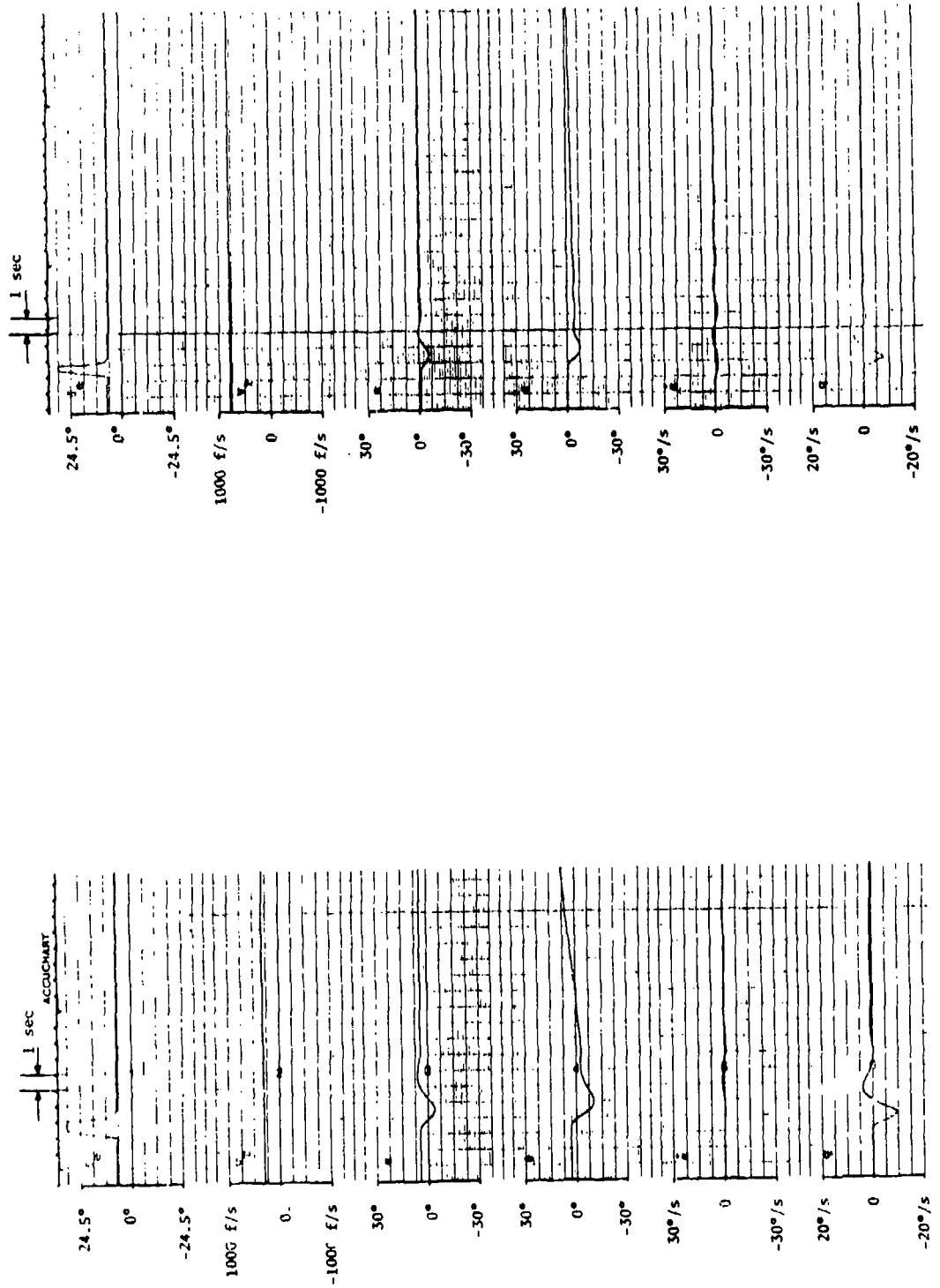
MODE	FLIGHT CONDITION	SIMULATED AIRCRAFT			DESIRED AIRCRAFT		
		ξ	ω_n	τ	ξ	ω_n	τ
Short Period	Low Q^*	.6	1.5	-	.614	1.42	-
	High Q^*	.4	2.86	-	.48	2.94	-
Rolling	Low Q	-	-	1.4	-	-	1.5
	High Q	-	-	1.4	-	-	1.44
Dutch Roll	Low Q	.035	.967	-	.0093	.923	-
	High Q	.05	1.57	-	.054	1.69	-

* Low Q : $h = 5000'$ * High Q : $h = 25000'$
 $V = 274.8$ $V = 763.4$
 $\alpha = 7.19^\circ$ $\alpha = -36^\circ$
 $Q = 77.4$ $Q = 310.3$

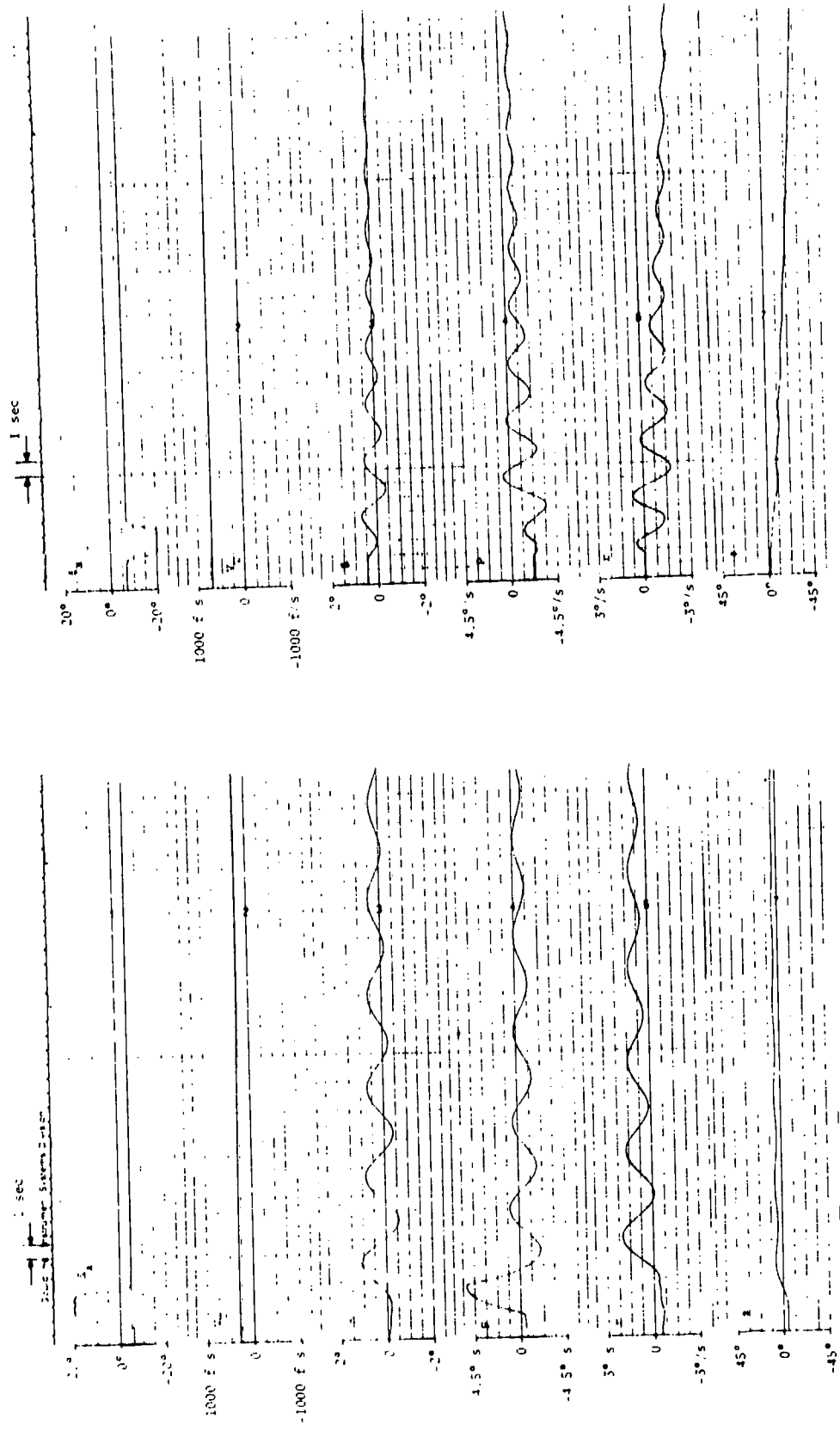
3.4.2 Rehosting of IFTC Algorithms

The IFTC algorithms, developed on previous AFFDL programs, were incorporated in a closed-loop simulation through a general purpose IBM-370 computer. This IBM computer was not dedicated to the Simulation Laboratory but was accessed through a real-time monitor.

The KC-135 cockpit simulator was upgraded by rehosting the IFTC algorithms from the IBM-370 computer to a dedicated PDP-11/70 simulation computer.



HIGH Q FLIGHT CONDITION
LONGITUDINAL AIRCRAFT RESPONSE TO PULSE ELEVATOR DEFLECTION
FIGURE 33



HIGH Q FLIGHT CONDITION
 LOW Q FLIGHT CONDITION
 LATERAL AIRCRAFT RESPONSE TO PULSE AILERON DEFLECTION
 FIGURE 34

Because of the unreliability of the real-time monitor, this change in the mechanization of the simulation increased the time availability and efficiency of the simulator. Simultaneously with this rehosting of the software, the algorithms were upgraded to include racetrack pattern and spiral climb capability of the aircraft.

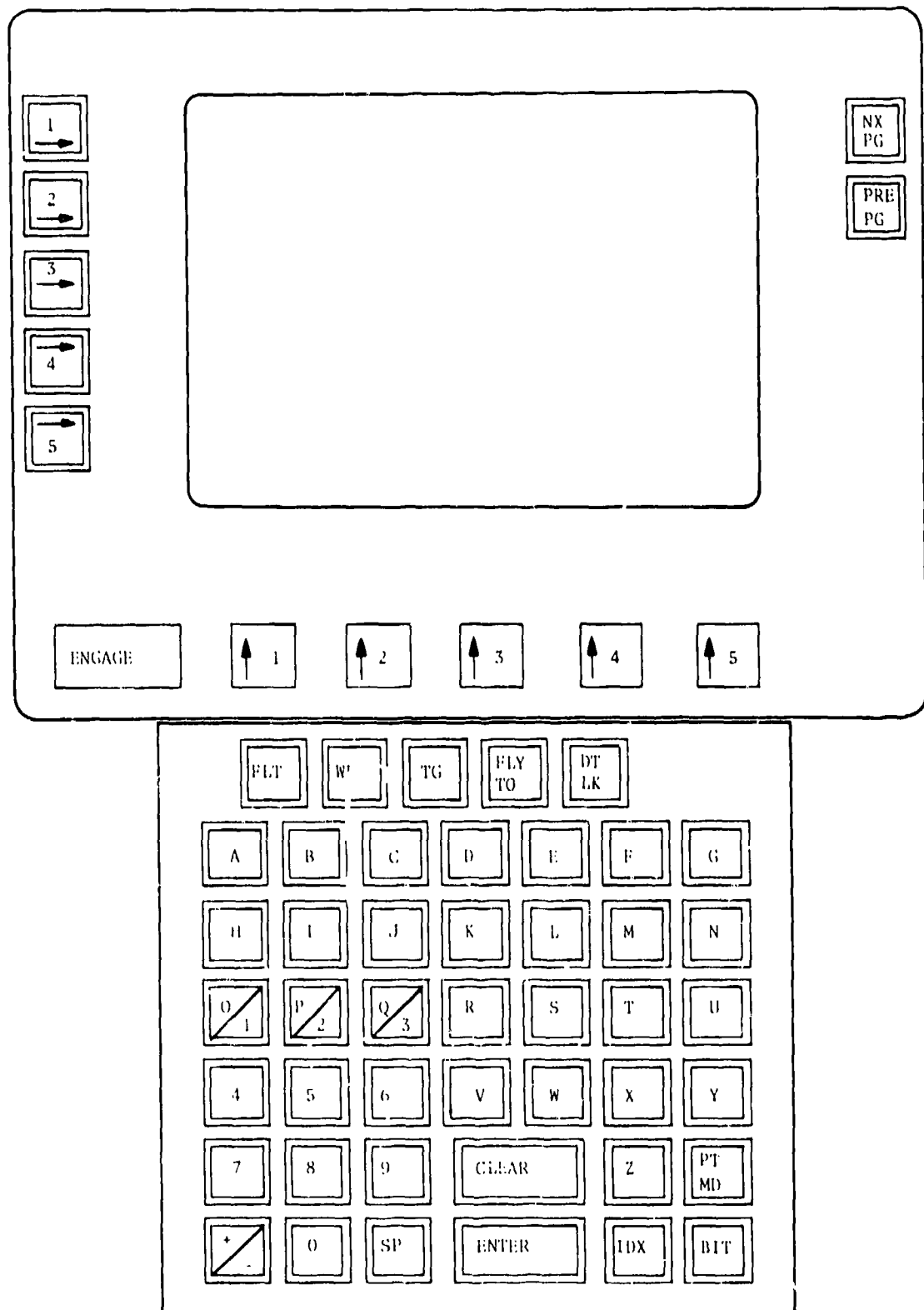
The planned incorporation of the threat avoidance algorithms was never completed because the specific form of the algorithms, suitable for implementation on our airborne avionics computer, was not available.

The review of the software during the rehosting process provided several areas for simplification and improvement of the software to improve portability and performance.

3.4.3 Controller/Display Modification

The controller/display in the cockpit was modified by addition of a refresh memory to provide increased performance of the display and to provide modified row/column matrix select keys to improve the flexibility of menu select and modification functions.

Figure 35 is a faceplate of the controller/display currently installed in the transport cockpit.



NEW DUAL SEAT COCKPIT CONTROLLER/DISPLAY CONFIGURATION
FIGURE 35

RECOMMENDED FLIGHT TEST PLAN

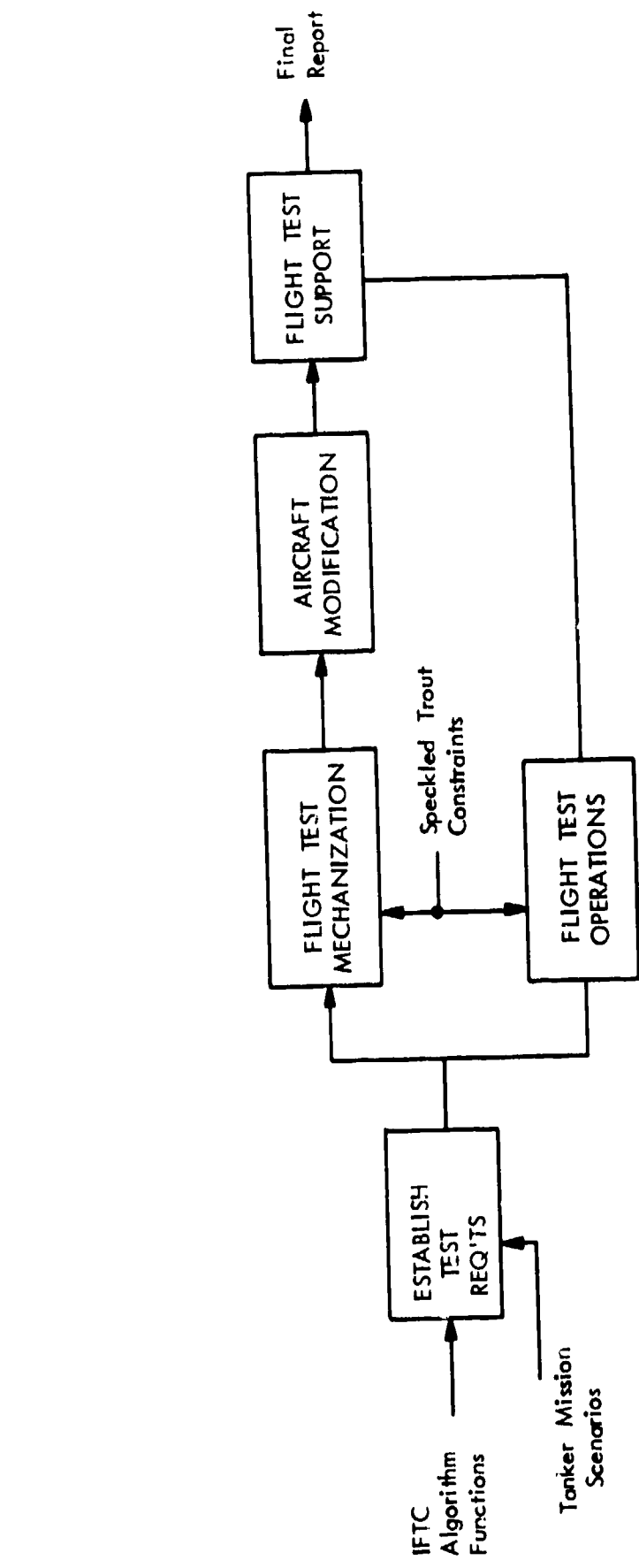
Although the optimal flight trajectory control algorithms are not yet state-of-the-art for systems, the baseline classical integrated flight trajectory control algorithms have been simulated but not demonstrated in an operational aircraft. The purpose of this flight test plan is to define a program that will use the Speckled Trout aircraft to demonstrate the operational utility of the conventional IFTC algorithms in the KC-135 tanker mission.

4.1 FLIGHT TEST PLAN OVERVIEW

The major tasks and other relationships for the flight test plan are shown in Figure 36, Task Flow Diagram.

Typical KC-135 Tanker mission scenarios are analyzed for operational requirements of the avionics system. These requirements are then compared to the unique capabilities of the IFTC algorithms to establish the principal flight test requirements of time control and in-flight mission redirect. The avionics system mechanization and flight test scenarios that are necessary to demonstrate the test requirements are limited to mechanical and operational constraints of the flight test aircraft. The mechanized constraints are primarily cockpit panel space and rack availability for the equipment. The operational constraints are the limited time availability for modifications to the aircraft and the requirement to maintain a flightworthy operational avionics suite throughout this test program. Our basic concept to achieve these difficult operational restrictions is to configure a three-phase modification and test procedure.

Air Force personnel will perform the actual equipment installation, check out the data collection, perform the data and analysis with support from LSI. The Air Force is currently developing the software for an operational flight program and critical elements of the avionics update program. This system--which will be tested functionally on the bench and operationally in a fixed-base simulator--will contain the IFTC algorithm functional capabilities. This system, or an existing LSI commercial-hardware equivalent with software modifications, is proposed for this flight test.



TASK FLOW DIAGRAM, FLIGHT TEST PLAN
FIGURE 36

4.2 FLIGHT TEST FUNCTIONAL REQUIREMENTS ANALYSIS

The mission of the KC-135 aircraft is to provide air refueling and/or air/land stores delivery anywhere in the world while operating with a three-man crew. This general mission requirement, and the specific operational scenarios of three typical missions⁸, both explicitly and implicitly define the functional requirements for the avionics system of the aircraft. The detailed functional requirements for navigation, guidance, flight plan management, communications, performance management, control and display are outlined in the following paragraphs. These detailed functional requirements provide the basis for the flight test system mechanization (Section 4.3).

4.2.1 General Navigation

A fundamental avionics system requirement is the capability to determine the aircraft position and velocity, with respect to the current mission plan and to other aircraft, with a minimum crew workload.

These general capabilities imply the following specific requirements:

- a. Communications with mission control and other mission aircraft.
- b. Measurement of relative position/velocity vectors with respect to other mission aircraft using cooperative and/or non-cooperative sensors.
- c. Knowledge of, and ready access to, current navigation data associated with foreign and domestic route structures, airways, waypoints, navigation aids and terminal areas for mission planning.
- d. Utilization of existing and future civil and military external navigation aids.

Because enemy action may shut down these external navigation aids during all or part of some missions (e.g., Mildenhall EWO mission) the aircraft must achieve the minimum acceptable navigation performance with only self-contained dead reckoning equipment.

For minimum crew workload the navigation system must have the capability to automatically select the best available combination of internal/external navigation sensors, throughout the mission, and integrate their outputs to obtain a best estimate of the aircraft navigation state.

⁸R.P. Madero, TAACE Scenario Update, Bunker-Ramo Document No. 4506-020-5100-9, May 1979.

4.2.2 Guidance

The basic air refueling mission, particularly those involving SAC receivers, requires precise ARCP/ARCT rendezvous. Explicit in this basic mission requirement are functional avionics system capabilities for precise mission time control and in-flight mission redirect.

The general requirement for precise time control implies the following specific capabilities for the avionics system:

- a. Automatic generation of a reference flight path in four dimensions that is constrained only by the dynamics of the aircraft and the waypoints specified by missions planning.
- b. Automatic prediction of the future position and velocity of the aircraft from the estimates of the present aircraft state as generated by the navigation system.
- c. Automatic generation of steering and throttle commands that will minimize errors between the aircraft present position and the desired position of the mission plan.

The general requirements for precise in-flight mission redirect implies specific capabilities for easy reference path modification by manual inputs from the crew (see Controller/Display, Section 4.2.5). These changes in reference path may be required to avoid unforeseen threats such as weather (mildenhall EWO mission) with minimum disruption of the SAC receiver mission plan. Or, the reference path may require a change in order to reach out in performing a rendezvous in minimum time with fighter aircraft returning from the battle area with unsufficient fuel to make the original ARCP (BODO contingency mission).

Also implicit in the general requirements for precise time control and in-flight mission redirect is the specific requirement to minimize tanker fuel consumption in order to maximize fuel available for offloading (see Performance, Section 4.2.4). This specific requirement results from the fact that the KC-135, in flight, draws fuel from the same fuel supply that is used to refuel the receivers.

4.2.3 Flight Plan Management

The functional requirements of the navigation system for knowledge of and access to a current worldwide navigation data base of the guidance system to generate a reference flight path through mission waypoints specified in four dimensions imply the following two functions for flight plan management:

- a. Accept, edit, and store the navigation data associated with commercial and military route structures, airways, waypoints, navigation aids and terminal areas. These data must be updated every month.
- b. Accept, edit and store the particular mission waypoint sequence at the initiation of each mission.

For minimum crew workload and aircraft system reaction time (preflight preparation), this data should be loaded automatically into the avionics system (see Controller/Display).

4.2.4 Performance

The KC-135 aircraft, in flight, draws from the same fuel supply that is used to refuel the receivers. The functional requirement of aircraft performance management is to minimize the fuel consumed by the tanker in order to maximize the fuel available for offloading. In order to meet this functional requirement, the mission time constraint of ARCT should be compatible with the mission position constraint of ARCP. For example, at 250 KIAS refueling velocity, a time constraint of ± 1 minute corresponds to a position constraint on ARCP of ± 5 nautical miles. The associated fuel savings is approximately 200 pounds per minute.

Minimum fuel consumption enroute implies the following required capabilities:

- a. Control of the fuel offloaded from various tanks in order to maintain proper c.g. of the aircraft to minimize aerodynamic drag of the aircraft.
- b. Flight mode control, within constraints of the mission planning to achieve a specified ARCP/ARCT, for minimum fuel consumption. These modes, for example, include maximum economy climb-out, cruise, and descent, and wind trades to obtain operating altitude for minimum fuel burn during cruise.
- c. Operation of the engines at optimum engine pressure ratio for minimum fuel consumption through all flight regimes.

In addition, in order to assure maximum time in the rendezvous refueling pattern (BODO contingency mission), the Aircraft Performance Management System must continuously compute projected fuel remaining at end of mission.

4.2.5 Controller/Display

The principal function of Controller/Display is to allow efficient management of the aircraft by the crew. In general, this requires both specific dedicated displays and integrated controller/displays that are functionally interactive with the crew. Specifically, these requirements include:

- a. Integrated alphanumeric controller/displays for monitoring and controlling system operational modes, flight plans, and aircraft system status.
- b. Integrated graphics displays for showing the aircraft situation in both horizontal and vertical planes and in relation to the current flight plan, identified threats such as weather, and friendly and bogey aircraft in the operational area.
- c. Dedicated displays for warning of critical system malfunction and for monitoring and control of aircraft dynamics and engine performance (altitude, altitude, airspeed, engine pressure ratio).
- d. Dedicated controls for automatic entry of initial flight plan data and navigation data base.

4.2.6 Communications

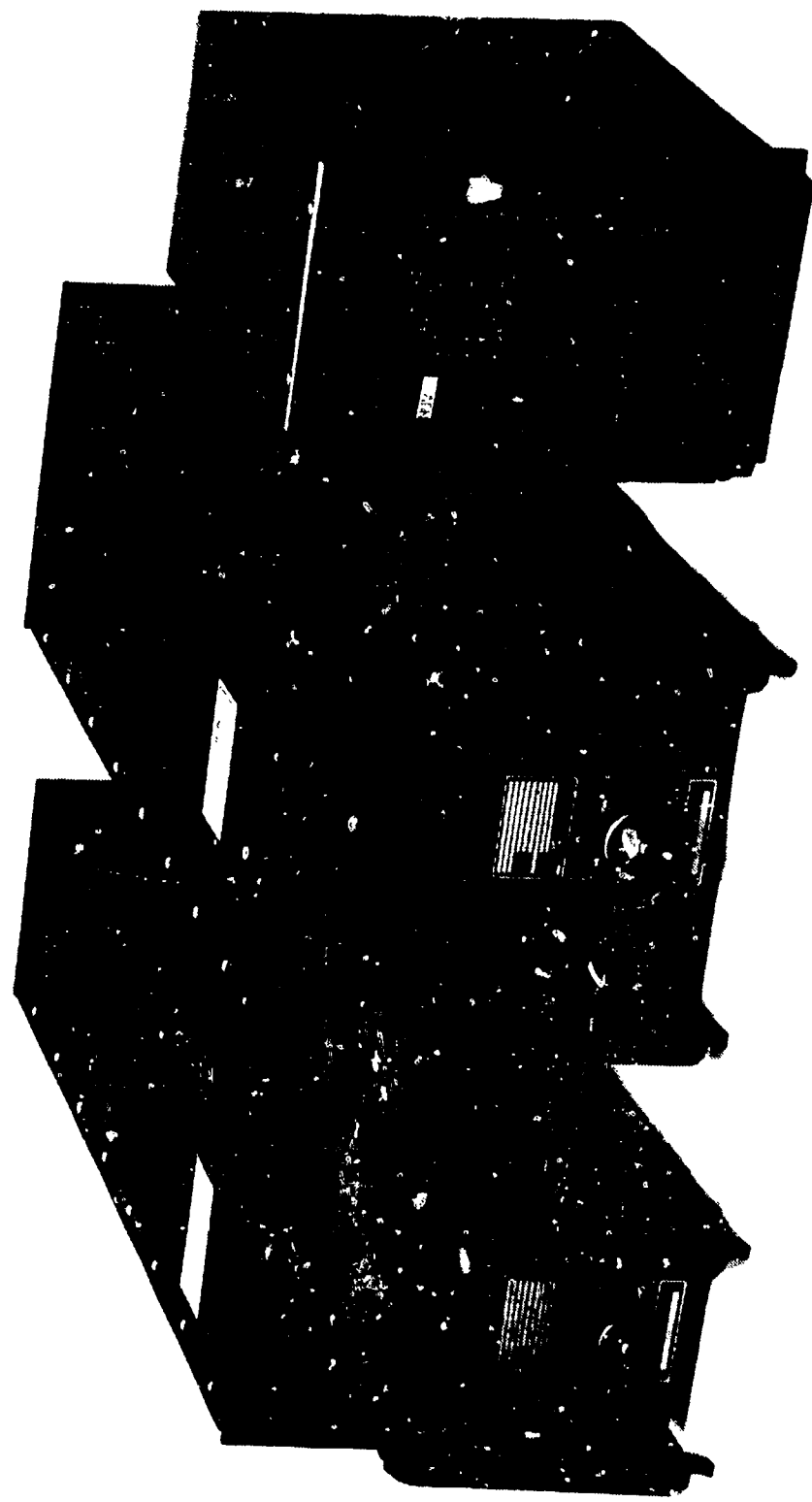
The aircraft must have direct communications with other operational units in the mission, the fuel receivers, and ground control. The required information includes status of area friendly and enemy aircraft, weather patterns that may affect the mission, and ground control missions redirect information.

4.3 FLIGHT TEST SYSTEM MECHANIZATION

The proposed flight test avionics system mechanization is based on our commercial Performance Navigation Computer System (PNCS), developed for the Boeing Aircraft Company Models 727 and 737 aircraft and/or the system currently being developed by ASD/EN for the KC-135 avionics update program.

4.3.1 Functional Description

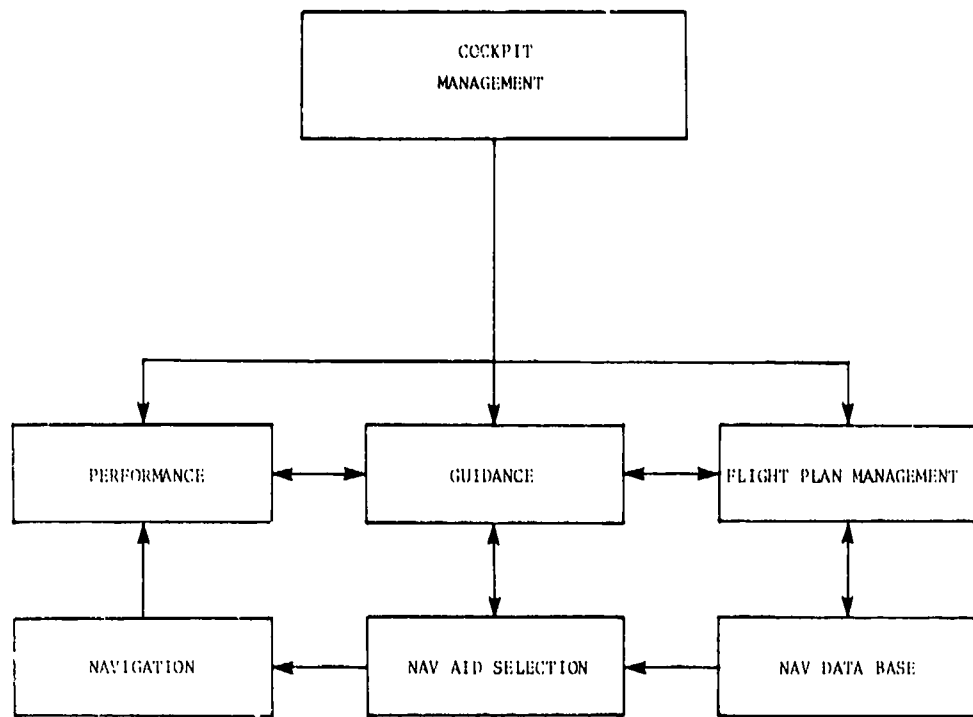
The PNCS shown in Figure 37 is a functionally integrated performance/guidance mission management system. The system software that is currently being adapted and modified for the KC-135 avionics update program includes the trajectory generator, path prediction, and guidance algorithms of the Integrated Flight Trajectory Control system.



PERFORMANCE NAVIGATION COMPUTER SYSTEM

FIGURE 5-

The functional block diagram of the proposed flight test system is shown in Figure 38.



FUNCTIONAL BLOCK DIAGRAM, FLIGHT TEST SYSTEM
FIGURE 38

The cockpit management function allows pilot interactive interface with the mission management system through a conventional controller/display unit and a multifunction display with graphics capability. This interface allows control of the system by access, insertion, and modification of data in the flight plan management, guidance, and performance functions of the system.

The flight plan management function includes flight plan selection, editing, insertion or deletion, and waypoint sequencing.

The flight plan management function maintains two flight plans: engaged and temporary. The engaged flight plan controls the aircraft through guidance and cockpit management functions. The editing function of the engaged flight plan is limited to providing supplementary information from the navigation data base to the cockpit management function to define the airports, navaids, and waypoints associated with the plan. The temporary flight plan may be modified by waypoint insertion and/or deletion through interaction with the cockpit management function and using data from the navigation data base and guidance function. The temporary flight plan may become the engaged flight plan or request from the cockpit management function.

The waypoints of both the engaged and temporary flight plans are sequenced, as a function of the current state of the aircraft, on command from the guidance function. The major guidance functions are path prediction, path generation, and steering.

Path prediction processing generates time-of-flight parameters based on the specified waypoint sequence of the flight plan and the desired performance mode of operation.

Guidance path processing generates the reference aircraft flight path to correspond to the waypoint sequence that defines the flight path. This function also uses the current aircraft state from the navigation function to determine the progress of the aircraft in relation to the desired or reference flight path. Guidance path processing also generates a modification to the refueling holding point pattern to make the KC-135 turn out ahead of the receiver aircraft for refueling rendezvous, and for capture of the flight path on takeoff and ILS beam on landing. The steering function generates lateral and longitudinal steering commands and throttle commands.

The navigation function integrates aircraft state measurement data from on-board dead-reckoning and ground-based position sensors. The navigation function draws on a supply of reference data that is carried on board. This navigation data base includes location and characteristics of ground-based navigation aids, standard approach and departure routes in landing sites, and standard airways.

The performance functions are takeoff, c.g. control, flight mode control, and performance data computation.

Takeoff calculates data to predict successful takeoff based on aircraft weight, outside air temperature, wind vector, runway length and condition and possible loss of one engine.

The c.g. calculation computes and controls total c.g. of the aircraft based on fuel burned and offloaded from each fuel tank.

The flight mode computes target EPR and airspeed commands for all flight modes: Takeoff, climb, cruise, descent, hold, maximum continuous, go-around, and turbulence.

The performance processing generates data used by the flight crew to investigate various flight profiles. This data, which would normally be obtained by reference to a flight operations manual, consists of data load, flight level intercept, flight level investigation, ground speed, range and endurance, fuel, temperature, landing flap/speed, trip planning, and wind. This data is shown to the pilot either in the form of α -N advisories or in its direct effect on the generated flight path on the map display.

4.3.2 Physical Description

The phase modular character of the proposed flight test allows initial limited objective tests with a system mechanization that provides less than the full functional capability required for the total mission management system. This system partitioning, however, also provides a piecemeal approach to implementing a new avionics system in the test aircraft so that down-time for installation and checkout are limited and flight test risks are reduced.

Three successively more complete system configurations are proposed for flight test: baseline, interim, and full-up mission management system.

4.3.2.1 Phase One Configuration: Baseline System

For Phase One of the flight demonstration program, a single-thread, baseline system will be installed. This baseline system consists of the following units:

- One Mission Management Computer Unit (MMC)
- One Fuel Savings Advisory System Computer (FSAS)
- One Controller/Display Unit (CDU)

The inputs required from the auxiliary equipment currently on the Speckled Trout aircraft to generate the fuel savings (performance) functions are the following:

- a. An accurate source of total air temperature data which is available from the Honeywell CADC (HG-180/W-747).

- b. Air data inputs of pressure altitude from the CADC.
- c. Calibrated or indicated airspeed from the CADC.
- d. Engine bleed air status for anti-ice and cabin pressure.

To generate the guidance and navigation functions, the required inputs are the following:

- a. Magnetic heading for heading/airspeed dead reckoning navigation.
- b. Range and bearing from ground-based reference points provided by VOR/TACAN stations.
- c. Present position and velocity information from the inertial navigation system (INS).

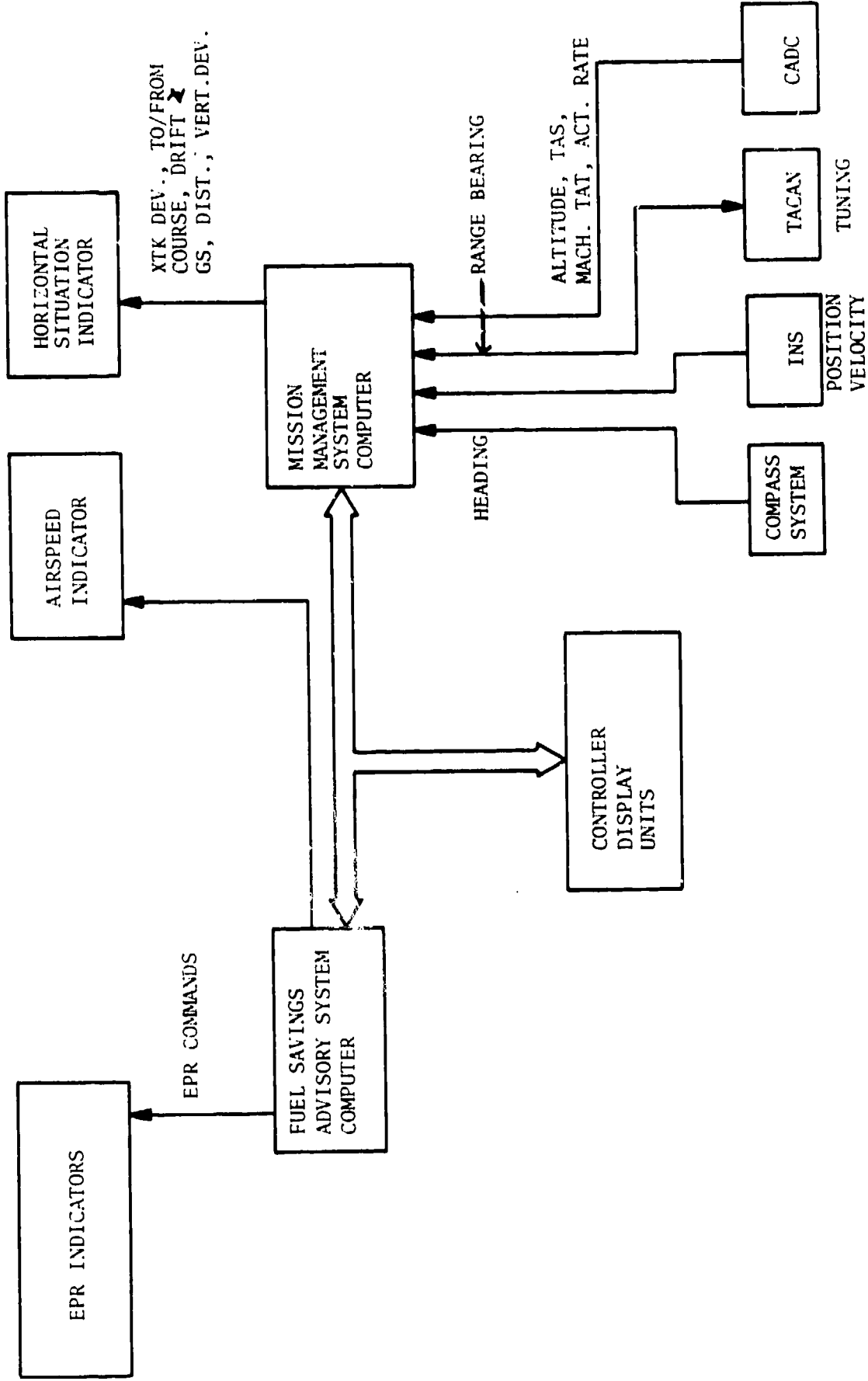
The baseline system output information will be supplied as advisory flight instrument indications to the copilot only. These advisory indications will be as follows:

- a. Copilot's ADI fast/slow needle or MACH/IAS-driven bug for time control.
- b. Copilot's HSI for V-NAV and L-NAV guidance as follows:
 - The course pointer to indicate a course representing the sum of measured track angle error and drift angle (TKE + DA).
 - The drift angle cursor.
 - The lateral deviation bar, which displays a linear displacement representing cross-track error (XTK).
 - Ground speed and distance.
 - Engine pressure ratio command.

The baseline system interconnect block diagram is shown in Figure 39.

For all system configurations, the mission management computer fuel savings computer and in-flight data recorder for flight test analysis are mounted in the equipment bays.

COPILOT INSTRUMENTS



INTERFACE DIAGRAM, BASELINE SYSTEM
FIGURE 39

4.3.2.2 Phase Two Configuration: Interim System

For Phase Two, the system will be expanded by addition of a multifunction display that will have graphics capability for HSI and HSD/VSD information. The HSD/VSD will show the horizontal/vertical projections of the flight plan with defining waypoints as well as present position of the aircraft and time prediction.

This MFD will also have capability for overlay of weather radar signals on the HSD information to show relation of the projected flight path to local weather conditions.

The interim system may be interfaced to the Speckled Trout to provide copilot advisories only for manual control or, as an option, can be directly interfaced to the AFCS/autothrottle to provide completely automatic guidance and control of the vehicle.

The interface diagram of the interim system is shown in Figure 40.

4.3.2.3 Phase Three Configuration: All-up MMS

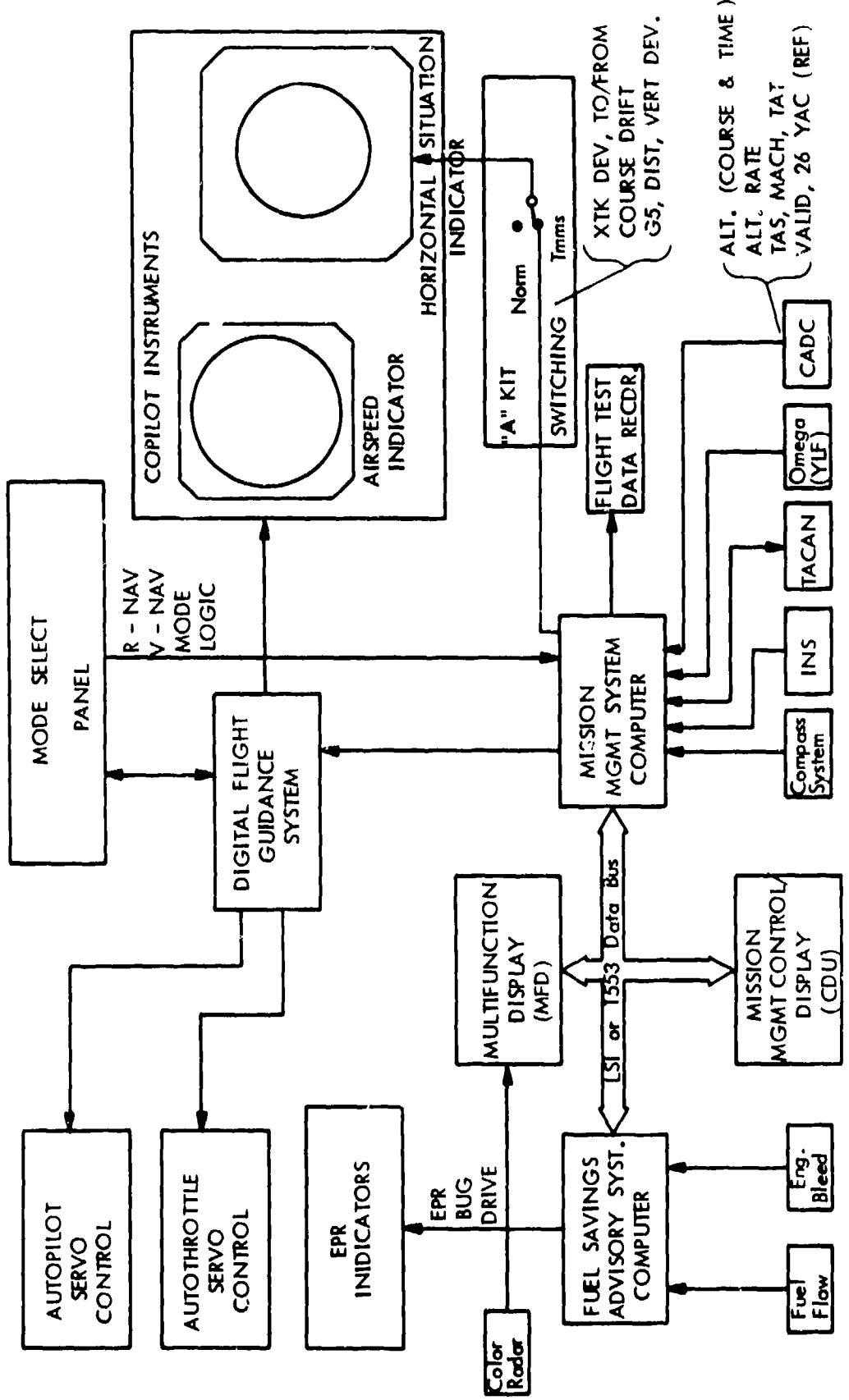
The final all-up mission management configuration is a dual redundant system. To upgrade the interim system to the final configuration requires the following additional units.

- Mission Management Computer (optional)
- Control/Display Unit
- Multifunction Display Unit
- Fuel Management Panel

The additional mission management computer is optional since it is not a flight safety critical item and may be required only as a backup bus controller if the system elements are integrated by a MIL-STD-1553 data bus. As an alternate solution, the FSAS computer function may be expanded to act as a backup bus controller.

The additional CDU and MFD are to provide the mission management system interface to the pilot's side of the cockpit.

The fuel panel is miniaturized with respect to the existing equipment. This allows space on the cockpit control panel for the additional electronic displays. This fuel panel, however, provides an additional important function of controlling fuel out of the tanks so that the c.g. of the tanker is maintained at approximately ideal location for minimum drag and hence minimum fuel consumption.



INTERFACE DIAGRAM, INTERIM SYSTEM
FIGURE 40

Figure 41 is the interface diagram for the complete flight test mission management system.

4.3.3 Flight Test System Installation Plan

Although the final installation configuration must be determined through a formal Space Allocation Requirement Program (SARP) and a formal Cockpit Configuration Review Board (CCRB), an on-site inspection of the Speckled Trout aircraft was conducted in order to recommend a preliminary plan for the hardware installation.

4.3.3.1 Avionics Equipment Bay Installation

The avionics equipment bays directly aft of the flight deck, as confirmed by Speckled Trout project personnel, is the appropriate area for installation of the "B" kit component of the Tanker Mission Management System. However, because these avionics equipment bays are space critical, and the space available for equipment installation frequently changes, we currently have no specific equipment mounting recommendations. These specifics will be established during the installation design phase of the proposed flight test program.

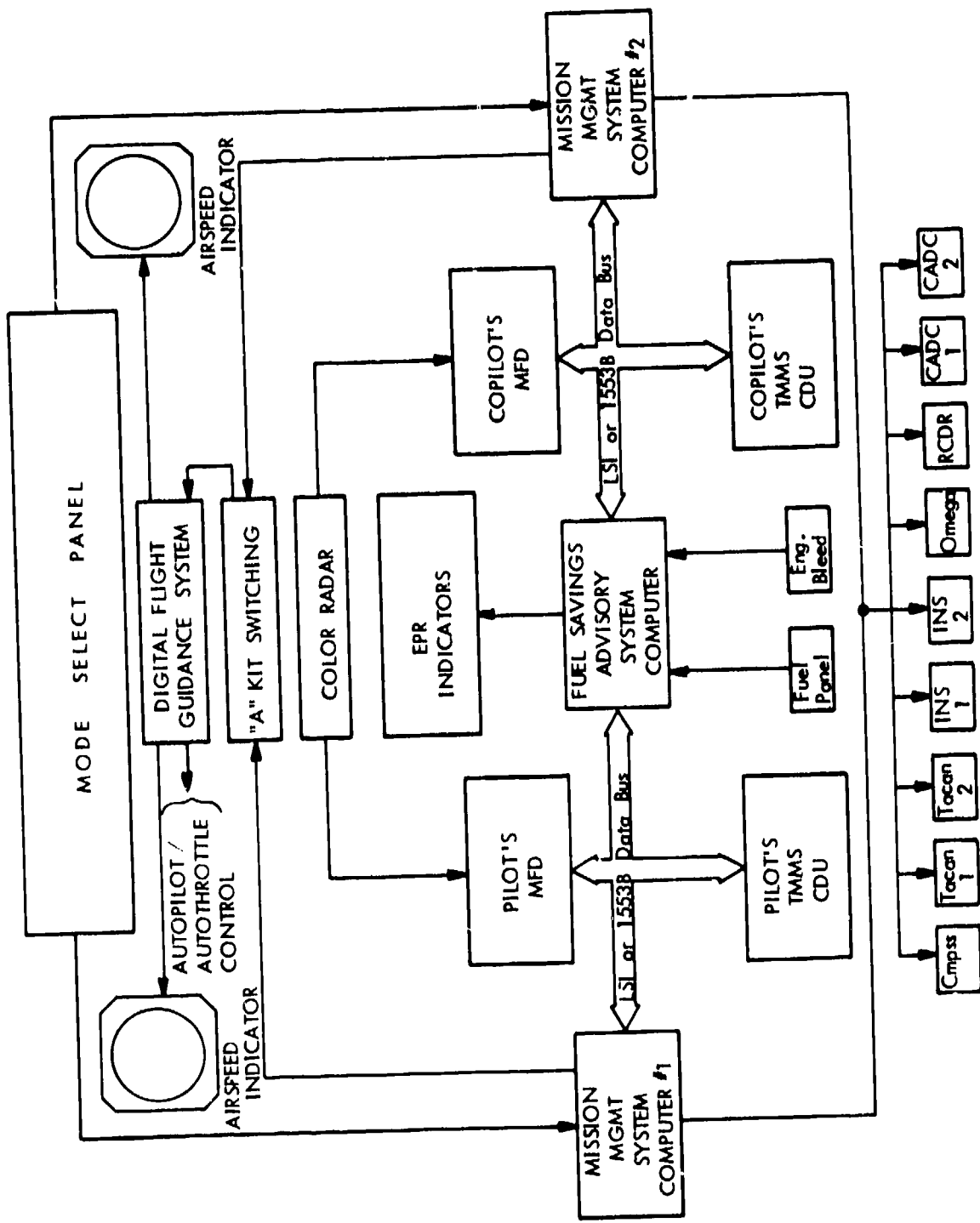
4.3.3.2 Cockpit-Mounted Controller/Display Units

The Speckled Trout aircraft cockpit was evaluated for installation of the critical control and display equipment required for each avionics system required for the proposed three-phase flight demonstration program. The modularity of the flight test program and equipment allows an installation plan that is compatible with limited downtime availability of the aircraft and the necessity of maintaining the aircraft in almost continuous flight-ready status.

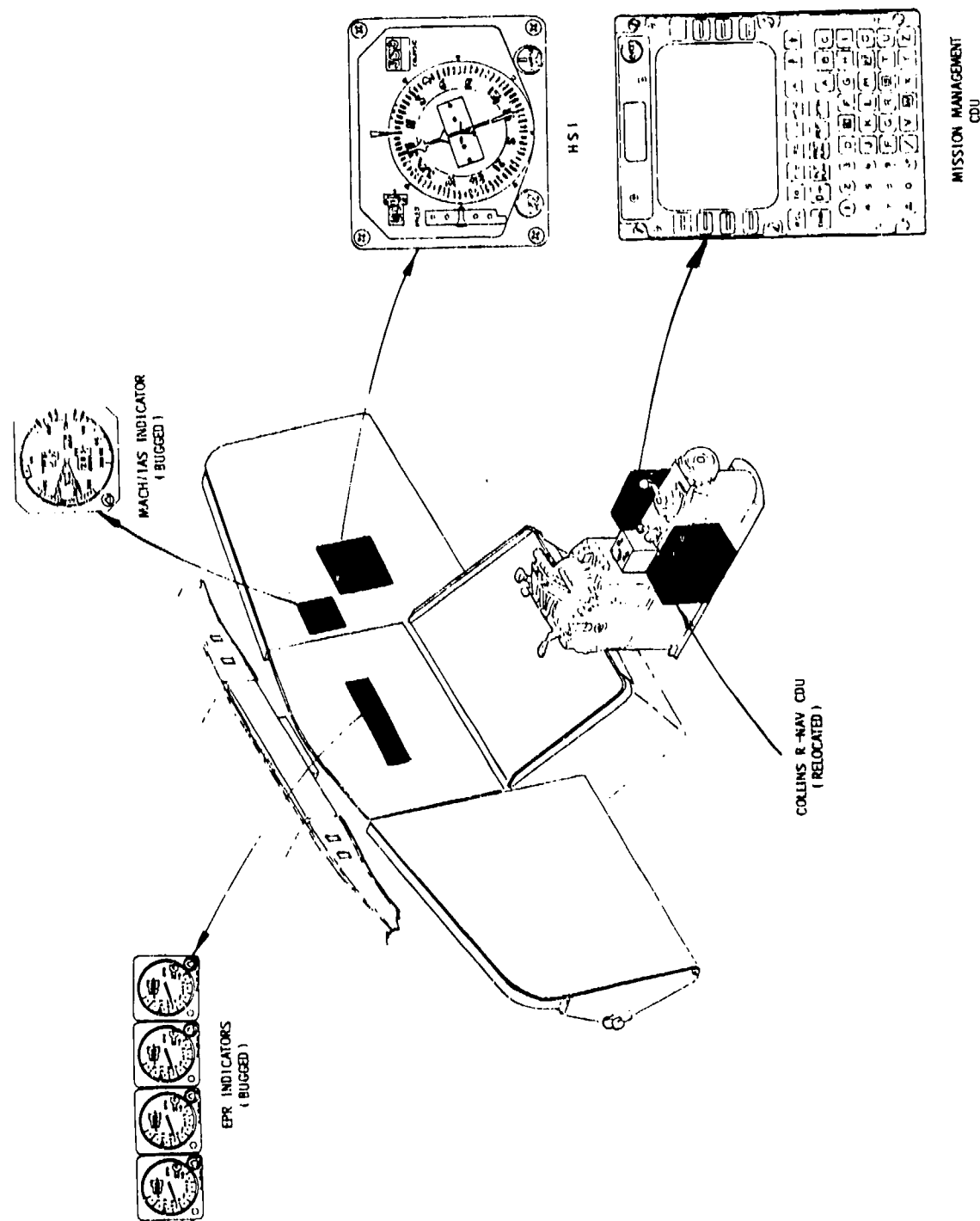
Phase One cockpit equipment installation tasks are minimal, requiring only the following:

- a. Relocating the Collins R-NAV system CDU from the right side to the left side of the center console.
- b. Installation of the Tanker Mission Management System CDU in the space vacated by relocating the Collins CDU.
- c. Replacement of the existing EPR indicators with EPRs equipped with driven bugs.
- d. "A" kit wiring and switching for interfacing the TMMS with the copilot's existing MACH/IAS indicator and HSI.

This configuration is illustrated in Figure 42.



INTERFACE DIAGRAM, MISSION MANAGEMENT SYSTEM
FIGURE 41



BASELINE SYSTEM INSTALLATION
FIGURE 42

Phase Two cockpit equipment installation tasks are the following:

- a. Relocation of the Collins R-NAV map control to the left side of the center console.
- b. Replacement of the pilot/copilot color weather radar indicator with a multifunction display (MFD) and MFD controller.
- c. "A" kit additions to interface the Digital Flight Guidance System with the TMMS.

This configuration is illustrated in Figure 43.

Phase Three involves the replacement of the Collins R-NAV system with a full dual channel mission management system, requiring the following installation actions (see Figure 44).

- a. Replacement of the copilot's HSI with the MFG installed for Phase Two.
- b. Replacement of the pilot's HSI with a second MFD.
- c. Replacement of the pilot's Collins R-NAV CDU with a second TMMS CDU, and the removal of the R-NAV map display.

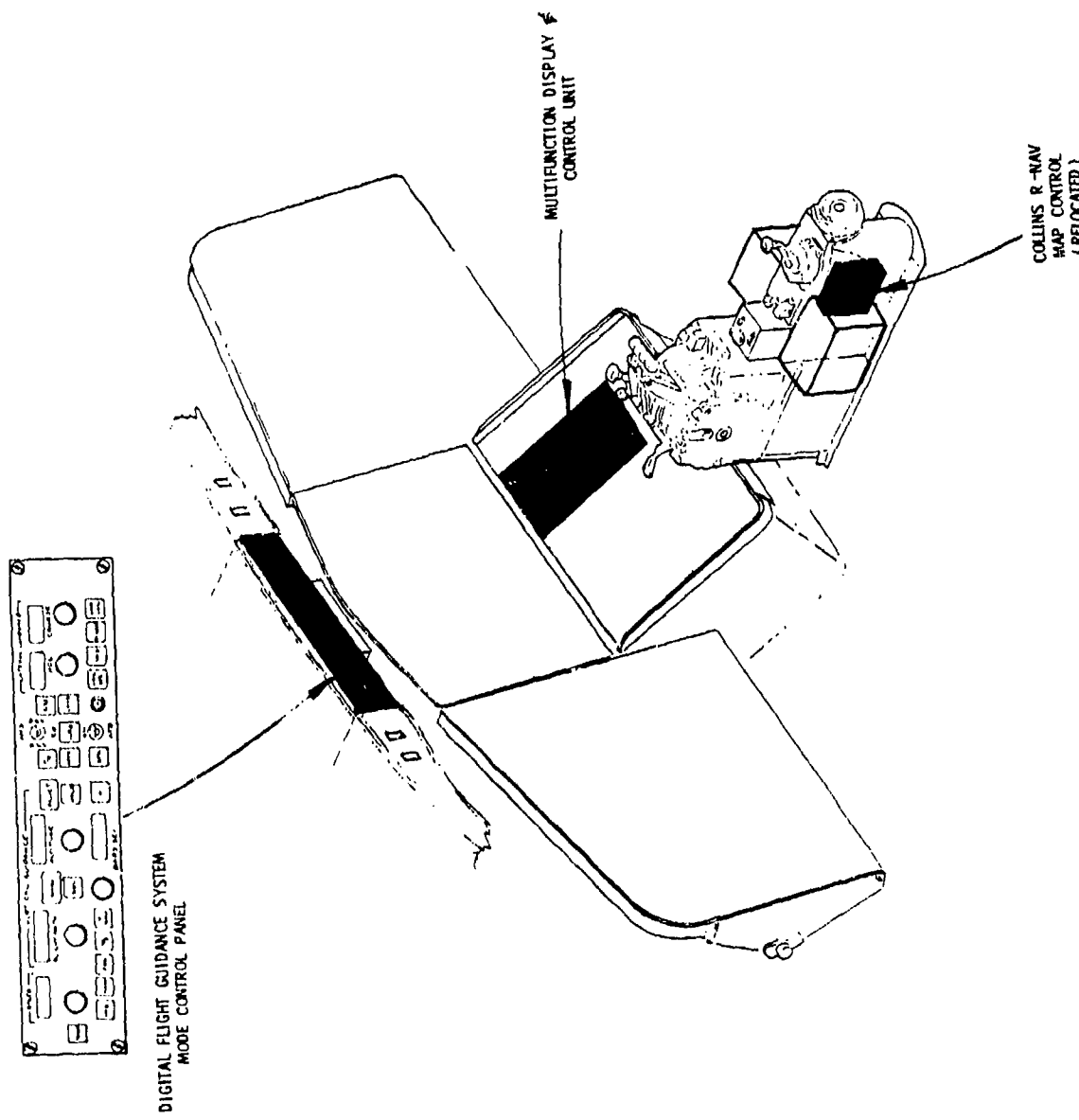
Note

For the Speckled Trout application, it may be more appropriate to install the second TMMS CDU at the navigator's station, along with a third MFD and MFD controller.

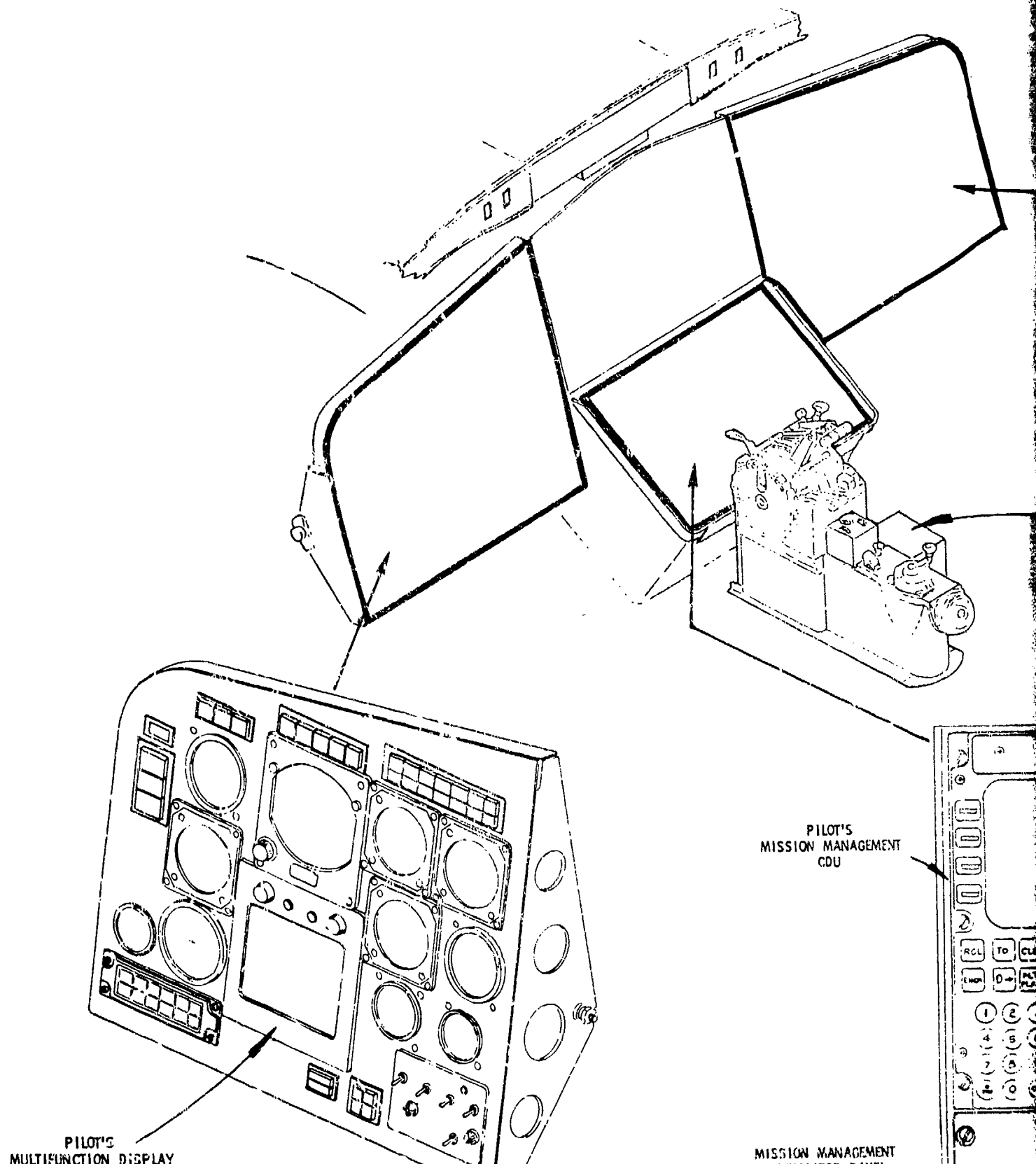
- d. Removal of the Collins R-NAV CDU, and RCA Primus color radar indicator and controller from the navigator's station.
- e. "A" kit wiring to interface the pilot's MFD and CDU with other units of the TMMS. Also, "A" kit switching for selection of active TMMS channel.
- f. Addition of LSI's miniaturized fuel management panel.

4.4 FLIGHT TEST OPERATIONS

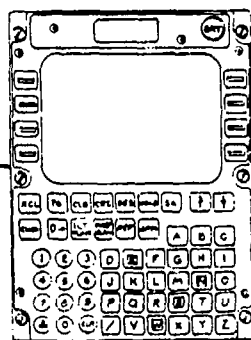
The modular characteristics of system mechanization, as defined in Section 4.3, allows a sequence of flight tests, as shown in Figure 45, to demonstrate the functional and operational capabilities.



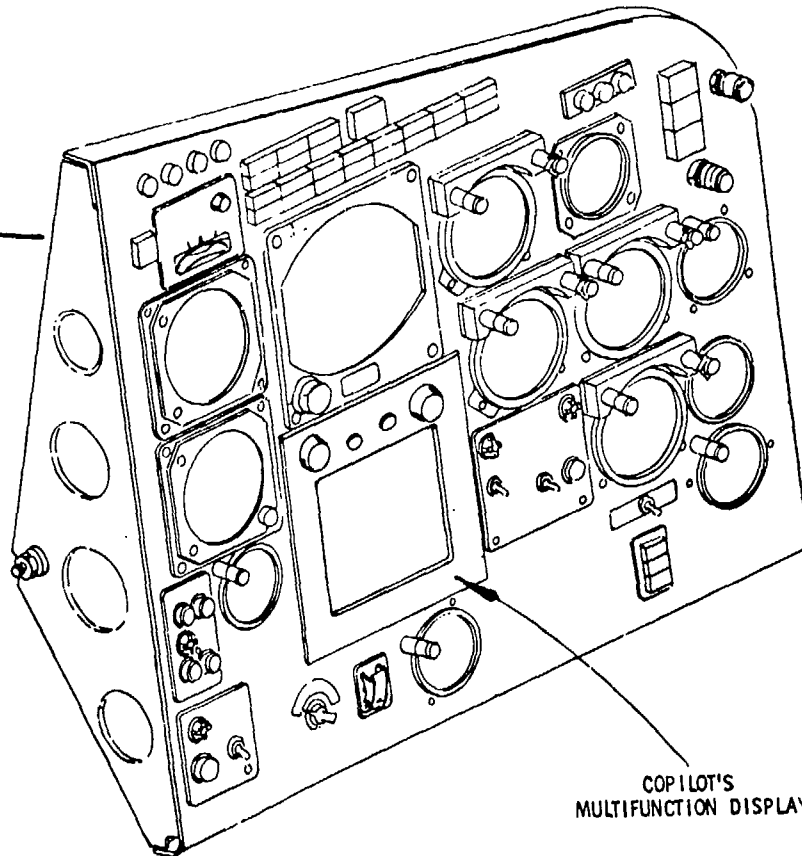
INTERIM SYSTEM INSTALLATION
FIGURE 43



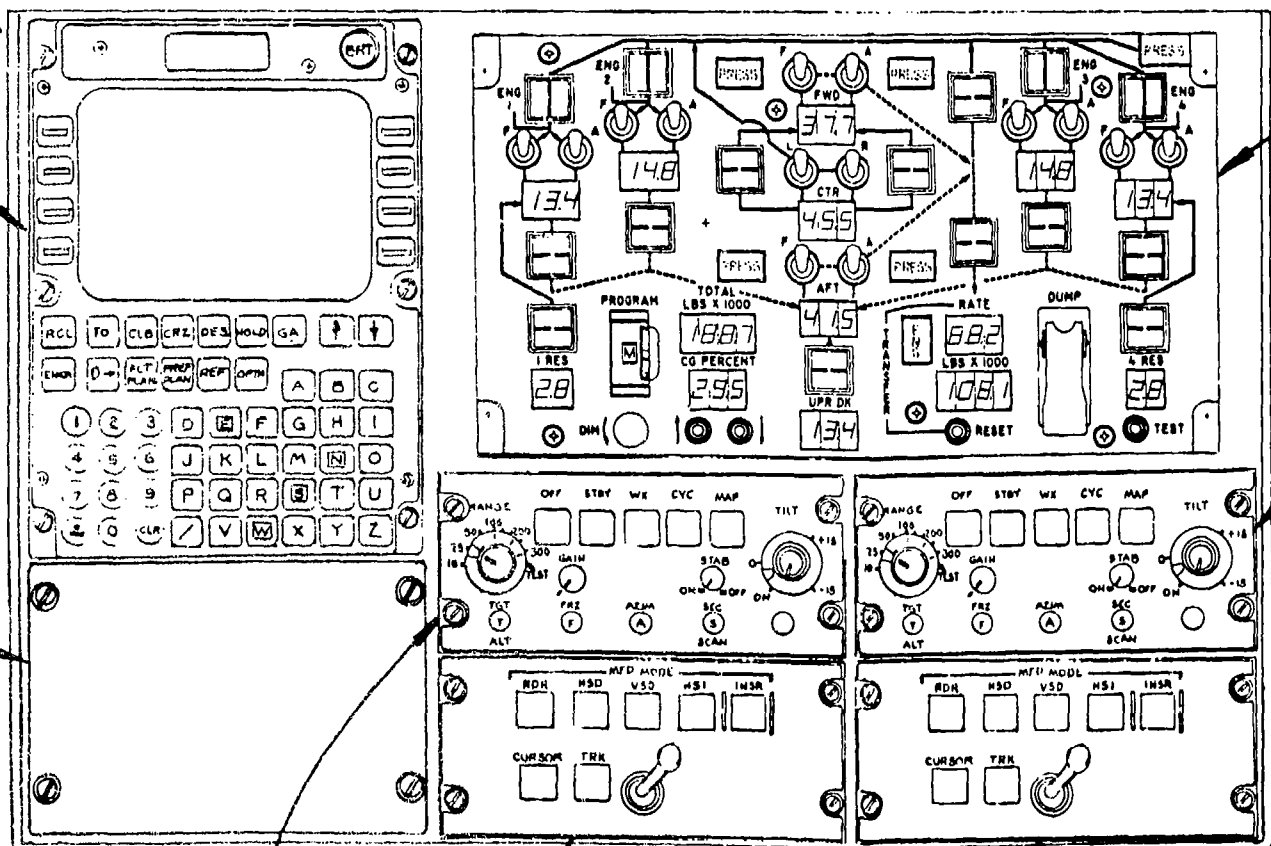
FINAL CONFIGURATION INSTALLATION
FIGURE 44



PILOT'S
RADAR SET CONTROL



COPILOT'S
MULTIFUNCTION DISPLAY



PILOT'S
RADAR SET CONTROL

PILOT'S
MULTIFUNCTION DISPLAY
CONTROL UNIT

FUEL MANAGEMENT
PANEL

COPILOT'S
RADAR SET CONTROL

COPILOT'S
MULTIFUNCTION DISPLAY
CONTROL UNIT

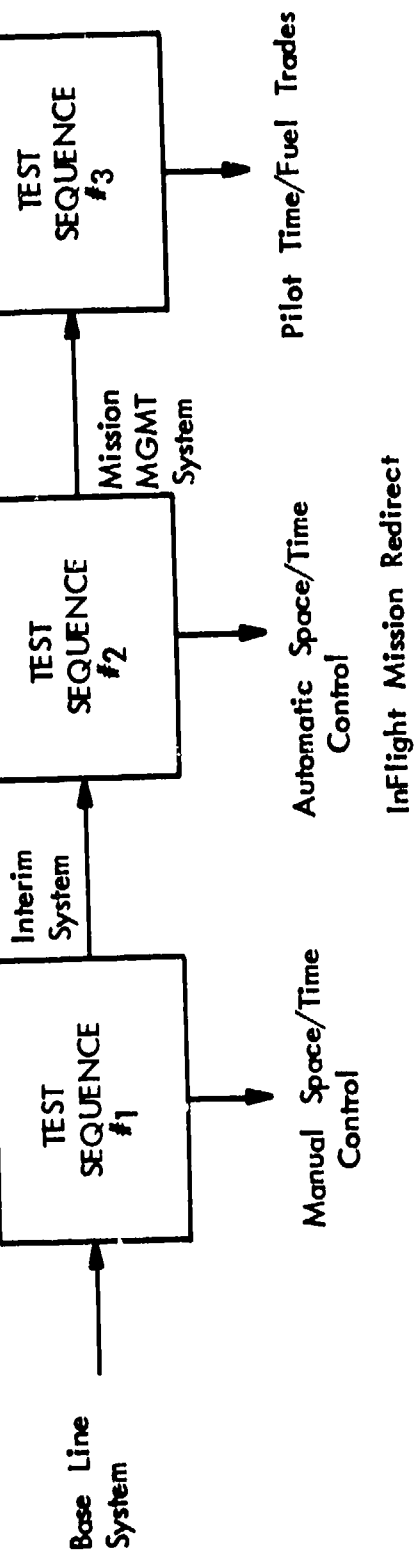


Figure 50 - FLIGHT TEST SEQUENCE

FLIGHT FIGURE 45

Test sequence 1, using only the baseline system, will demonstrate the basic space/time command functions of the system with the control loops for guidance, time control, and performance closed through the pilot.

Test sequence 2, with the upgraded interim system, will repeat the basic time/space/performance control flight test program but with automatic control by coupling the system outputs directly to the autopilot/ autothrottle system. In addition, the interim system, by incorporation of a multifunction display, will allow flight test demonstration of in-flight mission redirect capabilities.

Test sequence 3, with the full mission management system installed, will demonstrate all of the functional and operational capabilities, including time/fuel trades by the pilot manager, and operation without a navigator as required for the KC-135 mission.

All flight tests must be conducted on a range that has a TACAN station at one or more designated waypoints and that is instrumented to track position and time of the aircraft along selected portions of the flight trajectory. The position and timing errors of the ground tracking system must be small compared to the accuracy requirements of the avionics. An initial estimate of allowable errors of the tracking system is ± 500 feet position and ± 1 second time.

4.4.1 Test Sequence 1

To test the integrated performance/guidance capability of the baseline system to control aircraft position/time, the flight profile must be configured to exercise the detailed functions. Then the profiles must incorporate the following characteristics:

VNAV

- a. Takeoff at EPR limit.
- b. Climb at maximum rate for noise abatement profile to intermediate flight level.
- c. Climb at maximum economy from intermediate to cruise flight level.
- d. Cruise at maximum economy.
- e. Change to new cruise flight level.
- f. Cruise to top of descent and descend on maximum economy.
- g. Approach on ILS beam.

LNAV

- a. Capture initial flight plan (i.e., initial flight leg will be displaced in direction by up to 45 degrees from the runway direction).
- b. At least one each of the following types of waypoints:
 - Fixed with direct flyover. Approach and departure headings will differ by more than 45 degrees.
 - Fixed without flyover. Approach and departure headings will differ by more than 60 degrees.
 - Floating waypoint defined by the specified flight path heading intersecting a VOR radial.
- c. Racetrack pattern for rendezvous with receiver aircraft.
- d. Manual override of automatic guidance/control with subsequent return and recapture of the flight plan.
- e. Typical holding pattern at a terminal.
- f. Approach and capture of IGS landing beam.

4.4.2 Test Sequence 2

The flight test profiles of sequence 2 will be the same as for sequence 1, except that on at least some of the tests, the pilot will modify the flight plan on the following schedule:

- a. On cue from data stored in the computer as part of the flight plan, the pilot will investigate alternate LNAV waypoints and VNAV flight levels to circumvent a specified threat area that is identified on the initial flight plan. This threat could, for example, be a severe weather area. The criterion for selection of alternate routes will be the time required to reach the designated ARCP.
- b. On cue from data stored on the computer as part of the flight plan, the pilot will investigate alternate mission termination points to accommodate unexpected shutdown of the landing field specified in the initial flight plan. The criterion for alternate selection will be minimum fuel requirements (maximum fuel available for offloading) to complete the mission after achieving ARCP/ARCT.

- c. After excursion from the initial flight plan, by manual override of the aircraft control, return by Direct-To some future waypoint in the original plan. The criterion for selection of the waypoint is achieving ARCP within ARCT allowable time deviations and with minimum fuel expenditure.

4.4.3 Test Sequence 3

The primary purpose of test sequence 3 is to demonstrate the total functional capability of the complete mission management system. This is in contrast to sequences 1 and 2 that are designed primarily to test the functional capability of the IFTC algorithms.

A secondary purpose of test sequence 3 is to investigate typical mission success probability when operating without a navigator. The redundant controller/displays of the complete mission management system makes possible a flight test that specifies a realistic pilot/copilot work assignment, allowing both crew members to interactively operate the system.

The actual flight test plan should simulate, as nearly as possible but with shortened time schedules, the typical mission scenarios used to generate the system requirements (Section 4.2).

4.5 AIRCRAFT INSTALLATION AND CHECKOUT

Design based on successful experience and complete documentation of both the modifications to the aircraft and the adapter A-Kits assures straightforward installation of the avionics system in the aircraft.

The modification design will assure the physical, functional, and operational integration of the aircraft with the total avionics system comprised of elements currently on the aircraft and provided by the Air Force, and those which LSI designs and develops.

The total modification will be documented in a Class II Modification Document, Part I and Part II.

4.5.1 Class II Modification Document Details

Part I of the Modification Document will contain only preliminary design data. Part II will contain this design data, expanded and detailed, as well as pre-airworthiness flight test data and post-airworthiness flight test results.

The design data includes drawings, analyses and airworthiness flight test plans. Detailed information shown on the drawings includes the following:

- a. Mounting methods, mounting hardware, supports, fixtures, and mounting position of each unit.
- b. The specific location of each unit in the aircraft.
- c. Sway space clearance provided for each unit installed.
- d. Avionics equipment, airframe material, or hardware to be re-located or modified due to the installation.
- e. List of materials or parts list required for installation. The list will include the equipment to be installed and the installation material or hardware, including interconnecting cables.

The engineering analyses in the design data include hazard or flight safety, mass properties (weight and balance), structures, electrical load, electromagnetic compatibility and stability control.

The flight test plan for verification of airworthiness of the modified test vehicle contains test objectives, a resolution of Air Force and LSI responsibilities in accomplishing the flight test, test criteria and procedures, including profiles to demonstrate the operational airworthiness of the vehicle, and test schedules. Test data requirements, data reduction and analysis requirements, and flight test format are part of this test plan.

This test plan will be preliminary in Part I and updated and modified for the final version in Part II of the Class II Modification Document.

In addition to updated versions of major sections of Part I, the Part II Modification Document also contains Operating/Maintenance Instructions, lists of applicable supporting documentation and spare parts, pre-airworthiness flight test data and post-airworthiness flight test results.

A partial flight manual will provide the necessary ground and flight operation, maintenance, and inspection instructions for the modified test aircraft.

4.5.2 Aircraft Installation Design

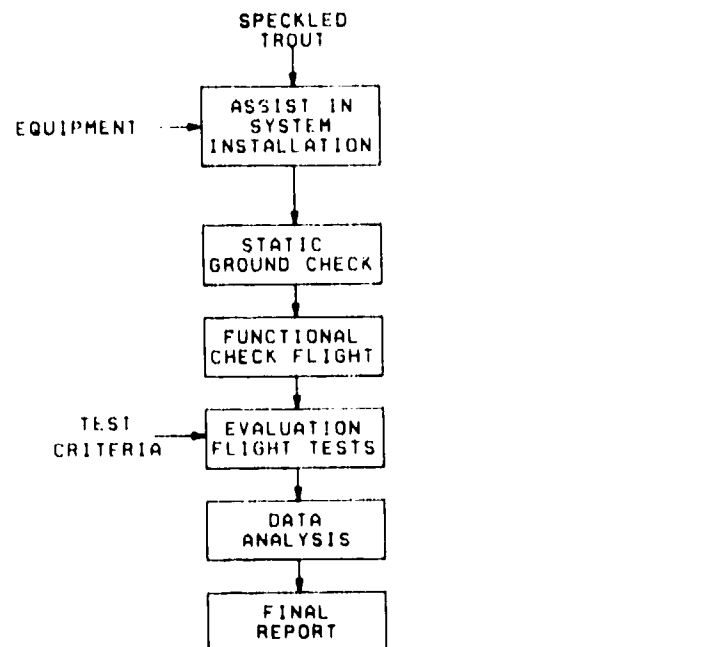
The aircraft Class II modification to install and integrate the avionics system into the test aircraft must be in accordance with MIL-P-27733 and safety of flight requirements.

The pilot's and copilot's main instrument panels, as shown in Figure 44, will be redesigned. All new Controller/Display equipment will be supplied as GFE. New instrument panels will be provided as part of the A-Kit. Electrical interface of this equipment, as well as all other elements of the total avionics system, will be included in our integration design.

Flight safety during the program is assured by the modularity of flight test avionics and test plan and by an engineer specifically assigned the responsibility for coordinating all safety-related activities, analyses, and reports. The safety efforts must begin at the start of the program and carry through completion. The efforts, results, and conclusions will be documented in a Preliminary Hazard Analysis and a Final System Hazard Analysis.

4.6 FLIGHT TEST SUPPORT

LSI will provide support to the Air Force for modification of the test aircraft and installation of all Group A and Group B equipment as defined by the Class II Modification Document. Specific support tasks (Figure 46) include ground testing, systems calibration and checkout, preparation of the aircraft for functional check flights, actual flight testing, integration support of advanced systems, equipment maintenance, environmental assessment and field support.



211370

SYSTEM DEMO TASK FLOWCHART - PHASE III

FIGURE 46

Air Force personnel at Detachment 1, 4950th Test Wing (Speckled Trout) will actually accomplish the modification, installing both the equipment which LSI will supply and equipment furnished by the Air Force.

4.6.1 Aircraft Modifications

LSI support will assure that aircraft modifications comply with all applicable military specifications, the approved Class II Modification Document, and Air Force Quality Control standards and procedures.

The applicable military specifications are MIL-P-27733, MIL-I-45208, MIL-STD-882, and T.O. 1-1A-14. The Class II Modification Document will be modified as necessary as the airframe modification progresses to incorporate the actual physical configuration of the system.

The Air Force will prepare the test aircraft and remove any equipment from the test aircraft that is necessary to accomplish installation of the respective Group A and Group B kits.

All Group A components of the system will be installed in accordance with AF-approved Class II modification documentation, MIL-I-45208, and Air Force Quality Assurance procedures. LSI and government inspections will be conducted during modification.

4.6.2 Ground Checkout

A careful ground checkout -- including EMI tests, system calibration and functional tests -- assures that the test aircraft is ready for the Air Force functional test flight.

EMI testing verifies that EMI integrity within the aircraft is not affected by the equipment installation.

System functional testing verifies proper installation, alignment, calibration, and operation of all systems and disturbed systems.

These final ground flight preparation checks include weight and balance check, compass rose swing (if required), hydraulics check, landing gear check, 90-day calendar inspection (if required), brake and tire check, nose wheel steering check, and fuel level.

The test aircraft is now ready for a functional check flight by Air Force flight crew to verify system operation prior to formal flight testing. LSI will correct any deficiencies found during this functional check flight. This correction of deficiencies, if any are found, and an acceptable functional flight test complete the modification/installation phase.

4.6.3 Data Analysis

LSI will develop test criteria and provide data analysis support that will maximize the demonstration results with a minimum number of flight hours.

For this task, on-site engineers and technicians will be established, supported by engineers in Grand Rapids as required, to assure effective operation of the avionics system.

Flight test criteria will be developed to demonstrate the system airworthiness. This task includes definition of all the operational data requirements, including source, function, and analysis methods.

The basic performance criteria are consistent non-glitching operation of the integrated system and consistent output of the data bus parameters to the Data Recording System.

These criteria are incorporated as the flight test plan of the Class II Modification Document.

Following the flights, LSI will evaluate the data obtained by the on-board recording equipment as well as the observations of the flight crew. This flight test data will be summarized for inclusion in both the interim and final flight test reports.

CONCLUSIONS AND RECOMMENDATIONS

This report shows that the complexity of generating a four-dimensional trajectory using optimal techniques was too great to allow more than a cursory examination of the problem within the time and money constraints of the program. The principal problem was in defining an optimization algorithm that could readily satisfy the initially defined cost function.

A two-step approach of separating the horizontal plane and vertical plane projections of the desired trajectory was investigated briefly. This approach, while analytically more amenable, was not attempted because of the inherent reductions in performance.

Optimal control of the aircraft by a linear quadratic regulator to the trajectory generated by classical algorithms was investigated. Although technically feasible, this technique proved to be too costly in terms of on-board avionics computer capabilities to justify the probable degree of performance improvement.

A three-phase plan for flight verification of the classical Flight Trajectory Control algorithms and for demonstration of their operational capabilities was defined. This flight test plan will utilize the Speckled Trout test aircraft and existing avionics hardware with modified software.

This plan is recommended as a program follow-on because it will do the following:

- a. Provide an experimental data base for the utility of the Flight Trajectory Control concept -- particularly in monitoring preplanned time on target with in-flight redirect;
- b. Establish the computer resources of the on-board avionics to implement the Flight Trajectory Control concept;
- c. Establish operational characteristics of the concept for application to an integration with other developmental capabilities of advanced aircraft such as terrain-following and integrated fire/flight control.

APPENDIX A

AIRCRAFT TRANSFER FUNCTIONS

10 AIRCRAFT TRANSFER FUNCTIONS

10.1 SHORT PERIOD MODE

The two-degree-of-freedom Short Period Mode approximation is given by the following:

$$\frac{q}{\delta_e}(s) = \frac{(M_{\delta_e} + Z_{\delta_e} M_{\dot{W}})s + (Z_{\delta_e} M_W - M_{\delta_e} - M_{\delta_e} Z_W)}{s^2 - (V_T M_{\dot{W}} + Z_W + M_q)s + (M_q Z_W - V_T M_W)}$$

where

$$M_{\delta_e} = \frac{\rho S V_T^2 c}{2 I_{YY}} C_{m_{\delta_e}}$$

$$Z_{\sigma_e} = \frac{\rho S V_T^2}{2m} (-C_{L_{\delta_e}})$$

$$M_{\dot{W}} = \frac{\rho S c^2}{4 I_{XY}} C_{m_{\alpha}}$$

$$M_W = \frac{\rho S V_T}{2 I_{YY}} C_{m_{\alpha}}$$

$$Z_W = \frac{\rho S V_T}{2m} (-C_{L_{\alpha}} - C_D)$$

$$M_q = \frac{\rho S V_T c^2}{4 I_{YY}} C_{m_q}$$

For both flight conditions, the values of the aerodynamic coefficients are the following:

Aerodynamic Coefficient	Flight Condition	
	Low Q	High Q
$C_{m\delta_e}$	-.688 (1/rad)	-.481 (1/rad)
$C_{L\delta_e}$.223 (1/rad)	.149 (1/rad)
$C_{m\alpha}$	-4.7 (1/rad)	-5.4 (1/rad)
$C_{L\alpha}$	-1.09 (1/rad)	-1.32 (1/rad)
C_D	4.56 (1/rad)	5.54 (1/rad)
C_{mq}	.049	.0152
	-15.1 (1/rad)	-15.25 (1/rad)

Solving for the stability derivative, the following results are achieved:

Stability Derivative	Flight Condition	
	Low Q	High Q
M_{δ_e}	-.93	-2.61
Z_{δ_e}	-10.23	-27.4
M_w	-8.48×10^{-4}	-5.05×10^{-4}
M_w	-.00536	-.00938
Z_w	-.769	-.927
M_q	-.749	-1.092

Therefore, for the low Q flight condition,

$$\frac{q}{\delta_e} (s) = \frac{-0.921(s+0.717)}{s^2 + 1.75s + 2.05}$$

and for the high Q flight condition,

$$\frac{q}{\delta_e} (s) = \frac{2.6(s+0.83)}{s^2 + 2.4s + 8.17}$$

10.2 $\frac{r}{\delta_r} (s)$ TRANSFER FUNCTION

The 3-degree-of-freedom lateral-directional equations of motion are the following:

$$\begin{bmatrix} s - Y_V & -\left(\frac{g}{V_T}\right) & 1 & \begin{bmatrix} \beta(s) \\ \phi(s) \\ r(s) \end{bmatrix} \\ -L_\beta & s^2 - L_p s & -\left(\frac{I_{XZ}}{I_{XX}}\right)s - L_r & \\ -N_\beta & -\left(\frac{I_{XZ}}{I_{ZZ}}\right)s^2 - N_p s & s - N_r & \end{bmatrix} = \begin{bmatrix} Y_{\delta_R}^* & 0 & \begin{bmatrix} \delta_R \\ \delta_a \end{bmatrix} \\ L_{\delta_R} & L_{\delta_a} & \\ N_{\delta_R} & N_{\delta_a} & \end{bmatrix}$$

where

$$Y_V = \frac{\rho S B}{4m} C_{y_\beta}$$

$$Y_{\delta_R}^* = \frac{\rho S V_T}{2m} C_{y_{\delta_R}}$$

$$L_\beta = \frac{\rho S V_T^2 b}{2 I_{XX}} C_{\ell_\beta}$$

$$L_{\delta_R} = \frac{\rho S V_T^2 b}{2 I_{XX}} C_{\ell_{\delta_R}}$$

$$L_p = \frac{\rho S V_T b^2}{4 I_{XX}} C_{\ell_p}$$

$$L_{\delta_A} = \frac{\rho S V_T^2 b}{2 I_{XX}} C_{\ell_{\delta_A}}$$

$$L_r = \frac{\rho S V_T b^2}{4 I_{XX}} C_{\ell_r}$$

$$N_{\delta_R} = \frac{\rho S V_T^2 b}{2 I_{ZZ}} C_{n_{\delta_R}}$$

$$N_{\beta} = \frac{\rho S V_T^2 b}{2 I_{ZZ}} C_{n_{\beta}}$$

$$N_{\delta_A} = \frac{\rho S V_T^2 b}{2 I_{ZZ}} C_{n_{\delta_A}}$$

$$N_r = \frac{\rho S V_T b^2}{4 I_{ZZ}} C_{n_r}$$

$$N_p = \frac{\rho S V_T b^2}{4 I_{ZZ}} C_{n_p}$$

The lateral-directional aerodynamic coefficients for both flight conditions are given below.

Aerodynamic Coefficient	Flight Condition	
	Low Q	High Q
C_{n_p}	-.026 (1/rad)	.021 (1/rad)
C_{y_β}	-.676 (1/rad)	-.756 (1/rad)
C_{λ_β}	-.186 (1/rad)	-.17 (1/rad)
C_{λ_p}	-.364 (1/rad)	-.306 (1/rad)
C_{λ_r}	.203 (1/rad)	.129 (1/rad)
C_{n_β}	.128 (1/rad)	.142 (1/rad)
C_{u_r}	-.158 (1/rad)	-.148 (1/rad)
$C_{y_{\delta_R}}$.211 (1/rad)	.179 (1/rad)
$C_{\lambda_{\delta_R}}$.0099 (1/rad)	.0184 (1/rad)
$C_{\lambda_{\delta_a}}$.0253 (1/rad)	.0198 (1/rad)
$C_{n_{\delta_R}}$	-.0843 (1/rad)	-.0733 (1/rad)
$C_{n_{\delta_A}}$	0 (1/rad)	.0034 (1/rad)

Solving for the stability derivatives, the following results are achieved:

Stability Derivative	Flight Condition	
	Low Q	High Q
N_p	-.0318	.0386
Y_v	-.0269	-.0156
L_β	-2.31	-8.46
L_p	-1.07	-1.305
L_r	.6	.55
N_β	.684	3.04
N_r	-.201	-.272
$Y_{\delta R}^*$.0352	.0431
$L_{\delta R}$.123	.916
$L_{\delta A}$.314	.985
$N_{\delta R}$	-.45	-1.57
$N_{\delta A}$	0	.073

Substituting the stability derivatives into the lateral-directional equations of motion, we have the following for the low Q flight condition:

$$\begin{bmatrix} s+0.0269 & -0.117 & 1 \\ 2.31 & s^2+1.07s & -0.074s-0.6 \\ -0.684 & -0.0319s+0.0318s & s+0.201 \end{bmatrix} \begin{bmatrix} \beta(s) \\ \phi(s) \\ r(s) \end{bmatrix} = \begin{bmatrix} 0.0352 & 0 \\ 0.123 & 0.314 \\ -0.45 & 0 \end{bmatrix} \begin{bmatrix} \delta_R(s) \\ \delta_A(s) \end{bmatrix}$$

and for the high Q flight condition:

$$\begin{bmatrix} s+0.0156 & -0.0422 & 1 \\ 8.46 & s^2+1.305s & -0.074s-0.55 \\ -3.04 & -0.0319s^2-0.0386s & s+0.272 \end{bmatrix} \begin{bmatrix} \beta(s) \\ \phi(s) \\ r(s) \end{bmatrix} = \begin{bmatrix} 0.0431 & 0 \\ 0.916 & 0.985 \\ -1.57 & 0.073 \end{bmatrix} \begin{bmatrix} \delta_R(s) \\ \delta_A(s) \end{bmatrix}$$

The aircraft transfer function $\frac{r}{\delta_R}(s)$ is obtained using the IBM 370 program LISA.

For the low Q flight condition:

$$\frac{r}{\delta_R}(s) = \frac{-0.447(s+1.25)[(s-0.0934)^2+(.437)^2]}{(s+1.26)(s+0.00589)[(s+0.00856)^2+(.923)^2]}$$

and for the high Q flight condition:

$$\frac{r}{\delta_R}(s) = \frac{-1.54(s+1.44)[(s-0.0976)^2+(.436)^2]}{(s+1.39)(s+0.00668)[(s+0.0913)^2+(1.69)^2]}$$

$$10.3 \quad \frac{\phi}{\delta_A}(s) \Big|_{r+\delta_R} \quad \text{TRANSFER FUNCTION}$$

The equation relating $r(s)$ to $\delta_R(s)$ is the following:

$$\delta_R(s) = \left(\frac{100}{Q}\right)(2)\left(\frac{10}{s+10}\right)\left(\frac{s}{s+1}\right)\left(\frac{15.7}{s+15.7}\right)r(s)$$

Modifying the lateral-directional transfer function matrix, we have the following for the low Q flight condition:

$$\begin{bmatrix} s+0.0269 & -0.117 & 1. & -0.0352 \\ 2.31 & s^2+1.07s & -0.074s-0.6 & -0.123 \\ -0.684 & -0.0319s^2+0.0318s & s+0.201 & 0.45 \\ 0 & 0 & -(31,400/Q)s & s^3+26.7s^2+182.7s+157 \end{bmatrix} \begin{bmatrix} \beta(s) \\ \phi(s) \\ r(s) \\ \delta_R(s) \end{bmatrix} = \begin{bmatrix} 0 \\ 0.314 \\ 0 \\ 0 \end{bmatrix} \delta_A(s)$$

and for the high Q flight condition:

$$\begin{bmatrix} s+0.0156 & -0.0422 & 1. & -0.0431 \\ 8.46 & s^2+1.035s & -0.074s-0.55 & -0.916 \\ -3.04 & -0.0319s^2-0.0386s & s+0.272 & 1.57 \\ 0 & 0 & (-31,400/Q)s & s^3+26.7s^2+182.7s+157 \end{bmatrix} \begin{bmatrix} \beta(s) \\ \phi(s) \\ r(s) \\ \delta_R(s) \end{bmatrix} = \begin{bmatrix} 0 \\ 0.985 \\ 0.073 \\ 0 \end{bmatrix} \delta_A(s)$$

The aircraft transfer function, $\left. \frac{\phi(s)}{\delta_A} \right|_{r \rightarrow \delta_R}$, is obtained by using the analysis program LISA.

For the low Q flight condition:

$$\left. \frac{\phi(s)}{\delta_a} \right|_{r \rightarrow \delta_R} = \frac{.315[(s+0.146)^2 + (.547)^2](s+1.75)(s+6.87)(s+17.1)}{[(s+0.0468)^2 + (.713)^2](s+1.25)(s+0.00463)(s+6.29)(s+3.09)(s+17.25)}$$

and for the high Q flight condition:

$$\left. \frac{\phi(s)}{\delta_a} \right|_{r \rightarrow \delta_R} = \frac{.993[(s+0.628)^2 + (1.54)^2](s+1.75)(s+6.87)(s+17.1)}{[(s+0.395)^2 + (1.35)^2](s+1.61)(s+0.00556)(s+1.75)(s+7.03)(s+17.1)}$$

APPENDIX B

STOCHASTIC THREAT MODEL

STOCHASTIC THREAT MODEL

In order to develop a robust algorithm for resource allocation, it is necessary to take into account the stochastic nature of the threat environment. If the solution were to consider only those threats which absolutely were known to exist, then it would leave the aircraft vulnerable to "pop-up" threats. On the other hand, if the algorithm were to consider all possible pop-up threats which conceivably might appear, then it would tend to avoid threats which in fact never materialize. Such a worst-case policy is also inappropriate. What is required is an analytical procedure which results in a proper trade-off of flight path between known present threats and possible future threats. Such a procedure is developed in this section.

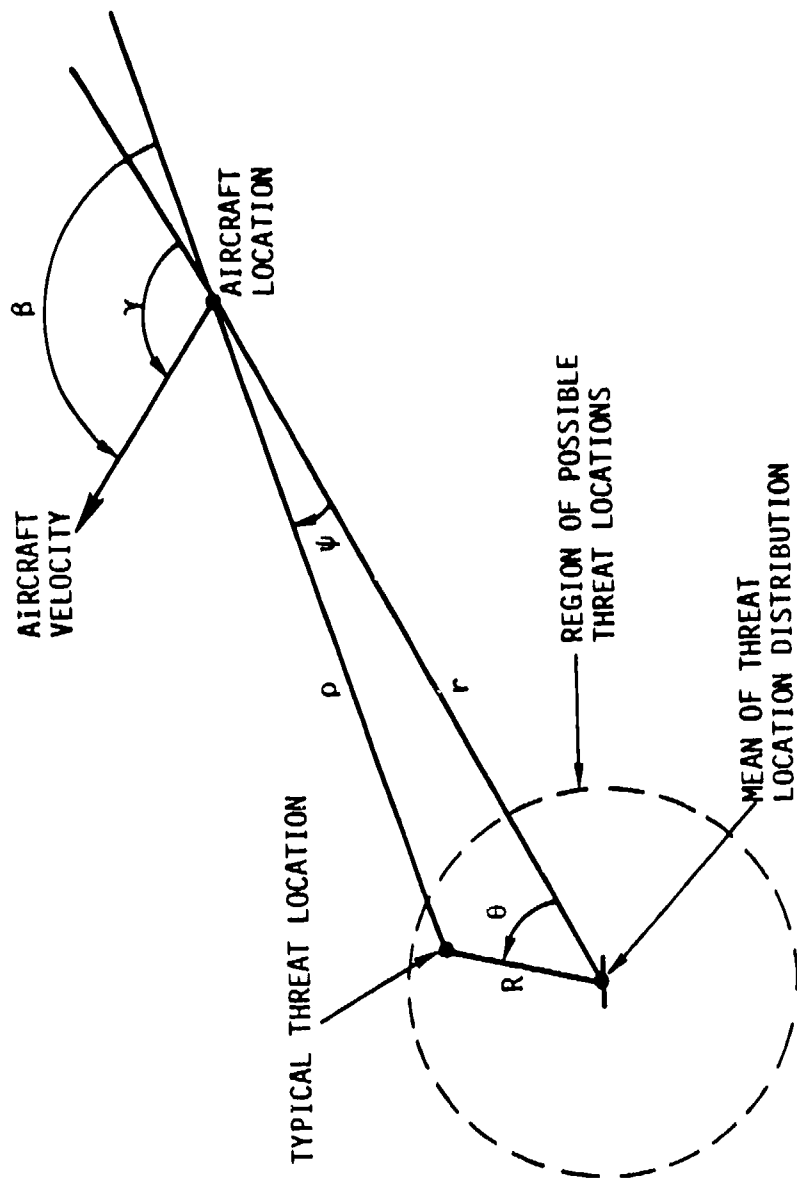
Three types of information are assumed to be available to the aircraft for each known present and potential future threat. They are as follows:

1. a probability that the threat actually exists;
2. a probability distribution for the location of the threat given that it does exist; and
3. a threat model specified by the conditional probability of aircraft survival given that the threat actually exists and is at a known location, as a function of the aircraft's position and velocity relative to the threat.

The equations are derived which transform this information into an unconditional threat model. Then, certain simplifying assumptions are described which allow the rapid real-time computation of the unconditional threat model.

20.1 DERIVATION OF GENERAL EQUATIONS

For each threat, assume that a value for the probability that the threat exists, $P(X)$, is known. $P(X)$ will be near 1 for presently known threats, and will be less for postulated, future pop-up-type threats. Furthermore, a probability distribution of each threat's location is assumed to be known. The form of the distribution is arbitrary, although simple analytic expressions such as uniform or Gaussian distributions are reasonable assumptions and certainly more tractable than quantized representations requiring numerical integration. This distribution is expressed conveniently in polar coordinates (see Figure B-1), relative to the man threat location denoted $f(R, \theta)$. The threat model is a function of three position/velocity variables, as follows:



THREAT/AIRCRAFT GEOMETRY
FIGURE B-1

$P(S|\rho, \beta, z, A, X)$ = Probability of aircraft survival per unit time for horizontal separation ρ , aircraft approach angle β , aircraft altitude z , resource allocation A , and conditioned upon the threat existing.

The desired threat model which is to be derived below is the unconditional model (i.e., no dependence on the random variable X) with respect to the mean of the threat distribution:

$P(S|r, \gamma, z, A)$ = Probability of aircraft survival per unit time for horizontal separation between the aircraft and the mean of the threat distribution r , angle of aircraft velocity with respect to the line joining the aircraft and the threat center γ , aircraft altitude z (see Figure 1), and resource allocation A .

The first step in the derivation is to distribute the unconditional probability over the two mutually exclusive events of the threat's existence and its nonexistence $P(\bar{X})$.

$$P(S|r, \gamma, z, A) = P(S|r, \gamma, z, A, X)P(X) + P(S|r, \gamma, z, A, \bar{X})P(\bar{X}).$$

But, if the threat does not exist, then the survival probability must be unity. So:

$$P(S|r, \gamma, z, A) = P(S|r, \gamma, z, A, X)P(X) + 1 - P(X). \quad (B-1)$$

The next step is to distribute the conditional probability appearing on the right side of the above equation over all possible locations for the threat, as:

$$P(S|r, \gamma, z, A, X) = \iint f(R, \theta)P(S|\rho(R, \theta), \beta(R, \theta), z, A, X) dR d\theta \quad (B-2)$$

where (using the laws of sines and cosines and Figure B-1)

$$\rho(R, \theta) = R^2 + r^2 - 2Rr \cos \theta \quad (B-3a)$$

$$\beta(R, \theta) = \gamma + \psi(R, \theta) \quad (B-3b)$$

where

$$\sin \psi = \frac{R \sin \theta}{\rho} \quad (B-3c)$$

$$\cos \psi = \frac{r - R \cos \theta}{\rho} \quad (B-3d)$$

Thus, a general solution to the problem exists. Given the three items of information about a threat, the following procedure may be used to develop the unconditional threat model. For a given value of r, γ, z and A , the conditional probability $P(S|r, \gamma, z, A, X)$ may be calculated by numerical integration of equation B-2, using equations B-3a through B-3d. Then the desired unconditional probability may be obtained by using equation B-1.

20.2 SIMPLIFICATION OF GENERAL EQUATION

In the preceding section, relationships between the conditional and unconditional probabilities of survival were derived in general. In this section, the general equations will be simplified so that rapid real-time computation is possible.

The first thing to note is that the mission-planning dynamic-programming algorithm does not operate on the probability of survival directly, but rather on the negative logarithm of the survival probability. Therefore, the following notational convention is adopted:

$$E(\text{variables}) \triangleq -\ln [P(S|\text{variables})] \quad (B-4)$$

The quantized unit of time proposed for the mission planner will be a short enough length of time that all survival probabilities are nearly 1. Hence, the following approximation is of excellent numerical accuracy.

$$E(\text{variables}) \approx 1 - P(S|\text{variables}) \quad (B-5)$$

Applying the above relationship to equation B-1,

$$\begin{aligned} P(S|r, \gamma, A, z) &= 1 - P(X) [1 - P(S|r, \gamma, A, z, X)] \\ 1 - P(S|r, \gamma, A, z) &= P(X) [1 - P(S|r, \gamma, z, A, X)] \quad (B-6) \\ E(r, \gamma, A, z) &\approx P(X) E(R, \gamma, z, A, X) \end{aligned}$$

and then to equation B-2,

$$\begin{aligned} E(R, \gamma, z, A, X) &= 1 - \iint f(R, \theta) P(S|\rho, \beta, z, A, X) dR d\theta \\ &= \iint f(R, \theta) dR d\theta - \iint f(R, \theta) P(S|\rho, \beta, z, A, X) dR d\theta \quad (B-7) \\ &= \iint f(R, \theta) [1 - P(S|\rho, \beta, z, A, X)] dR d\theta \\ E(r, \gamma, z, A, X) &\approx \iint f(R, \theta) E(\rho, \beta, z, A, X) dR d\theta \end{aligned}$$

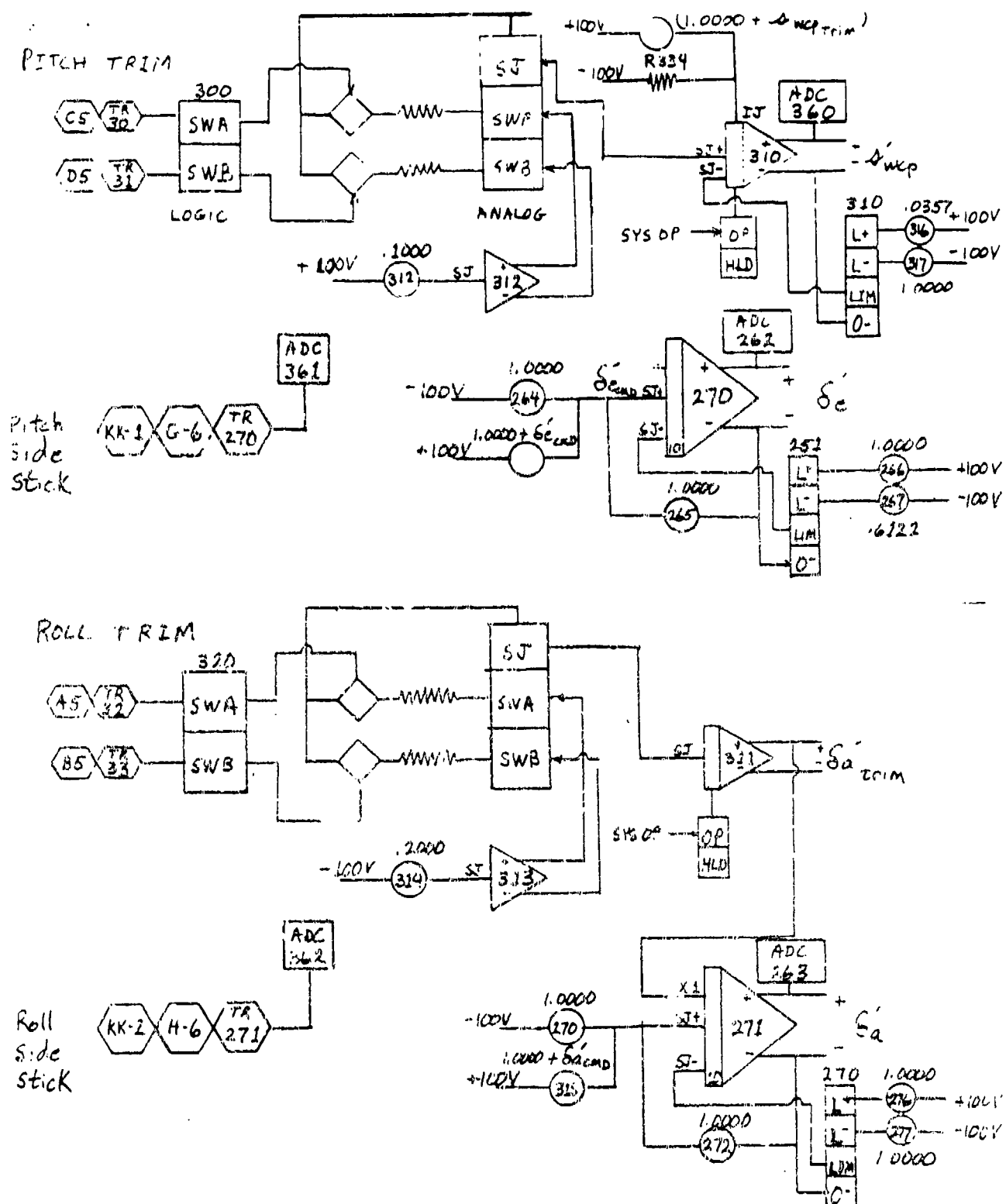
and combining the results (equations B-6 and B-7) give the following:

$$E(r, \gamma, z, A) \cong P(X) \iint f(R, \theta) E(\rho, \beta, z, A, X) dR d\theta \quad (B-8)$$

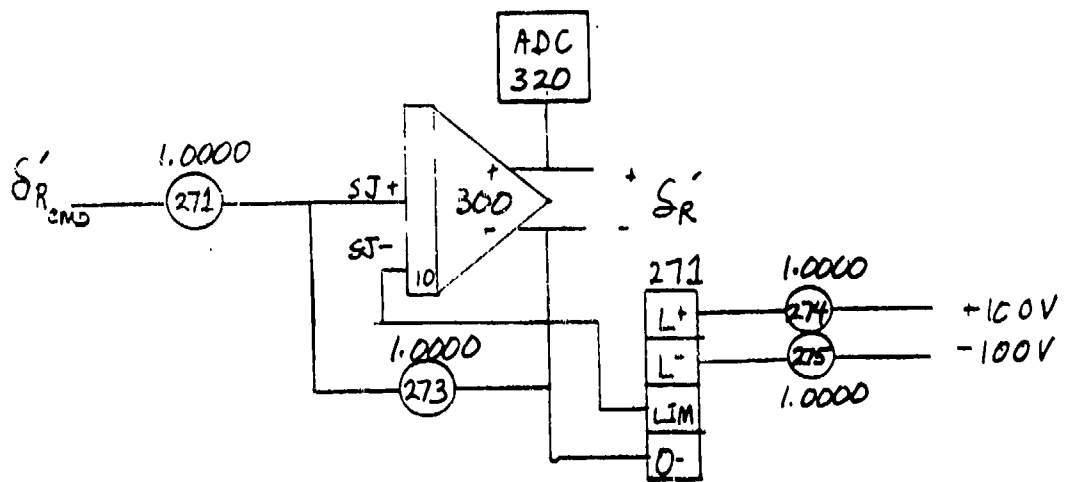
Equation B-8 may be used for numerical integration, along with equations B-3a through B-3d and using a uniform or Gaussian probability density function for $f(R, \theta)$ as appropriate. This procedure is perfectly general as long as the unit of time is taken to be small enough so that the approximation in equation B-5 is valid.

APPENDIX C-1

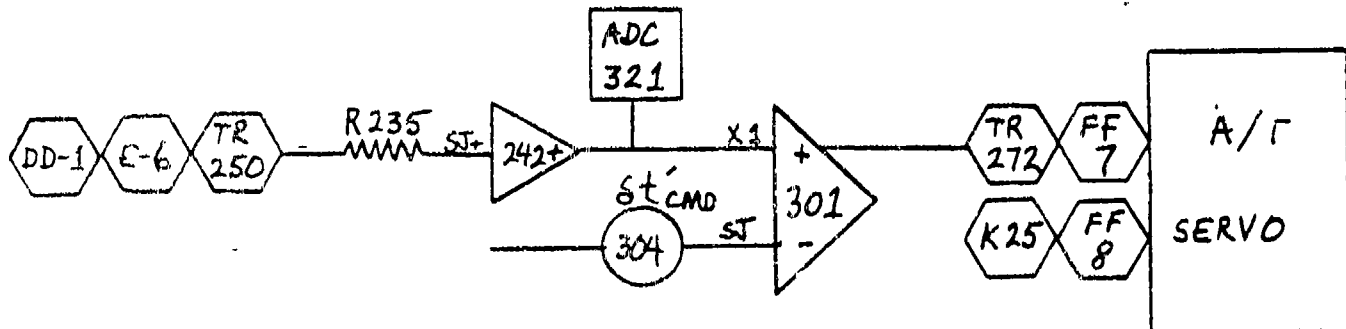
ANALOG CIRCUIT DIAGRAMS



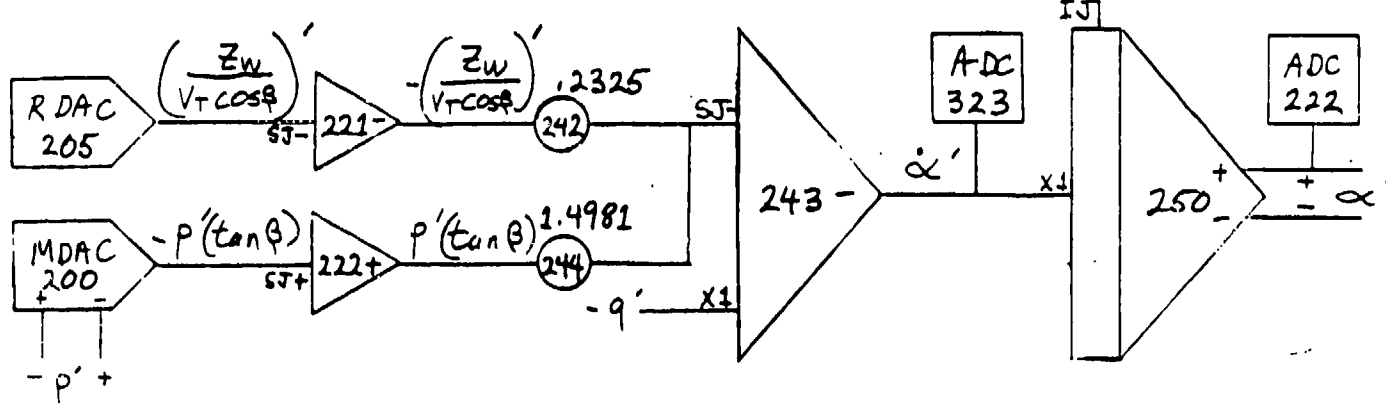
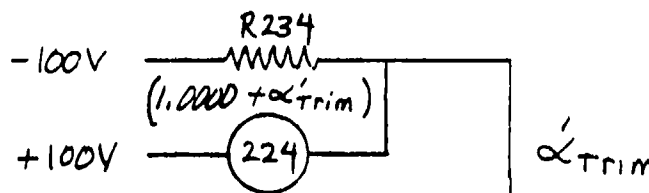
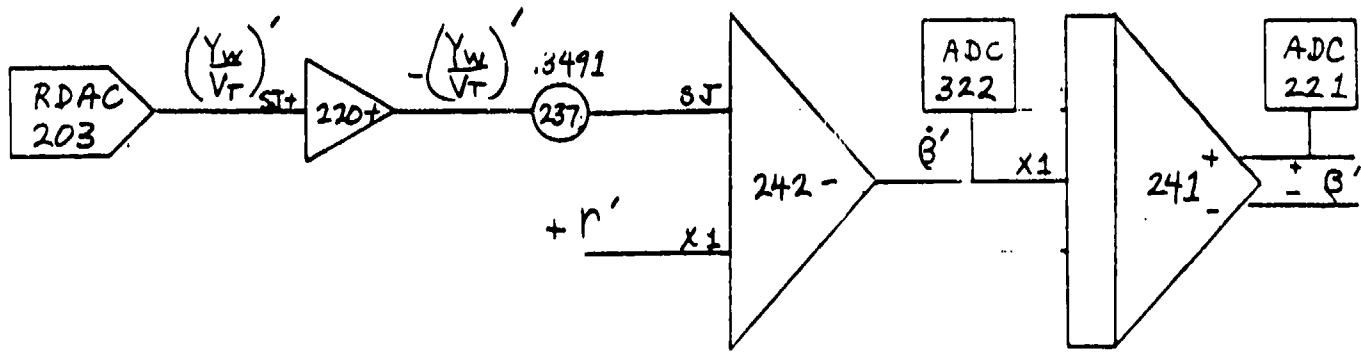
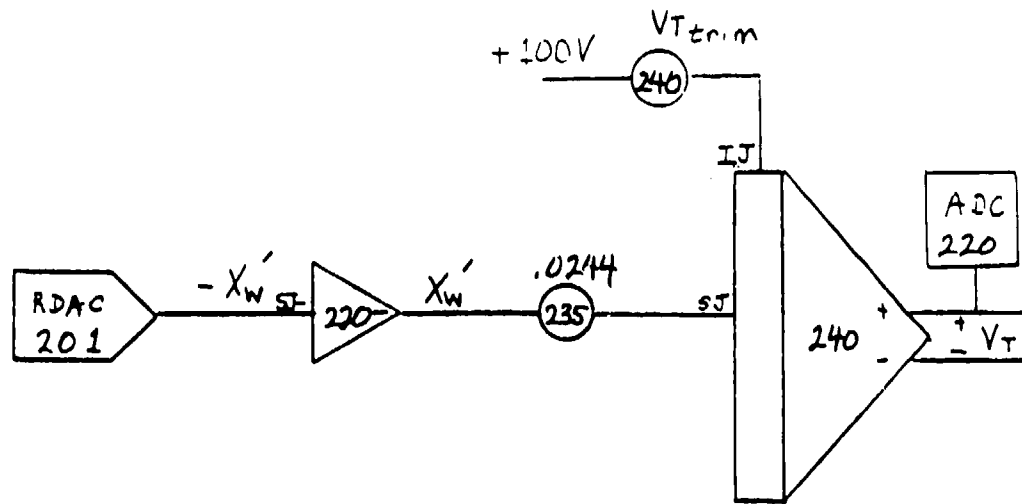
SIDE STICK INPUTS, TRIM AND CONTROL SURFACE DYNAMICS

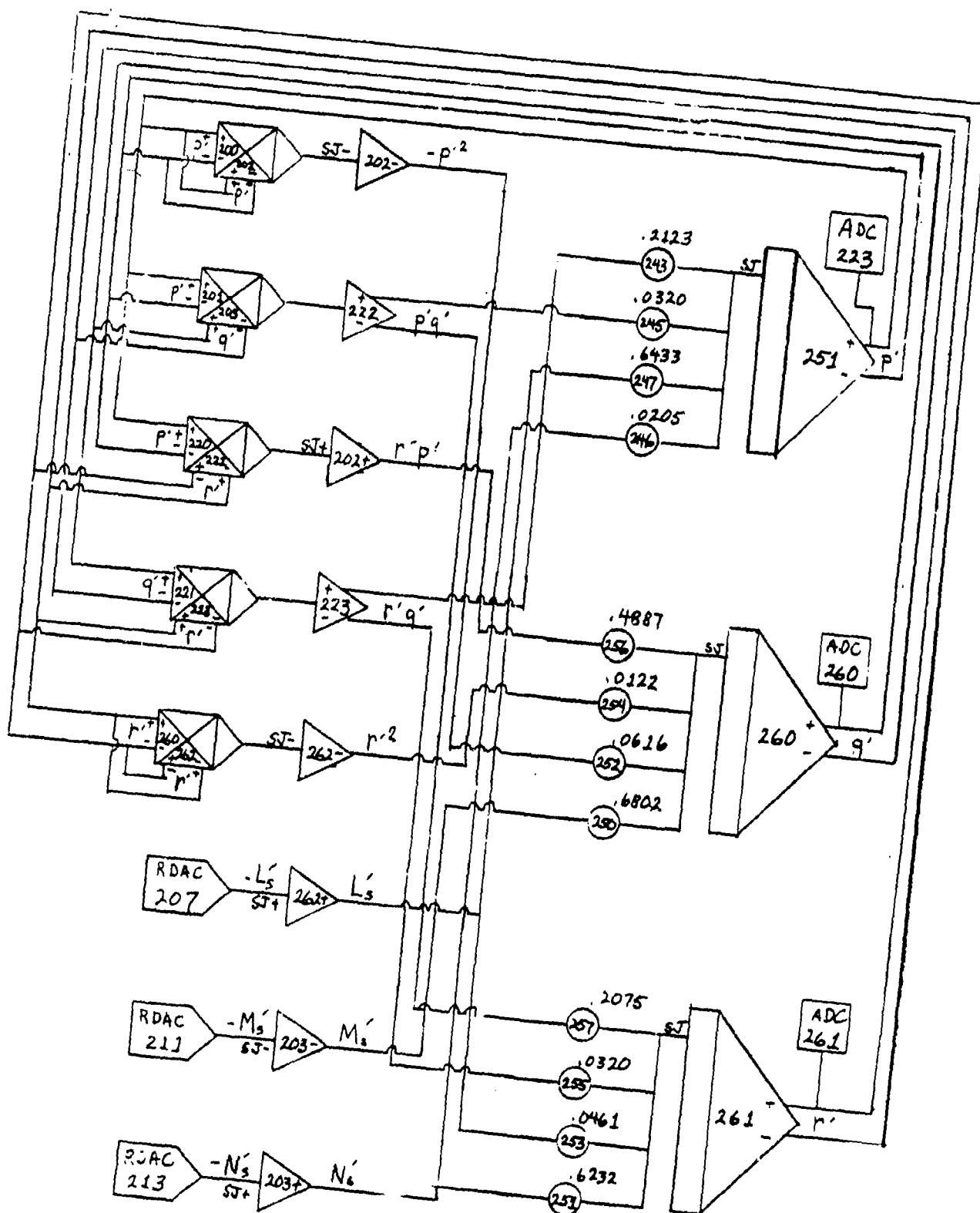


Rudder Dynamics



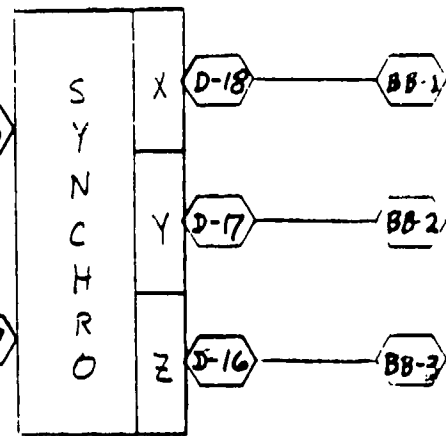
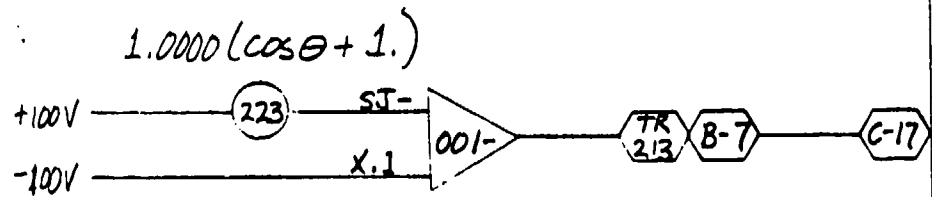
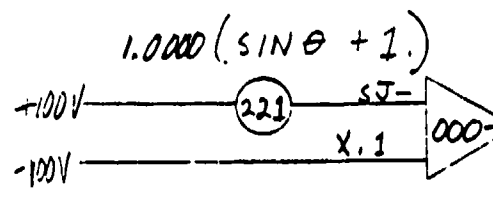
AUTOTHROTTLE



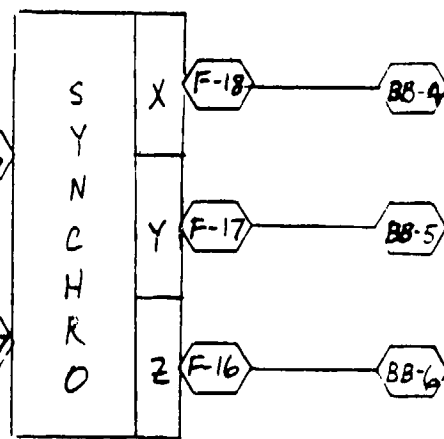
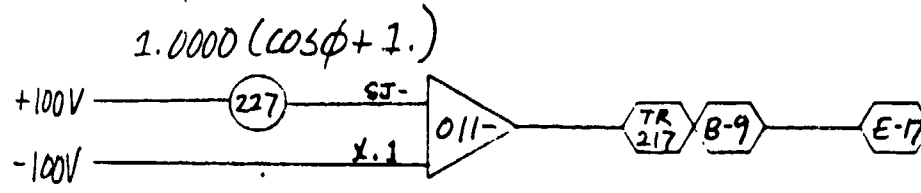
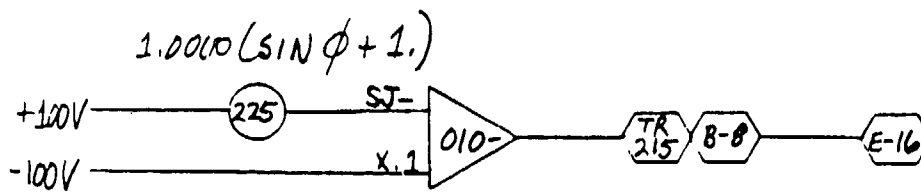


Rotational Dynamics

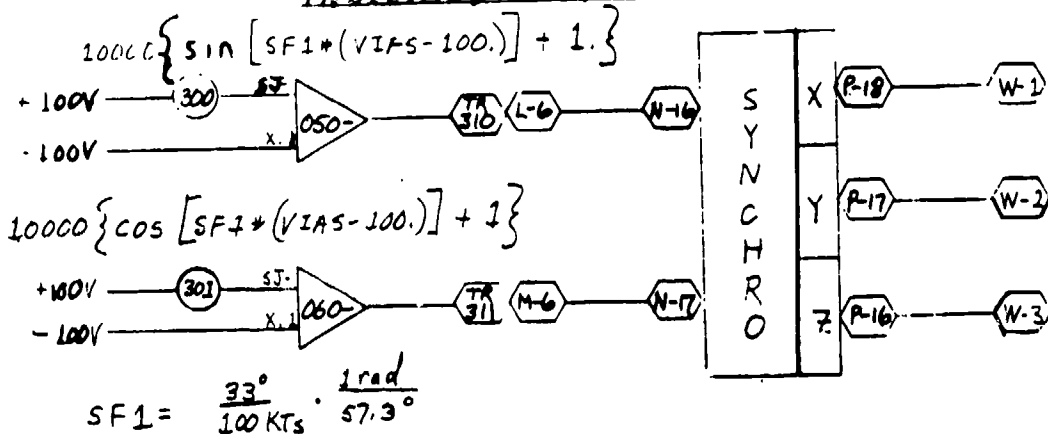
AIRCRAFT PITCH



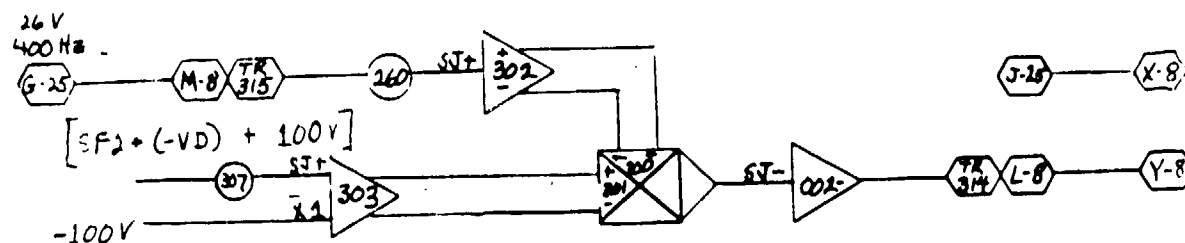
AIRCRAFT PITCH



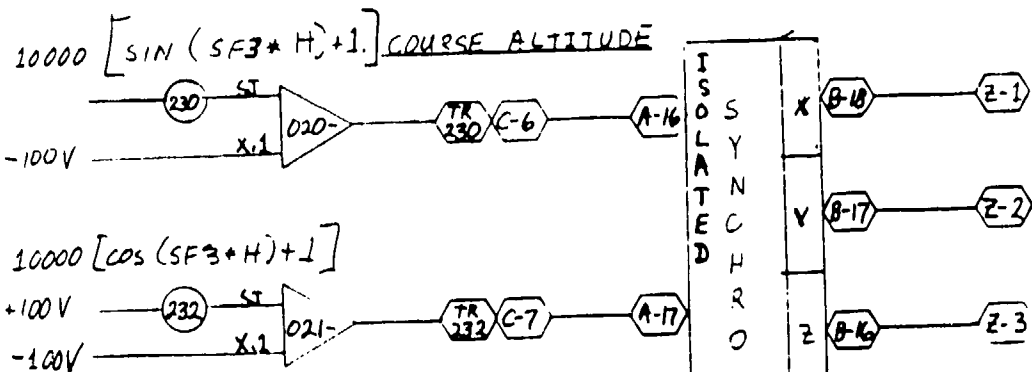
INDICATED AIRSPEED



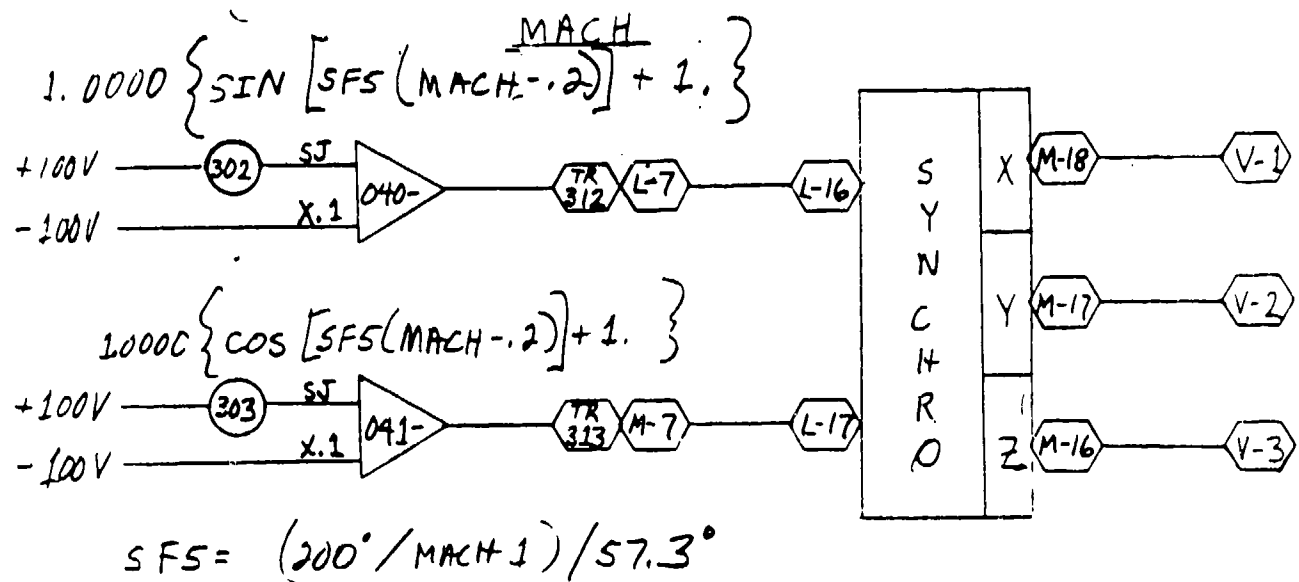
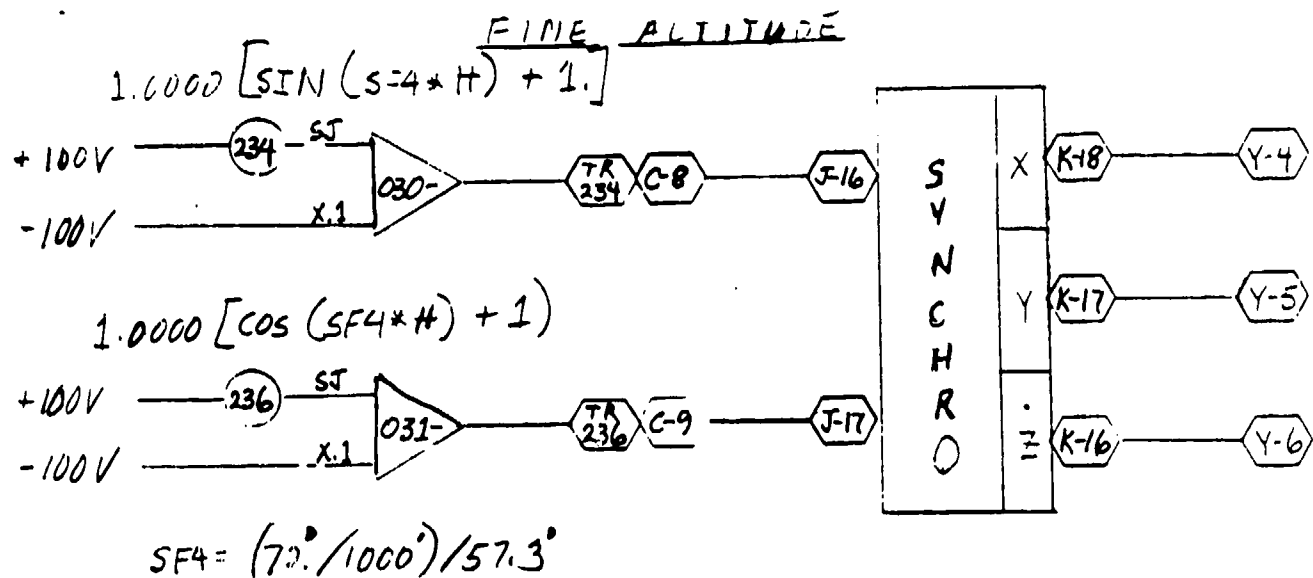
VERTICAL VELOCITY



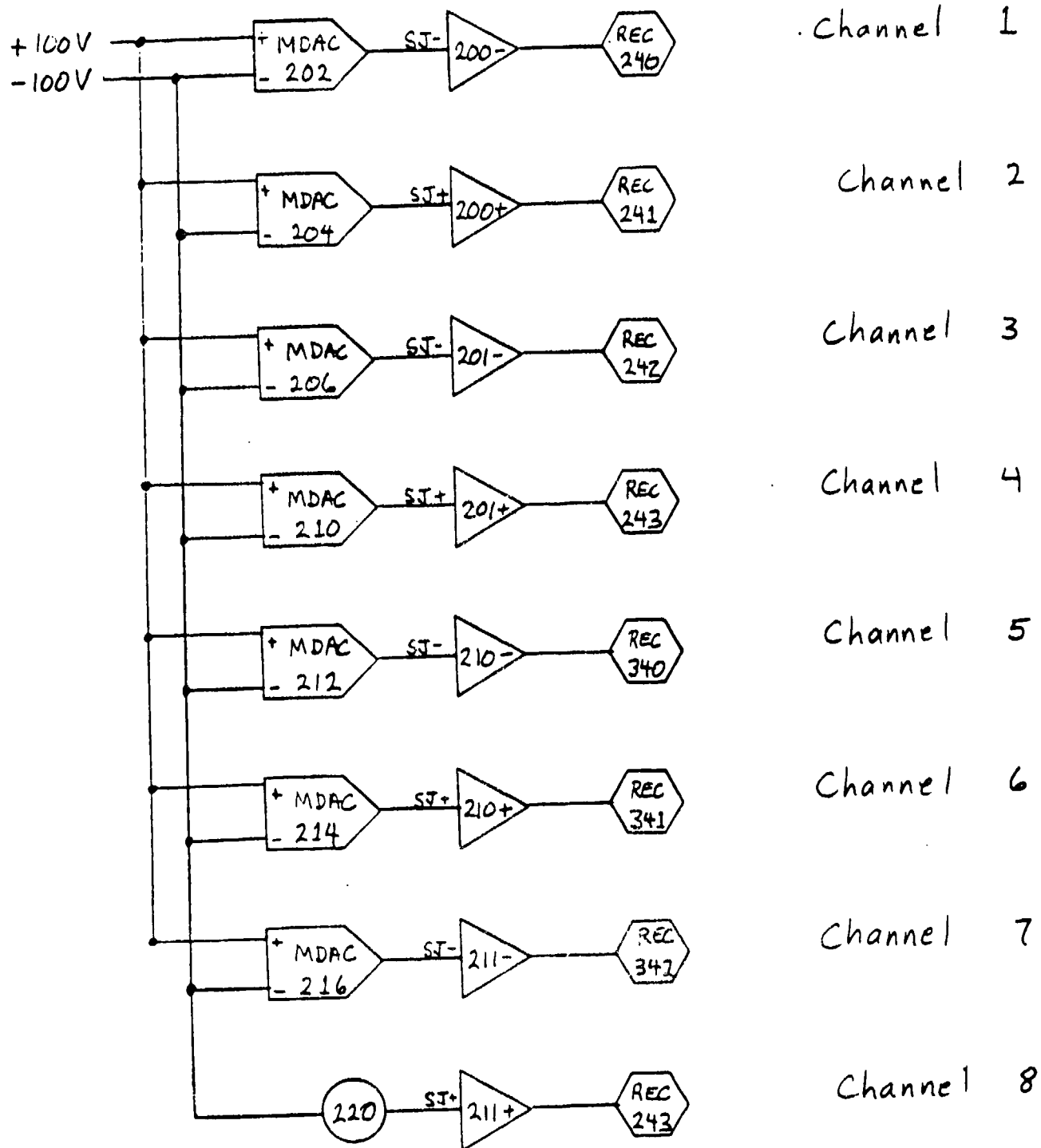
$$SF_2 = 60. \times .025 = 1.5 \quad 1000 \text{ f/m} = .25 \text{ V}$$



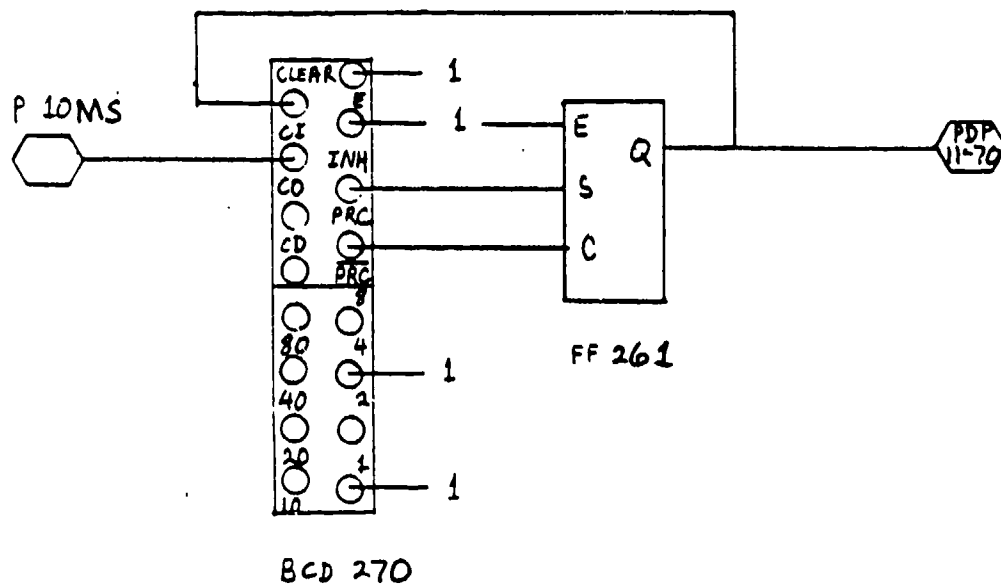
$$SF_3 = (2.67^\circ / 1000') / 57.3^\circ$$



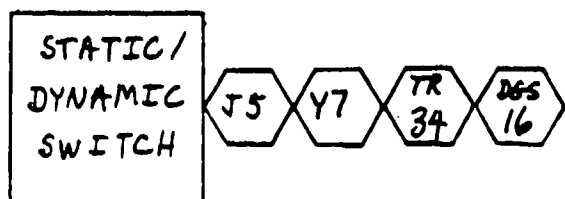
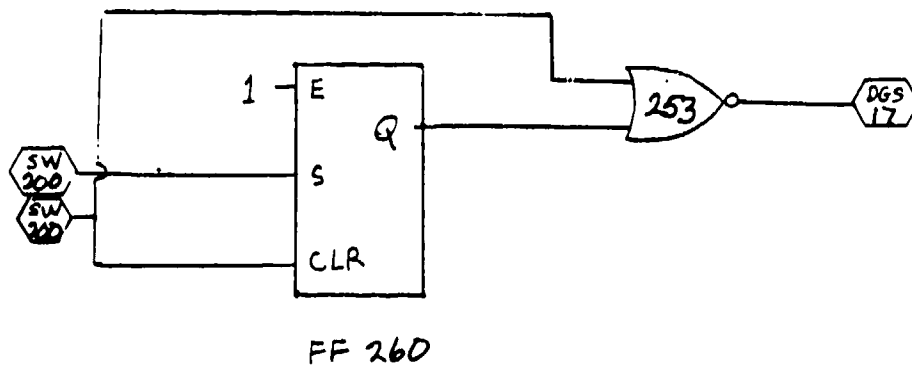
RECORDER - AD4



50 MS CLOCK



PROGRAM TERMINATE



APPENDIX C-2
DIGITAL FLOW CHART

